Transient Protein Interactions:
The case of pseudoazurin and nitrite reductase

PROEFSCHRIFT

ter verkrijging van de graad van Doctor aan de Universiteit Leiden,

op gezag van de Rector Magnificus Dr. D. D. Breimer,

hoogleraar in de faculteit der Wiskunde en

Natuurwetenschappen en die der Geneeskunde,

volgens besluit van het College voor promoties te

verdedigen op donderdag 7 april 2005

te klokke 14.15 uur

door

Antonietta Impagliazzo

geboren te Rome in 1971

Promotiecommissie

Promotor:	Prof. dr. G.W. Canters
Co-promotor:	Dr. M. Ubbink
Referent:	Prof. dr. J. J. G. Moura (Universidade di Lisboa)
Overige leden:	Prof. dr. J. Brouwer
	Prof. dr. E. J. J. Groenen
	Prof. dr. S. S. Wijmenga (Radboud Universiteit Nijmegen)
	Dr. M. Prudêncio (Instituto Gulbenkian de Ciência)

A mia nonna

Cover front: Schematic presentation of the interaction between nitrite reductase and pseudoazurin

Cover back: Ribbon presentation of pseudoazurin. The ribbon size and colors are a function of the experimental cross saturation transfer upon nitrite reductase binding (see Fig. 5.3, page 78).

Cover kindly designed by Elena Impagliazzo, www.phantatomix.com.

Contents:

Abbreviations:

$\Delta\delta_{Bind}$ chemical shift perturbation arising from complex formation

$\Delta\delta_{Avg}$ the average $\Delta\delta_{Bind}$ of the $^1H^N$ and ^{15}N nuclei of an amide

ET   electron transfer

HSQC   heteronuclear single quantum coherence spectroscopy

IPTG   isopropylthio-β-D-galactoside

Mol. eq.   mole equivalent

K_a protonation constant

K_d dissociation constant

K_d^{app} apparent dissociation constant

K_m Michaelis-Menten constant

k_{off} dissociation rate constant

k_{on} association rate constant

NMR   nuclear magnetic resonance

NOESY   nuclear Overhauser enhancement spectroscopy

TOCSY   total correlation spectroscopy

c.s.t.   cross saturation transfer

Proteins

PAZ   pseudoazurin from *Alcaligenes faecalis* S-6

PAZ Cu I   pseudoazurin with copper in the reduced form

PAZ Cu II   pseudoazurin with copper in the oxidized form

PAZ Zn II   zinc substituted pseudoazurin

NiR   nitrite reductase from *Alcaligenes faecalis* S-6

NiR Cu-Cu   nitrite reductase with copper in the type 1 and type 2 sites

NiR Cu-T2D   nitrite reductase type 2 copper depleted

NiR Co II-Co II   cobalt substituted nitrite reductase

Laz   azurin from *Neisseria gonorrhoeae*

Azupsa   azurin from *Pseudomonas aeruginosa*

AniA   nitrite reductase from *Neisseria gonorrhoeae*

PSI   photosystem I

cyt   cytochrome

Organisms

Ac. cycloclastes   *Achromobacter cycloclastes*

Al. xylosoxidans   *Alcaligenes xylosoxidans*

Al. denitrificans   *Alcaligenes denitrificans*

Al. faecalis S-6   *Alcaligenes faecalis* S-6

E. coli   *Escherichia coli*

N. gonorrhoeae   *Neisseria gonorrhoeae*

Ps. aeruginosa   *Pseudomonas aeruginosa*

Ps. aureofaciens　　　　　*Pseudomonas aureofaciens*
Ps. fluorescens　　　　　　*Pseudomonas fluorescens*
Pa. halodenitrificans　　　*Paracoccus halodenitrificans*
Pa. denitrificans　　　　　*Paracoccus denitrificans*
Ps. putida　　　　　　　　*Pseudomonas putida*
Ps. stutzeri　　　　　　　　*Pseudomonas stutzeri*

Chapter I

Introduction

Abstract

This chapter provides a general introduction to nitrite reductase and pseudoazurin, the subject of this thesis. The physiological context of the proteins is described and the structural and functional properties of nitrite reductase and cupredoxins are presented. Furthermore, an introduction to NMR exchange phenomena is provided. The chapter concludes with an overview of the thesis.

1.1   Transient complexes

Most proteins function by interacting with other proteins and participating in this way in many cellular processes. Hence, the understanding of those interactions is essential not only to comprehend fundamental biological processes, including events such as signal transduction, cell cycle regulation, immune response etc. but also to discover the reasons of many disorders associated with aberrant protein-protein interactions. Recent progress in technology gave access to much information on the characteristics of complex formation and this work describes one such contribution.

According to its function, each complex has its own characteristics. One is the complex stability which is correlated to the affinity of one protein for the other. The range of dissociation constants (K_d) observed in biological relevant protein-protein interactions is extremely wide ranging from 10^{-4} to at least 10^{-16} M.

In stable complexes, the specificity of the binding is determined by geometric complementarity of the protein surface. Examples are the complexes between antibodies and antigens (e.g. hen egg lysozyme binds to the variable domains of the HyHEL5 monoclonal antibody with a $K_d = 10^{-10}$ M (Sheriff, 1987) and those between proteases and protease inhibitors, (e.g. the pancreatic trypsin inhibitor (PTI) binds to trypsin with a $K_d = 10^{-14}$ M (Huber, 1974); similarly, the inhibitor barstar binds to the bacterial ribonuclease barnase with a $K_d = 10^{-14}$ M (Guillet, 1993; Schreiber, 1993). On the other end of the range are transient complexes, characterized by a much weaker binding which is correlated to their biological function. These complexes are often found in electron transfer chains as in photosynthesis, oxidative phosphorylation and denitrification, in which a high turnover rate of the complexes is needed in order to guarantee a continuous flow of electrons between redox partners. In redox chains, proteins function as electron carriers implying that a single protein needs to interact with two or more partners. Thus, the forces required for productive complex formation must be sufficient to allow inter-protein electron transfer to occur with multiple partners, but not so large as to impede prompt dissociation of the product complex. Thus, such transient complexes of redox proteins represent a compromise between fast turnover and affinity.

1.2   Interactions in protein-protein electron transfer complexes

Characteristics of electron transfer complexes are high association (k_{on}) and dissociation (k_{off}) rate constants, with K_d (k_{off} / k_{on}) in the µM – mM range. The structural basis for these characteristics has been reviewed recently (Crowley, 2003). The first step of complex formation is the formation of the encounter complex by two proteins occupying the same solvent shell after collision (Adam, 1968). The two proteins trapped in this aspecific association have a higher probability to recollide again (Northrup, 1992), adopting different conformations until the optimal one for the electron transfer is achieved.

Oppositely charged residues on the protein surfaces contribute to a pre-orientation of the diffusing reactants (Matthew, 1983), helping the formation of the active complex (Kannt, 1996; Schreiber, 1993) and prolonging the lifetime of the encounter complex (Sheinerman, 2000), thus increasing k_{on} toward the diffusion limit (10^8 - 10^9 M^{-1}s^{-1} for proteins). Charged

residues are thus involved in long range electrostatic interactions, which contribute to the binding energy (Sheinerman, 2000; Janin, 1997).

Non-polar residues contribute to the complex formation via hydrophobic interactions. Those interactions are considered to be the driving force in the stabilization of the association complex while the electrostatic interaction contributes to the initial recognition. The released water and the consequent increase in entropy more than compensates for the entropy loss (rotational and translational) of the proteins after the complex formation (Chothia, 1975). Redox proteins usually have a small hydrophobic surface area (Adman, 1991) involved in such hydrophobic interactions. This patch is located close to the redox centre, thus ensuring not only affinity, but specificity at the same time, since it assures that the redox centres are brought close to each other in the complex, enhancing the electron transfer rate.

The high k_{off}, essential for transient interactions, has been explained as a consequence of "poorly packed" interfaces (Crowley, 2004; Crowley, 2003; Crowley, 2002c). "Poorly packed" interfaces are not optimized in geometric complementarities, facilitating the interactions with a variety of partners, which is one of the characteristics of redox proteins. Furthermore, the process of re-solvation, which proceeds simultaneously with dissociation, may be facilitated by the presence of polar residues surrounding the hydrophobic area.

1.3   Nitrogen cycle

The nitrogen cycle (Figure 1.1) represents one of the most important nutrient cycles found in terrestrial ecosystems. Nitrogen is used by living organisms to produce a number of complex organic molecules like amino acids, proteins, and nucleic acids. The largest store of nitrogen is found in the atmosphere where it exists as a gas (N_2). Most plants obtain the nitrogen they need as inorganic nitrate from the soil solution. Ammonium is used less by plants for uptake because in large concentrations it is extremely toxic. Animals receive the required nitrogen they need for metabolism, growth, and reproduction by the consumption of living or dead organic matter containing molecules composed partially of nitrogen. Five main processes (Figure 1.1) are involved in cycling nitrogen through the biosphere, atmosphere, and geosphere: nitrogen fixation, dissimilatory nitrate reduction to ammonia, nitrification, denitrification and the anammox process. Microorganisms, particularly bacteria, play major roles in all of the principal nitrogen transformations.

Once nitrite is formed (step I in Figure 1.2), it can be converted in different processes: dissimilatory nitrate reduction to ammonia (DNRA, step I - IIa in Figure 1.2), denitrification (step IIb-IVb in Figure 1.2) which produces dinitrogen, or the more recently discovered anammox process (step IIc in Figure 1.2) in which dinitrogen is also formed.

Dissimilatory nitrate reduction to ammonia (DNRA, step I and IIa in Figure 1.2) is a pathway that covers the whole range between nitrate and ammonia (Cole, 1980). Ammonia is used as nitrogen source by microrganisms and plants for biosynthesis of many vital compounds, such as amino acids, proteins and DNA. Hereby, nitrate is first reduced to nitrite in a 2-electron step by a nitrate reductase, and subsequently the product nitrite is converted to ammonia in a 6-electron step catalyzed by a cytochrome *c* nitrite reductase or ferredoxin-nitrite reductase (Einsle, 2002; Murphy, 1974).
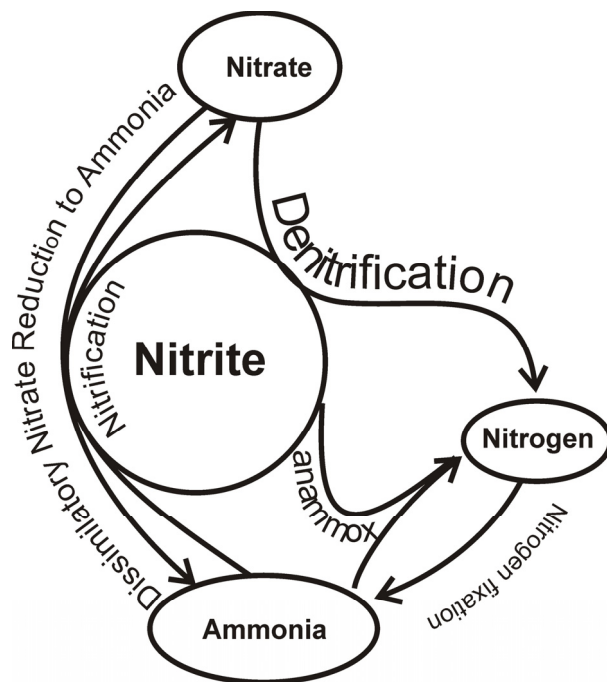
Figure 1.1: Scheme of the nitrogen cycle showing the main processes involved in it: nitrogen fixation, dissimilatory nitrate reduction to ammonia, nitrification, denitrification and the anammox process.

A short route for dinitrogen gas formation is represented by anaerobic ammonium oxidation (anammox) (Van de Graaf, 1995). Anammox is the microbiological conversion of ammonium and nitrite into dinitrogen gas (step IIc in Figure 1.2) (Jetten, 2001). The anammox process makes a significant (up to 70%) contribution to nitrogen cycling in the world's oceans (Thamdrup, 2002) and represents a viable option for biological wastewater treatment (Jetten, 2003; Jetten, 2001; Strous, 1999). The anammox reaction is carried out by a group of planctomycete bacteria. Two of those have been named provisionally: *Candidatus* "Brocadia anammoxidans" and *Candidatus* "Kuenenia stuttgartiensis".

Alternatively, nitrate (NO_3^-) can be reduced to N_2 during denitrification. Denitrification is a physiological process which occurs under anaerobic conditions and is crucial for energy generation of a variety of bacteria (Zumft, 1997). The importance of the process is given by the fact that it returns large amounts of fixed nitrogen to the atmosphere as part of the terrestrial nitrogen cycle. During denitrification nitrate is reduced to N_2 in four steps (Denitrification step I, II b – IV b in Figure 1.2), each one catalyzed by different metallo-enzymes.

The first enzyme, nitrate reductase, (NaR), is located in the cytoplasmic membrane with its active site accessible from the cytoplasmic side. Both nitrate and the reduction product nitrite are transferred by a specific carrier associated with NaR, across the membrane. Once nitrite is back in the periplasmic space, it is reduced by nitrite reductase (NiR). The nitric oxide reductase (NoR) is localized in the cytoplasmic membrane and releases its product N_2O back into the periplasmic space where the soluble enzyme nitrous oxide reductase (N_2oR) converts it into N_2.

Denitrifying processes and the enzymes involved in them, are also important from an ecological point of view: agriculture and industrial processes result in increased emission of nitrous oxide, which is an active greenhouse gas and contributes to depletion of the ozone layer (Bange, 2000; Robertson, 2000).

Other nitrogen containing compounds (such nitrate and ammonium salts) are introduced to the environment by the increasing use of nitrogen-rich fertilizers, destabilizing the ecosystem and leading to algal blooms and eutrophication. For this reason, monitoring nitrite levels in the environment has become an important task and recently nitrite reductase has been applied in a biosensor for nitrite detection (Ferretti, 2000; Sasaki, 1998).

Denitrifying bacteria occupy a wide range of natural habitats such as soil, water, foods and digestive tracts. In the absence of oxygen, those bacteria can use nitrogen oxide species as final electron acceptors. The cellular location of the denitrification enzymes has been determined for Gram-negative bacteria (Wasser, 2002; Averill, 1996) and is shown in Figure 1.3.
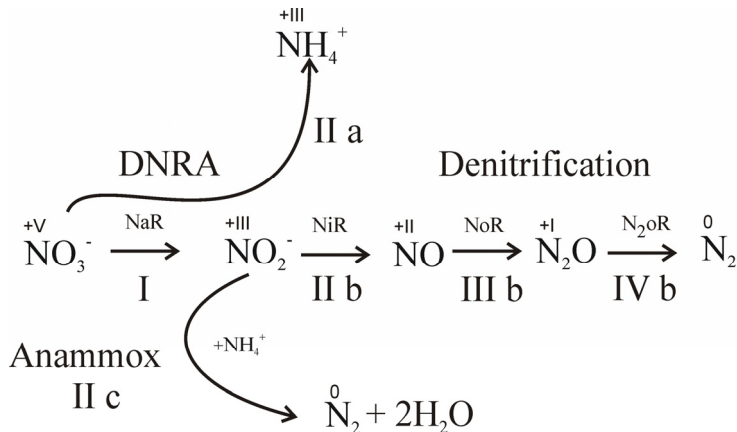
Figure 1.2: Scheme of possible reactions that nitrite can undergo after being formed from nitrate. **NaR**: nitrate reductase. DNRA (IIa): dissimilatory nitrate reduction to ammonia. Denitrification (IIb-IVb) (catalyzed by **NiR**: Nitrite reductase (IIb); **NoR**: Nitric oxide reductase (IIIb); **N₂oR:** Nitrous oxide reductase (IVb). Anammox process (IIc). The roman numbers above the nitrogen atoms refer to the oxidation state of this atom in each molecule.

Figure 1.3: Arrangement of the enzymes involved in denitrification process in Gram-negative bacteria: nitrate reductase (NAR) and nitric oxide reductase (NoR) are membrane bound proteins while nitrite reductase (NIR) and nitrous oxide reductase (N_2oR) are periplasmic enzyme.
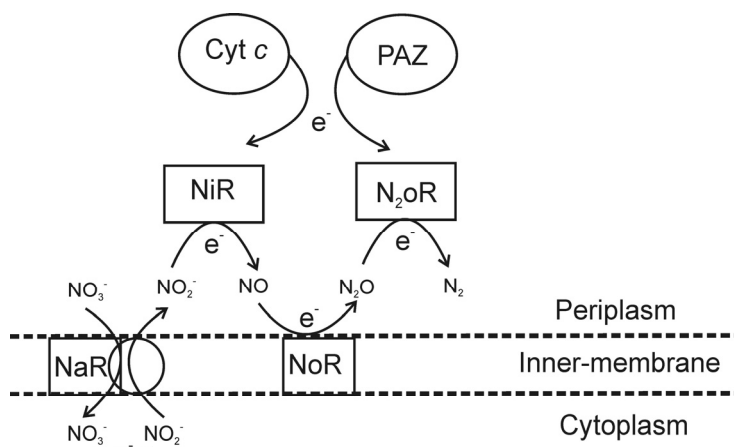
The work of this thesis is focussed on one of those denitrification enzymes: nitrite reductase (NiR). A more specific description will be given of NiR and its physiological partners belonging to two organisms: *Alcaligenes faecalis* S-6 and *Neisseria gonorrhoeae*.

1.4   Nitrite Reductase

Two types of nitrite reductase are known, one containing a single haem group in the catalytic site and one containing copper, both catalyzing the same reaction in the denitrification process:

$$NO_2^- + e^- + 2H^+ \rightleftharpoons NO + H_2O$$
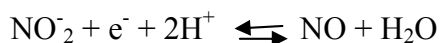
Nitrite reductases containing multi-haem prosthetic groups (pentahaem and sirohaem) can catalyze a six-electron reduction in the dissimilatory nitrate reduction to ammonia:

$$NO_2^- + 6e^- + 8H^+ \rightleftharpoons NH_4^+ + 2H_2O$$
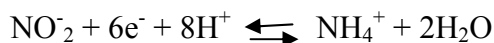
1.4.1   Haem Nitrite Reductase

Haem containing nitrite reductases have been isolated from various bacteria: *Pseudomonas aeruginosa* (Ota, 1961), *Thiobacillus denitrificans* (Huynh, 2004)*, Pseudomonas stutzeri* (Liu, 1983), *Paracoccus halodenitrificans (Mancinelli, 1986)*. Haem nitrite reductases are homodimers of two 60 kDa subunits. Each of the two polypeptide chains is folded into two domains: the alpha helical *c*-type cytochrome domain (*c* domain), and a rigid β propeller

domain (d_1 - domain). The *c*-haem is covalently bound to the *c*-domain, and is the site of electron entry for donor proteins. The d_1 haem is non-covalently bound to the d_1 - domain and resides in the pocket created by the antiparallel sheet motif (Williams, 1997).

Haem *c* receives electrons from a potentially wide variety of electron donors as it can be reduced by cytochrome *c*, azurin and pseudoazurin (Dodd, 1995; Moir, 1993; Parr, 1977). It rapidly reduces the Fe^{+3} haem d_1 back to the Fe^{+2} form after catalytic turnover of nitrite, ensuring that it is ready to interact with another substrate molecule (Averill, 1996). A wide variety of spectroscopic and ligand-binding studies have been carried out on various examples of haem nitrite reductases, elucidating the mechanism for reduction of nitrite by haem cd_1 and the role of specific residues on the d_1-haem active sites (Cutruzzola, 2001; Silvestrini, 1990; Walsh, 1981).

In the dissimilatory nitrate reduction to ammonia, nitrate is first reduced to nitrite by a molybdenum-dependent nitrate reductase, and subsequently nitrite is converted into ammonia in a six electron step by a multi-haem nitrite reductase like cytochrome *c* nitrite reductase or sirohaem-nitrite reductase.

Cytochrome *c* NiRs are pentahaem enzymes with interesting spectroscopic properties (Einsle, 1999). These NiRs belong to a growing family of structurally well characterized multi-haem proteins that are involved in electron transfer and redox chemistry of inorganic nitrogen and sulphur compounds. These proteins contain conserved structural motifs of haem centres, despite significant differences in primary sequence and protein structure (Einsle, 2000).

They have a molecular mass of ~55 kDa, are encoded by a single gene and have been found so far in *Escherichia coli* (Hussain, 1994), *Haemophilus influenzae* Rd (Fleischmann, 1995), *Sulfurospirillum deleyianum* (Einsle, 1999) and *Wolinella succinogenes* (Einsle, 2000). Crystal structures of pentahaeme cytochrome *c* nitrite reductase have been solved from *Sulfurospirillum deleyianum* (Einsle, 1999) and *Wolinella succinogenes* (Einsle, 2000) bacteria. Both enzymes form a stable dimer with a total of ten haem groups and two independent active sites.

Another type of nitrite reductases that is able to catalyze the reduction of nitrite into ammonium and those are the sirohaem nitrite reductases. Sirohaem is an iron tetrahydroporphyrin, covalently linked to an 4Fe-4S cluster (Crane, 1996; Murphy, 1974). There are two types of sirohaem NiRs: the higher plant chloroplast form of NiR is a monomeric protein (63 kDa) that uses reduced ferredoxin as the electron donor, and contains a single [4Fe-4S] cluster and a single sirohaem which serves as the binding site for nitrite (Dose, 1997). Fungal and bacterial NiR are homodimeric proteins that use NAD(P)H as the electrondonor. Both forms of NiR contain a sirohaem and iron-sulfur centres.

The ferrodoxin-dependent nitrite reductases have been found in the plants *Arabidopsis thaliana* (Tanaka, 1994), *Betula verrucosa* (Friemann, 1992), *Pinus sylvestris L.* (Neininger, 1994), *Spinacea oleracia* (spinach) (Back, 1988) and *Zea mays* (maize) (Lahners, 1988), and the cyanobacteria *Phormidium laminosum* (Merchan, 1995) and *Synechococcus sp*. (strain PCC 7942) (Luque, 1993).

NAD(P)H dependent NiR has been found in bacteria as *Bacillus subtilis* (Ogawa, 1995), *Klebsiella pneumoniae* (Lin, 1993) and *Aspergillus nidulans* (Johnstone, 1990) and in fungi

as *Leptosphaeria maculans* (Williams, 1995), *Neurospora crassa* (Exley, 1993) and *Fusarium oxysporum* (Kobayashi, 1995).

1.4.2   Copper Nitrite Reductase

Copper nitrite reductases (Adman, 2001) have been isolated primarily from Gram-negative bacteria: *Alcaligenes faecalis* S-6 (Kakutani, 1981c)*, Achromobacter cycloclastes* (Fenderson, 1991)*, Alcaligenes xylosoxidans* (Prudêncio, 1999; Abraham, 1993), *Pseudomonas aureofaciens* (Glockner, 1993) and recently from *Neisseria gonorrhoeae* (Hoehn, 1992a), but also from some Gram positive bacteria (Hoffmann, 1998) and fungi (Kobayashi, 1995). All the known Cu- nitrite reductases structures are trimeric, with a type1 copper centre in each monomer of ~37 kDa and three type 2 copper centres shared by adjacent subunits. Table 1.1 lists the properties of copper containing nitrite reductases with reference to their structure when available.

Nitrite reductases have been divided in green and blue according their colour, although they have very similar structures.

The type 1 copper centre is found in nitrite reductase as well as in cupredoxins such as azurin and plastocyanin. In these metal centres the copper is coordinated by one methionine thioether, one cysteine thiolate and two histidine imidazole groups. The cysteine ligand has been shown to be responsible for the ligand-to-metal charge transfer transition [S (Cys)→Cu II] which gives the protein its colour (blue or green), with an intense absorption band near 600 nm. The type 1 copper centre has an axial by flattened tetrahedron geometry and shows a rhombic EPR signal in green nitrite reductase while in blue nitrite reductase it has an axial by distorted tetrahedron geometry and axial EPR signal (Dodd, 1998; Inoue, 1998).

Table 1.1: Properties of copper containing nitrite reductases.

Organism	Mass subunit & Colour	pI	Electron donor	PDB	Ref.
Ps. aureofaciens	36.9 kDa blue	6.0	Azurin		(Glockner, 1993)
Al. xylosoxidans	36.5 blue	8.4	Cyt c_{553}	1BQ5	(Inoue, 1998)
Ac. cycloclastes	36.5 kDa green		Pseudoazurin	2NRD	(Adman, 1995)
Al. faecalis S-6	37 kDa green	4.5	Pseudoazurin	1AQ8	(Murphy, 1997)
Rhodobacter sphaeroides	37.5 kDa	5.2	Cyt c_2		(Tosques, 1997)
N. gonorrhoeae	36 kDa blue		Azurin	1KBW	(Boulanger, 2002)

The type 2 copper site does not show any visible band in the UV spectrum since there is no coordinating cysteine. The copper is coordinated by two histidines from one subunit and one histidine from the adjacent subunit and additionally it has a co-ordinated water molecule in the resting state. It shows a characteristic distorted tetrahedral geometry.

In copper nitrite reductase the type 1 centre accepts electrons from an electron donor (generally cupredoxins like azurin and pseudoazurin) and then donates it to the active site the type 2 copper centre (Suzuki, 1997).

Selective Cu depletion (Howes, 1994; Libby, 1992) has demonstrated that the type 2 site acts as the nitrite binding site and, more recently, this has been confirmed by different crystal structures of nitrite and NO bound nitrite reductases (Tocheva, 2004; Dodd, 1998; Murphy, 1997; Adman, 1995).

1.5   Cupredoxins

Cupredoxins, characterized by an intense blue colour, are small proteins (9-15 kDa), with a single domain structure, function as electron carriers in various redox chains. Cupredoxins can be classified into three subclasses according to their origin and characteristics (Messerschmidt, 2001): the first subclass is comprised of azurin, pseudoazurin, amicyanin, rusticyanin, halocyanin and auracyanin, all involved in bacterial respiratory electron

Table 1.2: List of cupredoxins azurins and pseudoazurins for which structures have been determined.

Subfamily	Organism	PDB entry	state	reference
Azurin	*Al. xylosoxidans*	1RKR	OX	(Li, 1998)
	Al. denitrificans	2AZA	OX	(Baker, 1988)
	Ps. aeruginosa	4AZU	OX	(Nar, 1991)
		5AZU		
	Ps. fluorescens	1JOI	OX	(Zhu, 1994)
	Ps. putida	1NOW	OX	(Chen, 1998)
	N. gonorrhoeae	n/a		
Pseudoazurin	*Al. faecalis S-6*	8PAZ	OX	(Libeu, 1997)
		3PAZ	RED	
	Ac. cycloclastes	1BQK	OX	(Inoue, 1993)
		1BQR	RED	
	Pa. denitrificans	1ADW	OX	Williams, '95
	Methylobacterium extorquens	1PMY	OX	(Inoue, 1994)

n/a: not available

transport. The second subclass is formed by proteins belonging to photosynthetic organisms, like plastocyanin. Stellacyanin, mavicyanin, and umecyanin, all plant proteins, belong to a third subclass.

Azurin and pseudoazurin are most relevant for the present work and will be discussed in more detail. Table 1.2 lists the organisms in which azurin and pseudoazurin have been found with reference to their structure.

The structures of several cupredoxins have been solved by X-ray and NMR techniques. Despite differences in sequence (sequence identity between some cupredoxins is less than 20% (Adman, 1991), these structures are well conserved, consisting of 6-13 β-strands which form a β-sandwich arranged in a Greek-key motif. Stability is provided by the 'hydrophobic core' between the two β-sheets. The type 1 copper site is located close to the surface at one end of the β-strands. The copper is strongly coordinated by the N^δ atoms of two histidine residues, a S^γ of a cysteine thiolate and weakly coordinated by an axial ligand which, in most cases, is a methionine thioether. The resulting coordination of the copper is intermediate between tetrahedral and trigonal. Spectroscopic studies indicate that the geometry of the copper-cysteine bond (bond length 2.13 ± 0.06 Å, torsion angle $Cu-S^\gamma-C^\beta-C^\alpha \sim -170°$ and $S^\gamma-C^\beta-C^\alpha-N \sim 170°$) is the most conserved feature of cupredoxins. Ligand positions seem to be unaffected by removal of the copper or replacement by different metals (Hg or Cd) (Blackwell, 1994), indicating that the coordination of the copper site is determined by the protein architecture rather than by the copper ion (Petratos, 1995; Shepard, 1990; Garrett, 1984). This polypeptide geometry of the copper ligation tunes the reduction potential, optimizes electron transfer and explains the similarities between the cupredoxin structures (Gray, 2000; Randall, 2000; Ryde, 2000; Larsson, 2000). Furthermore, it has been shown that the hydrogen bonding network in the ligand loop plays a key role in tuning the reduction potential (Machczynski, 2002).

1.6 Nitrite reductase and pseudoazurin from *Alcaligenes faecalis S-6*

1.6.1 *Nitrite reductase*

The copper-containing nitrite reductase (NiR) from the denitrifying bacterium *Al. faecalis* S-6 has been identified in 1981 and its function as an enzyme that catalyzes the reduction of NO_2^- to NO under anaerobic condition was reported (Nishiyama, 1993; Kakutani, 1981a; Kakutani, 1981c).

The crystallographic structure of NiR was published in 1994 (Kukimoto, 1994) which confirmed the trimeric structure (Figure 1.4a) and the presence of two coppers per subunit. A better refined structure of NiR from *Al. faecalis* was published in 1997 and it is used in this thesis [PDB:1AQ8] (Murphy, 1997). Each subunit contains two domains with a cupredoxin fold. His95, Cys136, His145 and Met150 are the ligands for the type 1 copper forming a flattened tetrahedron. The electron from the physiological electron donor, pseudoazurin, is transferred to the type 1 site on NiR. The type 1 copper atom lies about 4 Å from the protein surface and the distance to the type 2 copper is 12.6 Å. The two coppers are bound by adjacent residues in the sequence: type 2 Cu-His135 – Cys136 – type 1 Cu (Figure 1.4b), this linkage provides an efficient electron transfer pathway consistent with the observed first order electron transfer rate of 1.4×10^3 s^{-1} at pH 6 and 25°C (Suzuki, 2000).
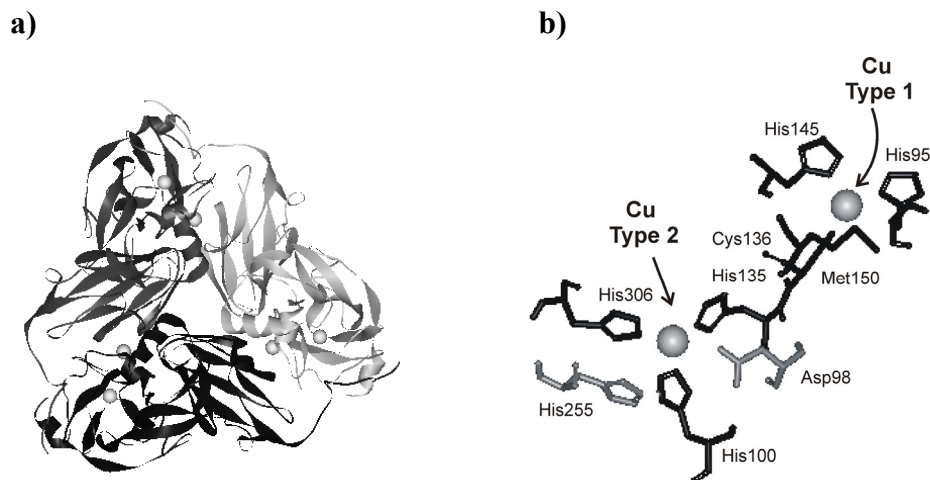
a)   b)

Figure 1.4: a) Structure of the trimeric nitrite reductase from *Al. faecalis* S-6 [PDB:1AQ8]. Each subunit indicated in light grey, dark grey and black contains both type 1 and type 2 copper spheres. **b)** Structure around the copper sites in NiR with the copper atoms represented by spheres. The copper ligands together with residues significant for the ET are represented by black sticks. The His306 ligand of the type 2 copper belongs to the adjacent monomer. Residues His135 and Cys136 provide a covalent link between the copper ions. Asp98 and His255 (from adjacent subunit) are grey coloured and have been demonstrated to be essential for the catalytic activity.

The type 2 site lies at the bottom of a deep channel (12-13 Å) situated in a pocket formed by apposition of domain II of one monomer and domain I of another. His100, His135 and His306 from the adjacent subunit are the ligands for the type 2 copper. These three histidine ligands, together with a molecule of solvent (H_2O), form a distorted tetrahedron. It has been shown for nitrite reductase from *Ac. cycloclastes* that these histidine residues remain oriented in the same way even upon removal of the type 2 Cu (Murphy, 1997; Adman, 1995). Furthermore, no significant structural or electronic differences of the type 1 site have been observed in NMR spectra upon depletion of the type 2 site (Dennison, 2000).

It has been observed that in a type 2 mutated nitrite reductase from *Al. xylosoxidans,* with a lower enzyme activity, the formation of an electron transfer complex with its physiological partner, azurin, restored the activity of the type 2 site, suggesting a coupling between the copper sites (Prudêncio, 2001). Furthermore, a recent study has shown that the presence of the nitrite substrate plays an important role in the modulation of the redox potential of the type 2 centre influencing the intramolecular electron-transfer rate between type 1 and type 2 copper centres (Pinho, 2004).

Two other residues present in the type 2 copper site seem to play an important role in the substrate binding and reduction: Asp98 and His255 (Figure 1.4b). Mutation of Asp98 reduces the activity to less than 1%, establishing that this residue is fundamental for the reaction mechanism (Zhao, 2002; Prudêncio, 2001; Boulanger, 2000; Kataoka, 2000;

Suzuki, 2000). Both residues have been shown not only to control the electron transfer process but also to provide a proton essential in the nitrite reduction process (Boulanger, 2000; Kataoka, 2000). Recent work on the basis of a comparison of the crystal structures of a NiR type2 copper nitrosyl complex and nitrite bound NiR, further confirms the importance of those residues and suggests a reaction mechanism for nitrite reduction (Tocheva, 2004). Nitrite binds with one of its oxygens to the type 2 copper in the oxidized state in a protonated form with the proton probably coming from Asp98. The electron coming from the type 1 site reduces the copper in the type 2 site causing a rearrangement of NO_2^- to release water and form a Cu I-NO^+ intermediate stabilized by the negative charge of Asp98.

Concerning the surface charge, NiR is characterized by 40 negatively charged and 27 positively charged residues resulting in a very negative surface charge with a theoretical pI of 5.56.

1.6.2 Pseudoazurin

Pseudoazurin (PAZ) is a member of the cupredoxin family of electron transfer proteins and has been shown to have a dual physiological role in the cells as an electron carrier to nitrite reductase for nitrite reduction under anaerobic conditions and as an inactivating factor of the enzyme under aerobic conditions in the presence of reducing agents such as ascorbate (Hormel, 1986; Kakutani, 1981b). The nucleotide sequence of the gene encoding pseudoazurin from *Al. faecalis* S-6 shows the presence of a typical N-terminal signal peptide sequence of 23 amino-acid residues. This suggests that the protein is secreted into the periplasmic space (Yamamoto, 1987). Pseudoazurins have also been found in several other bacterial species, like *Ac. cycloclastes* (52% sequence identity, Iwasaki, 1973), *Pseudomonas* AM1 (45%, Ambler, 1985), *Thiosphera pantotropha* (57%, Moir, 1993) and *Paracoccus pantotrophus* (50% Thompson, 2000).

Pseudoazurin from *Al. faecalis* contains 123 amino acid residues with a total molecular weight for the apo form of 13,397 Da. The three dimensional crystal structure of oxidized pseudoazurin (Figure 1.5a; PDB entry: 8PAZ (Petratos, 1988)) can be described as an eight stranded β-sandwich with the last 30 residues forming a hairpin motif of two α-helices. The copper atom is coordinated by His40, Cys78, His81, and Met86 in a distorted tetrahedral configuration. The structures of reduced pseudoazurin at two different pHs (7.8 and 4.4) have been determined (Vakoufari, 1994). A comparison between oxidized and reduced protein shows no changes in the main chain fold upon reduction. At low pH (4.4), Cu I and His81 move in opposite directions increasing the copper distance from the imidazole ring compared to the structure at pH 7.8. The distance Cu-$N^{\delta 1}$His becomes 3.1 Å, compared with 2.3 Å at pH 7.8, enough to indicate that His81 is not a copper ligand. At this pH the copper moves to a more trigonal position. Also Met 7 and Pro 35 move co-ordinately upon reduction (Libeu, 1997). The charge distribution on the surface of pseudoazurin (Figure 1.5a) is very peculiar compared with that of other cupredoxins. Eight lysines residues out of a total of 13 present in the protein (10, 38, 57, 59, 77, 106, 109, 117), together with Arg114, form a positively charged ring (Figure 1.5a, top panel) around the characteristic hydrophobic patch through which the histidine copper ligand protrudes slightly. A

characteristic molecular dipole-moment is created by the presence of four negatively charged residues (Asp29, 47, 94 and 100) at the other end of the protein.

1.7   The complex between nitrite reductase and pseudoazurin

Kinetic studies on protein-protein interactions between NiR and PAZ have been performed previously (Kukimoto, 1996; Kukimoto, 1995). In a mutagenesis study, 9 of the 13 lysines on PAZ surface were replaced indipendently with alanine or aspartate. These mutations had little effect on the rate of electron transfer to NiR, though some (involving Lys10, 38, 57 and 77) decreased the affinity between the two proteins as evidenced by an increase of the K_m. Similarly, site direct mutagenesis of NiR, where 10 negatively charged residues were independently replaced by alanine or serine, revealed the importance of several of these residues for pseudoazurin binding. The increased K_m value for both sets of charge mutants demonstrated the importance of the electrostatic interactions for complex formation.

The nature of the complex formation between three different nitrite reductases and five cupredoxins has been also analyzed (Murphy, 2002). Through electron donation experiments and surface charge analysis between nitrite reductases (green and blue) belonging to different organisms, and cupredoxins (azurins and pseudoazurin), it was demonstrated that azurins show a preference for blue nitrite reductases while pseudoazurins can give electrons to both green and blue nitrite reductases. It was suggested that the overall protein surface charge is an important factor in complex formation though a key role is played by the charge distribution and the surface compatibility around the docking sites.

The detailed role of the hydrophobic patch surrounding the exposed copper ligand in PAZ as well as the identity and the nature of the residues involved in the interaction remain unclear and are the object of study of the present work.

1.8   Nitrite reductase and azurin from *Neisseria gonorrhoeae*

1.8.1   Nitrite reductase

Nitrite reductase from the pathogen *N. gonorrhoeae* (AniA 36 kDa) is an outer membrane protein essential for cell growth under oxygen limiting conditions. The absence of oxygen and the presence of nitrite serve as environmental signals to induce the synthesis of AniA (Mellies, 1997). The AniA sequence shows a lipoprotein consensus sequence and shows moderate sequence similarity with other copper containing nitrite reductases (~30% identity). An additional 35 residues are present in the mature protein at the N- terminus, which serve as a linker between a membrane anchor (palmitoyl group) and the main catalytic part of the protein. Also 38 residues at the C-terminus have been proposed to assist the outer-membrane anchoring (Hoehn, 1992a; Hoehn, 1992b).

Also for AniA the type 1 and type 2 copper ligands as well as the active site residues Asp97 and His240, required for nitrite reducing activity in other nitrite reductases, are conserved (Boulanger, 2000; Kataoka, 2000).

The visible spectrum is characterized by absorbance maxima at 458 and 585 nm consistent with the blue colour of the protein. Though the sequence identity with green NiR from *Al. faecalis* S-6 is only 26%, their crystal structures are very similar. AniA is also trimeric and each monomer contains an N-terminal and a C-terminal domain folded into a Greek key β-sandwich. The type 1 copper atoms are buried within the N-terminal domain of each subunit 6 Å below the surface of the protein. The type 1 copper ligands are His94 $N^{\delta 1}$, His143 $N^{\delta 1}$, Cys135 S^{γ} and Met148 S^{δ}.

The type 2 copper is located at the bottom of 16 Å deep pocket formed by the N-terminal domain of one subunit and the C-terminal domain of another. The copper is coordinated through the $N^{\varepsilon 2}$ atoms of three histidine residues (His99, His134 and His289). A ligand water molecule completes the tetrahedral coordination of the type 2 copper site. The two copper sites are 12.5 Å apart and are connected through a defined pathway incorporating residues His134 type 2 ligand and Cys135 type 1 ligand. The structure of the active site is like in *Al. faecalis* NiR. In general, the most noticeable structural difference between the type 1 copper centres in green and blue nitrite reductases is the conformation of the side chain of the methionine copper ligand which has been suggested to be a factor determining the electronic structure of the copper site (Dodd, 1998; Inoue, 1998; Adman, 1995). The distance between the copper and the Met S^{δ} ligand is 2.6 ± 0.1 Å in AniA and identical in NiR. A difference between NiR and AniA regards the length of the loop located at the bottom of each subunit which is six residues shorter in *Al. faecalis* NiR compared with AniA. The extended loop might promote a more intimate interaction between AniA and the surface of the outer membrane (Boulanger, 2002). The second difference is found in a second, shorter loop called the "tower loop", which leads into a four-turn α-helix that extends towards the type 1 copper site. The deletion in this loop changes the surface profile of AniA near the type 1 copper site compared to *Al. faecalis* NiR, and this might affect the binding site for the electron donor protein.

The overall charge as well as the charge distribution is similar, with 40 negatively charged residues in both AniA and NiR and 30 and 27 positively charged residues, respectively. The theoretical pI is 5.33 and 5.56 for AniA and NiR, respectively.

1.8.2 Azurin

Azurin (Laz) has also been identified in *N. gonorrhoeae* as an outer membrane protein (Woods, 1989) and has been suggested to be the physiological electron donor to nitrite reductase (Boulanger, 2002). No crystal or solution structure is available, and thus *Ps. aeruginosa* azurin (Azu PDB entry:1E5Y (Nar, 1991)) which is the most closely related azurin on the basis of sequence similarity (57%, Figure 1.6) has been used to build a model for Laz (Figure 1.5b top panel) by homology modelling using the Swiss – Model server (Guex, 1997a).

The RMSD (root mean squared difference) value between the two azurins (Azu and LAZ) calculated on the backbone C carbon was 0.79 Å.

1.9   Pseudoazurin from *Al. faecalis* and azurin from *N. gonorrhoeae*: similarities and differences

The structure of PAZ and Laz are shown in Figure 1.5 a and b, respectively. The hydrophobic area around the copper centre is present in both PAZ and Laz but it is smaller in Laz. Moreover, Laz and PAZ show different electrostatic properties (Figure 1.5a and b, bottom panels).
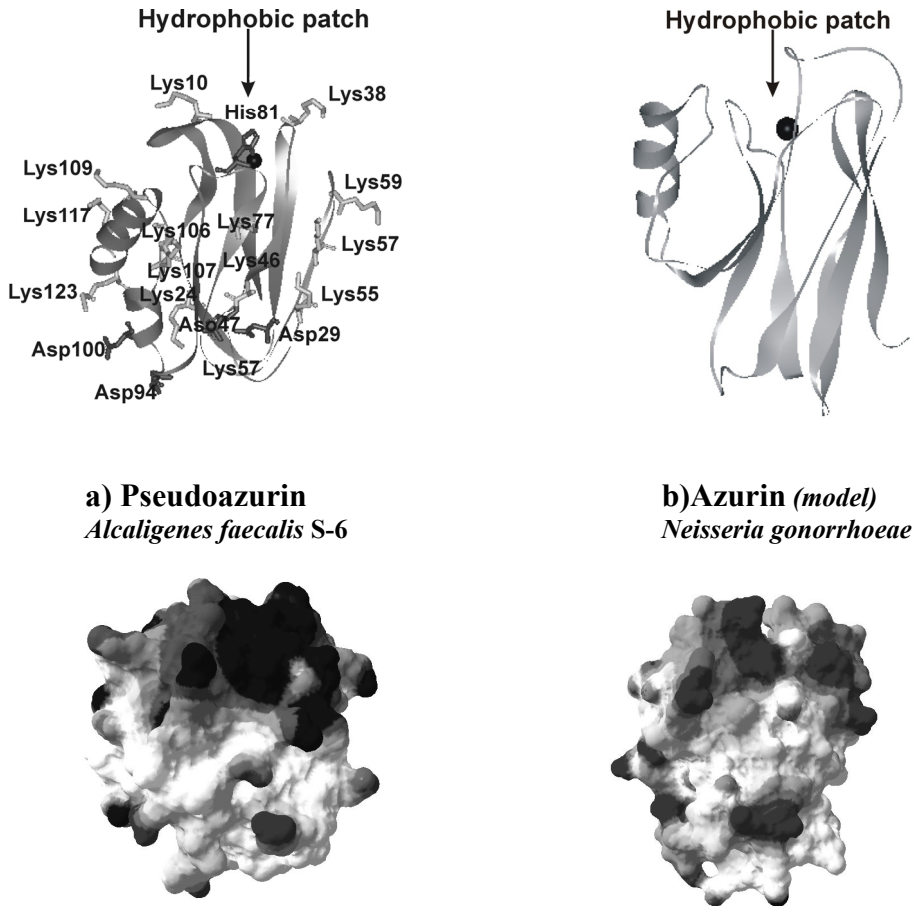

a) Pseudoazurin
Alcaligenes faecalis S-6

b)Azurin *(model)*
Neisseria gonorrhoeae

Figure 1.5: (Top panel) Ribbon structure of pseudoazurin (a) PDB entry: 8PAZ) with lysines and aspartate residues together with ligand His81 shown with sticks. Model ribbon diagram of Laz (b) obtained using homology modelling of Swiss – Model server (Schwede, 2003; Guex, 1997b; Peitsch, 1995) and using as model azurin from *Ps. aeruginosa* (PDB entry:1E5Y). Copper in both pictures a) and b), is indicated with a black sphere. The bottom panel shows the electrostatic potential surfaces of pseudoazurin (a) and azurin (b). The surfaces were created with Swiss-Pdb Viewer 3.7 with a colour range from blue for positive residues to red for negative ones. (For a color picture see Appendix).

```
Laz    1

       MKAYLALISA AVIGLAACSQ EPAAPAAEAT PAGEAPASEA PAAEAAPADA


Laz    51

        AEAPAA


               10         20         30         40         50         60
Laz    GNCAATVESNDNMQFNTKDIQVSKACKEFTITLKHTGTQPKASMGHNLVIAKAEDMDGVF
       ..:.. ...::.:::::. : :.:.::.::..:.: :. ::   :::: :.. : ::.::
Azu    AECSVDIQGNDQMQFNTNAITVDKSCKQFTVNLSHPGNLPKNVMGHNWVLSTAADMQGVV
               10         20         30         40         50         60


               70         80         90        100        110
Laz    KDGVGAA-DTDYVKPDDARVVAHTKLIGGGEESSLTLDPAKLADGD-YKFACTFPGHGAL
        ::.... : ::.:::::.::.:::::::.::..:.:.: .:: .:. : : :::::::.::
Azu    TDGMASGLDKDYLKPDDSRVIAHTKLIGSGEKDSVTFDVSKLKEGEQYMFFCTFPGHSAL
               70         80         90        100        110        120


       120
Laz    MNGKVTLV
       :.: .::
Azu    MKGTLTLK
```

Figure 1.6: Sequence alignment of Laz from *N. gonorrhoeae* and Azu from *Ps. Aeruginosa* has been performed using Align program available in GeneStream align Home Page at http://xylian.igh.cnrs.fr/bin/align-guess.cgi (Laz and Azu Swiss-Prot entry: P07211 and P00282, respectively). (**:**) indicates amino acid identity, (**.**) conservative replacement. The first 56 residues of the Laz sequence from *N. gonorrhoeae* represent the lipoyl attachment site and linker region.

PAZ (15 negatively charged residues and 12 positively ones) has a strong dipole, with a highly positive side around the metal centre due to a ring of lysines exposed on the surface and highly negative side on the opposite site of the protein. Laz (25 negatively charged residues and 14 positively charged ones) has a largely negative surface with some positively charged residues spread on the surface. It is remarkable that although green NiR from *Al. faecalis* and blue AniA from N. gonorrhoeae display similar overall charge distributions, the respective physiological partners, PAZ and Laz have such different charge distributions (Murphy, 2002).

1.10   Methods

The most important techniques for getting structural information about proteins or proteins complexes are X-ray diffraction (XRD) and NMR. XRD can provide high resolution structures. However, crystals are required which makes it less suitable for protein complexes, in particular those of a transient nature. NMR can be used to study the complexes in solution. Not only does it provide information about structural features of the complex, it can also be used to derive binding constants and dissociation rate constants, provided favourable condition are chosen. For the analysis of such data, it is important to consider the rates of binding and dissociation in relation to NMR parameters, such as relaxation times and chemical shifts. For this reason a brief overview of the effects of exchange in NMR spectra is provided below.

1.10.1   *NMR exchange and chemical shift perturbation mapping*

On an NMR experiment one is generally interested in measuring one or more different parameters such as chemical shift, J-coupling or relaxation, which may all be time dependent. If the molecule that is observed participates in a chemical or dynamic process (like protein-protein association) and if the variation in magnitude of the NMR parameter (expressed in frequency units) is similar to the characteristic frequency of the process, the NMR signal will be affected. The effect depends on the exchange rate (k) relative to the difference in the rates of the NMR parameter between the two states (ΔP). Three regimes are distinguished, slow ($k \ll \Delta P$), intermediate ($k \approx \Delta P$) and fast ($k \gg \Delta P$), see Table 1.3. For a molecule exchanging between state A and B, k_{exchange} is defined as:

$$A \xrightleftharpoons[k_B]{k_A} B \qquad\qquad k_{\text{exchange}} = k_{ex} = k_A + k_B$$

When, for example, one protein is titrated into a solution of a second protein (generally ^{15}N labelled), a nucleus of the latter protein may exchange between two different environments: that of the free state and that of the bound one. Each of these states will be characterized by different NMR parameters (e.g. chemical shift, scalar coupling or relaxation times).
According to the different regimes (fast, intermediate or slow) the ^{15}N-^{1}H HSQC spectra of the ^{15}N-labelled protein will change as described below.

Table 1.3: Definition of the type of exchange (slow, intermediate or fast) according to the NMR time scale of parameters such as chemical shift, scalar coupling and transverse relaxation.

NMR parameter (P)	Exchange rates *		
	slow	intermediate	fast
Chemical shift	$k_{ex} \ll \delta_a\text{-}\delta_b$	$k_{ex} \approx \delta_a\text{-}\delta_b$	$k_{ex} \gg \delta_a\text{-}\delta_b$
Scalar coupling	$k_{ex} \ll J_a\text{-}J_b$	$k_{ex} \approx J_a\text{-}J_b$	$k_{ex} \gg J_a\text{-}J_b$
Relaxation i = 1, 2	$k_{ex} \ll 1/T_{ia}\text{-}1/T_{ib}$	$k_{ex} \approx 1/T_{ia}\text{-}1/T_{ib}$	$k_{ex} \gg 1/T_{ia}\text{-}1/T_{ib}$

* k_{ex} in s[-1]; δ, J and T_i^{-1} in rad s[-1]

In the **fast exchange regime** for the chemical shifts a single averaged set of resonances will be observed. The chemical shifts for each resonance (δ_{obs}) will be a weighted average of the chemical shifts in the free (δ_a) and bound (δ_b) forms.

$$\delta_{obs} = p_a\delta_a + p_b\delta_b \qquad\qquad (\text{eq.1-1})$$

where p_a and p_b are the fractions of the free and bound protein, respectively.
Furthermore, due to the increased rotational correlation time of the complex compared to that of the free protein, *all* resonances exhibit a weighted average increase in the linewidth ($T_{2b}^{-1} > T_{2a}^{-1}$). The behaviour of a single resonance would look as in Figure 1.7a: by increasing the percentage of the ligand protein during a titration the signal of the observed residue will shift and broaden. If the ligand protein is very large, like in the case of NiR being titrated into ^{15}N-labelled PAZ, the line width increase can be so large that the signals already become undetectable when the observed protein is only bound for 10-20% of the time ($p_b = 0.1 - 0.2$). By fitting the chemical shift perturbation against the protein ratio, it is possible to extract the stoichiometry and the binding constant of the complex. By mapping the residues on the protein surface that are affected by the binding, it is possible to localize the binding area on the protein.
In the **slow exchange regime** ($k_{ex} \ll \Delta\delta$) it is possible to observe one set of resonances for the free protein and one for the bound one, provided that the size of the complex yields a line width small enough to allow observation of the signals. During the titration, the

intensities of the signals of the free protein will decrease due to the complex formation, while the intensities of those of the complex will increase. No effect of the binding will be observed on the linewidth of the signals of the free protein if also $k_{ex} << \Delta T_2^{-1}$. The behaviour of a single resonance would look as in Figure 1.7b: by increasing the percentage of ligand protein, the signal intensities of both free and bound ^{15}N-labelled protein change according to the fraction of bound protein. It should be noticed that in case of large complexes, the signal of the complex cannot be detected and consequently, a decrease of the intensity of the signal of the free protein will be the only sign that binding is occurring.
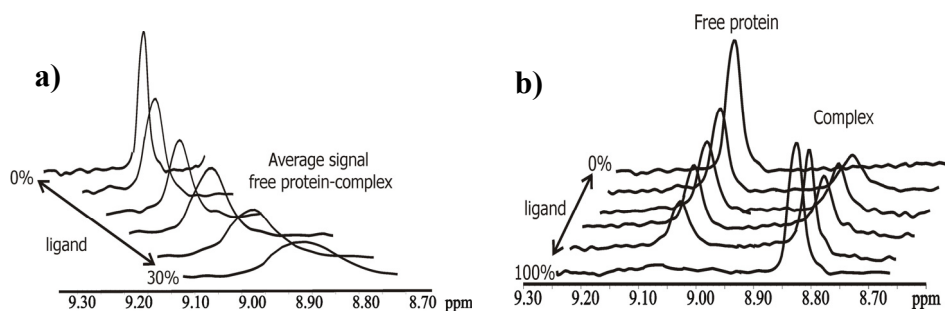

Figure 1.7: The behaviour of a single resonance during a titration with a binding partner. a) In fast exchange the position of the signal is shifting according to eq. 1-1. b) During slow exchange the signals of both the free protein (decreasing in intensity during the titration) and the bound protein (increasing in intensity during the titration) are present in the spectrum. The signals are drawn in perspective (no shift occurs).

1.11   Aim and scope of the thesis

Electron transfer complexes of metallo-proteins are fundamental in many natural processes. A protein-protein complex with a short metal-to-metal distance is required for rapid ET. However, the binding constant for complex formation is limited by the high dissociation rate constant, necessary for a high turnover rate. Thus, transient complexes of redox proteins represent a compromise between specificity and affinity. To understand the molecular details of transient complex formation, the nature of the interfaces needs to be characterised. The aim of the work described in the thesis, is to determine the characteristics of the complex between PAZ and NiR from *Al. faecalis* S-6. Various NMR techniques such as chemical shift perturbation analysis and cross saturation transfer have been used as tools for this investigation.

The first step of this work has been the complete assignment of PAZ which is presented in Chapter II.

In Chapter III binding studies of NiR and PAZ are described. Metal substituted forms of PAZ and NiR have been used to mimic the different oxidation states of the proteins. It is shown that binding properties are dependent on the redox state of PAZ. In the reduced form pseudoazurin exhibits a complex binding behaviour which has been modelled using a four state model.

In Chapter IV the influence of the pH on PAZ-NiR binding has been analyzed in order to explain the two different binding modes in the reduced state of PAZ. It is shown that pH modification affects the affinity between the two proteins.

In Chapter V cross saturation transfer is used as tool to determine the binding interface between PAZ and NiR, both in the reduced state. The procedure to efficiently express ^{2}H-^{15}N pseudoazurin required for this type of experiment is described.

The binding surface between pseudoazurin and NiR in the oxidized state has been determined via chemical shift perturbation mapping and this is described in Chapter VI.

Studies on the interactions on the recently described AniA and Laz from *N. gonorrhoeae* are reported in Chapter VII.

In Chapter VIII a general discussion and some concluding remarks are provided.

Chapter II

^{1}H, ^{13}C and ^{15}N resonance assignments of pseudoazurin from *Alcaligenes faecalis* S-6

Abstract

The complete assignments of the ^{1}H, ^{15}N and ^{13}C NMR spectra of Cu I pseudoazurin are presented, as well as the ^{1}H and ^{15}N assignments of the amide groups of the Zn II substituted form of pseudoazurin.

2.1 Introduction

Pseudoazurin (PAZ) is a copper-containing redox protein of 123 amino acids that can be isolated from denitrifying bacteria, like *Al. faecalis S-6* (Kakutani, 1981b). It functions as electron donor to a copper-containing nitrite reductase (NiR), which catalyses the reduction of nitrite to nitric oxide as part of the denitrification process. The proteins form a transient complex (Kukimoto, 1996; Kukimoto, 1995) to enable electron transfer from PAZ to NiR. The complex requires a high turnover to avoid that the electron transfer step, rather than the enzymatic conversion, becomes rate limiting. However, efficient electron transfer also requires the formation of a specific complex, with a short distance between the redox centres (Marcus, 1985). We aim to determine the dynamic and structural features of the complex of NiR and PAZ to understand how such proteins can associate and dissociate rapidly, yet with sufficient specificity to allow for electron transfer. NMR spectroscopy is the technique of choice to study the features of the complex under native conditions. A necessary step towards the determination of the complex interface is the assignment of the NMR spectra of ^{1}H, ^{15}N and ^{13}C of the free PAZ. Here such assignments are reported for the Cu I and Zn II substituted forms of PAZ.

2.2 Methods

The PAZ gene, coding for the mature protein, has been subcloned in pET-28a (+), creating a plasmid for expression in the cytoplasm of *E. coli*. The plasmid was kindly provided by Prof. M.E.P. Murphy and Dr. M. Boulanger (Univ. of Br. Columbia, Vancouver, Canada). The subcloning procedure introduced two additional residues at the N-terminus, a serine and an alanine. The protein was produced in *E. coli* strain HMS174, cultured on minimal medium containing $^{15}NH_4Cl$ (0.3 gr /L) and U-^{13}C- glucose (2 gr /L). Cultures were incubated at 37°C with shaking 250 rpm up to an OD_{600} of 0.7. Expression was induced with 0.5 mM IPTG, and 100 μM copper citrate was added simultaneously. Ten hours after induction, cultures were harvested by centrifugation. Cell pellets were resuspended in 20 mM phosphate buffer pH 7.0 containing 500 mM NaCl, 1 mM PMSF, DNase and 0.5 mM $CuCl_2$ and lysed using a French press cell (15.000 PSIG). After centrifugation for 15 min at 10.000 rpm the supernatant was dialysed against 20 mM phosphate buffer pH 7.0 and loaded onto a CM column equilibrated with the same buffer. PAZ eluted at circa 90 mM using a gradient of 0-250 mM NaCl. The fractions containing PAZ were concentrated using ultrafiltration methods (Amicon, YM3 membrane) and purified further on a Superdex 75 FPLC gel filtration column. The ratio between absorbances at 277 and 595 absorbance ratio of PAZ was 1.9 indicating a purity > 95% (Yamamoto, 1987), with a yield of 30 mg/L.

2.2.1 PAZ Zn II

To exchange copper for zinc in both ^{15}N-PAZ and ^{13}C-^{15}N PAZ, 0.5 ml of 200 mM KCN in 0.5 M of Tris-HCl pH 7.0 was added to 0.5 ml of PAZ Cu II (0.5 mM) in 0.1 M of Tris-HCl pH 7.0. As soon as the solution had lost the characteristic blue colour of PAZ Cu II, the

sample was loaded onto a G25 column equilibrated with 0.1 M of Tris-HCl pH 7.0 and 1 mM $ZnCl_2$. Fractions containing PAZ Zn II were detected by observing the absorbance at ~280 nm and washed with water and then the buffer was changed using ultrafiltration methods (Amicon, YM3 membrane) into 20 mM Na-phosphate pH 7.0. To remove possible traces of unfolded protein, the protein solution was purified over a CM column previously equilibrated with the same buffer. Using a gradient of 0-250 mM NaCl, PAZ eluted at circa 90 mM NaCl.

2.2.2   NMR sample

NMR samples contained 2-3 mM ^{15}N-PAZ Cu I or [15]N-^{13}C PAZ Cu I, 2 mM sodium ascorbate and either 10% or >99% D_2O in 20 mM potassium phosphate buffer pH 7.0.
Samples were placed in 5 mm Shigemi micro NMR tubes. All NMR spectra were acquired at 39ºC on a Bruker DMX 600 MHz NMR spectrometer. For PAZ Cu I assignment, backbone resonances were assigned using ^{15}N-HSQC, HNCA, HNCACB, HNCO and HNCACO spectra. Side-chain carbon and proton resonances were assigned using 2D ^{15}N-HSQC-TOCSY, 2D ^{15}N-HSQC-NOESY, ^{13}C-HSQC, H(CCO)NH, and HCCH-TOCSY spectra. Resonances of aromatic side-chains were assigned using ^{13}C-HSQC, HCCH-TOCSY and ^{13}C-HSQC-NOESY spectra optimised for detection of the aromatic region of ^{13}C spectrum.
The ^{15}N-^{1}H HSQC spectrum of ^{15}N PAZ Zn II was assigned on the basis of the corresponding spectrum of ^{15}N PAZ Cu I. The signals for which it was impossible to use such comparative method were assigned in the HNCACB spectrum obtained with a [15]N-^{13}C PAZ Zn (II) sample.
Spectra were processed with AZARA (http://www.bio.cam.ac.uk/azara/) and analysed with ANSIG for WINDOWS 1.0 (Helgstrand, 2000; Kraulis, 1989).

2.3   Results

Resonances for PAZ Cu I have been assigned for all the ^{1}H and ^{15}N amide, [13]C$^\alpha$ and CO nuclei in the backbone except for residues K46 and D47, which do not appear in the ^{1}H-^{15}N-HSQC spectrum, probably due to fast exchange with the solvent.
Resonances for all side chain have been assigned except for several nuclei in residues E13, I49, P80, M86, P108 and L115 and the Lys residues KI24, 38, 46, 57, 59, 77, 106, 107 and 109. In conclusion, the extent of PAZ assignment is: 98% of the amide resonances, 98% of C^α, 97% of H$^\alpha$, 96% of [13]CO, 94% of ^{1}H and ^{13}C side-chain resonances and 54% of aromatic ^{1}H and ^{13}C resonances.
Chemical shifts of all assigned nuclei have been deposited in the BioMagResBank (http://www.bmrb.wisc.edu) entry BMRB-6043.
The Chemical Shift Index (CSI) (Wishart, 1992) was used to derive secondary structure information from chemical shift data. The chemical shifts of HA, CA, CB and CO were compared to their random coil values and then assigned with a characteristic index for beta sheet, coil or helix. A secondary structure was calculated taking into account the presence

of more types of shift (HA, CA, CO, CB) for a single residue, in this case the program automatically calculates a consensus secondary structure (Figure 2.1a) using the Jafar program available on the web (http://www.sesame.wisc.edu/Jafar/jafar.html). The secondary structure derived from the chemical shift data matches the one observed in the crystal structure (PDB entry: 8PAZ) (Figure 2.1b) with the exception between residues 65-72 and 80-87 which are respectively β sheet and α helix according to the NMR while according to the X-ray there are no such secondary structure arrangements.

The assigned ^{1}H-^{15}N spectrum of PAZ Cu I and PAZ Zn II are shown in Figures 2.2 and 2.3 respectively. The assignments are listed in Tables 2.1 (PAZ Cu I) and 2.2 (PAZ Zn II).
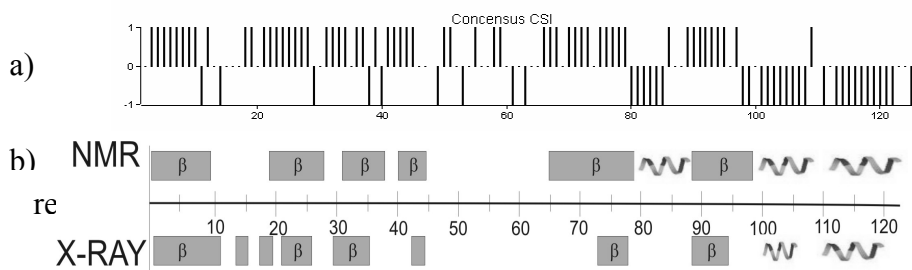

Figure 2.1: a) consensus CSI: each residue is assigned an index of 1 to indicate β sheet, 0 for coil, and -1 for α-helix; b) comparison between NMR and crystal structure (PDB entry: 8PAZ) secondary structure of PAZ; grey rectangles, β sheets; helix, α-helices.
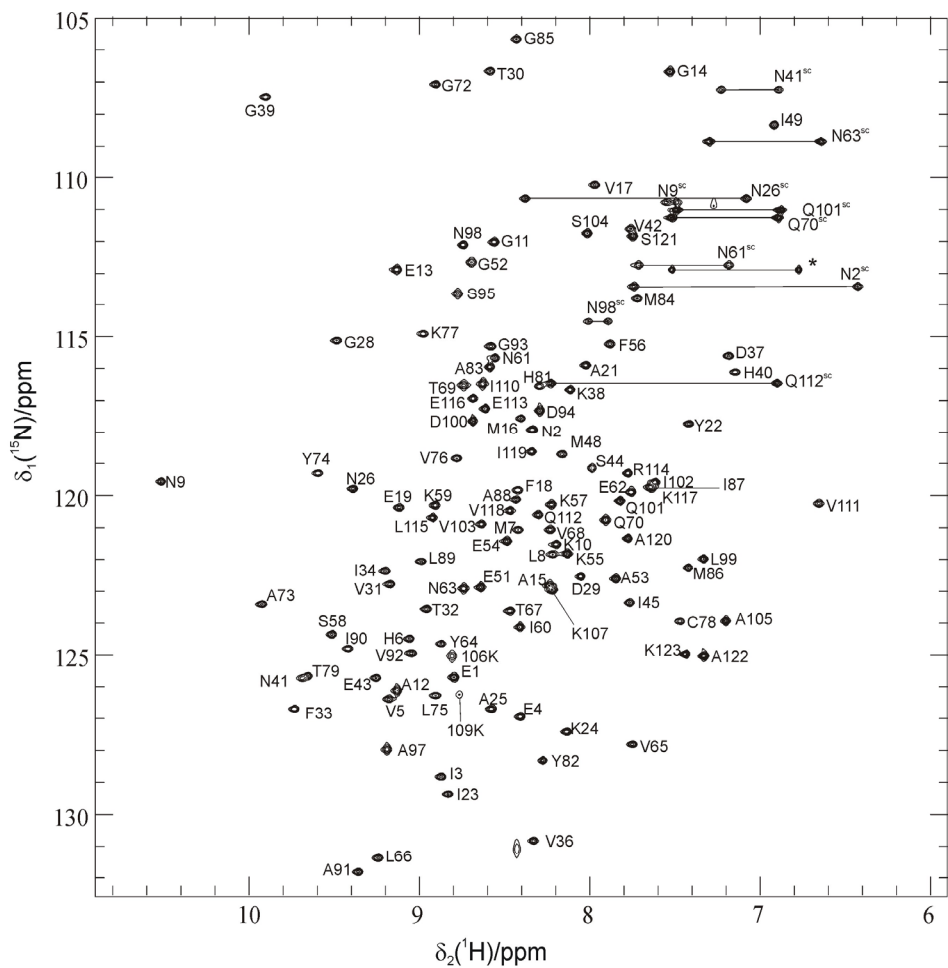
Figure 2.2. ^{1}H-^{15}N-HSQC spectrum of PAZ Cu I with assignments (20 mM potassium phosphate pH 7.0, 39ºC). Resonances of Asn and Gln side chains (sc) amides are connected by horizontal lines. The asterisk indicates the amide resonances of ^{15}N-acetamide, which was used as internal standard.
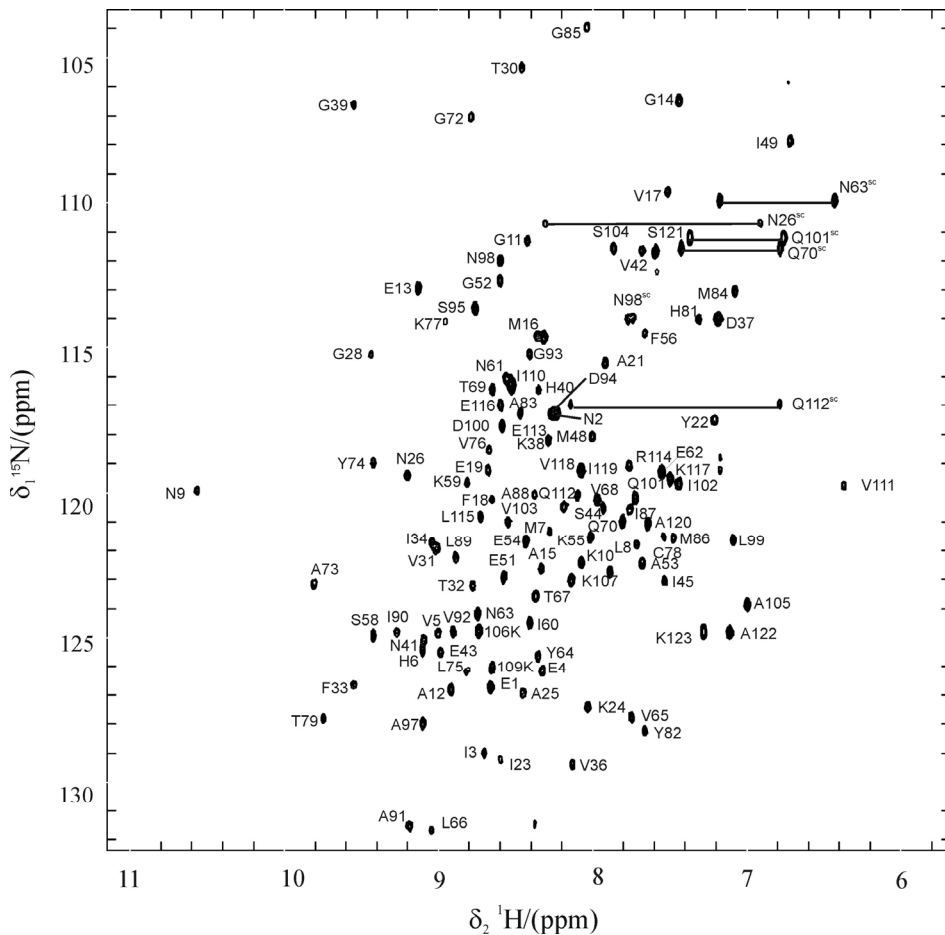
Figure 2.3. ^{1}H-^{15}N-HSQC spectrum of PAZ Zn II with assignments (20 mM potassium phosphate pH 6.5, 25ºC). Resonances of Asn and Gln side chains amides are connected by horizontal lines.

^{1}H and ^{13}C and ^{15}N resonances assignment of pseudoazurin from *Al.faecalis* S-6

Table 2.1: Assignment of PAZ Cu I at 39 °C, 20 mM sodium phosphate buffer pH 7 (n/a: not assigned)

Residue	^{15}N	^{1}H^{N}	C$^{\alpha}$	^{1}H$^{\alpha}$	C$^{\beta}$	^{1}H$^{\beta}$	CO	C$^{\gamma}$	^{1}H$^{\gamma}$	Others
-1 Ala	n/a	n/a	n/a	n/a	n/a	n/a	172.04			
0 Ser	111.3	7.66	n/a	4.41	63.82	3.84	172.40			
1 Glu	125.3	8.72	55.21	4.50	32.27	1.93	172.48	36.27	2.28; 2.22	
2 Asn	117.6	8.25	51.74	5.54	41.13	2.58 2.38	172.50			HD 7.66; 6.34, ND 113.03
3 Ile	128.4	8.79	61.04	4.12	40.40	1.60	173.33	28.69	1.38; 1.12	CG2 18.72; HG2 0.73, CD1 14.56, HD1 0.80
4 Glu	126.5	8.31	55.95	4.67	31.63	1.89; 1.71	172.81	37.42	2.18; 1.89	
5 Val	125.9	9.08	60.92	4.32	34.61	1.36	172.80	22.36	1.07	CG2 21.58, HG2 0.31
6 His	124.2	8.97	53.32	5.65	32.05	3.25; 2.93	172.42			HD2 6.79, CE1 135.40, HE1 8.31
7 Met	120.6	8.33	57.07	4.40	35.02	1.88; 1.32	173.87	33.82	2.04	
8 Leu	121.3	8.12	53.26	4.78	46.96	1.40		26.69	0.85	CD1 24.14, HD1 1.29, CD2 24.47, HD2 0.90
9 Asn	119.2	10.43	54.28	4.93	36.87	2.76	176.78			ND2 110.40, HD2 7.47; 7.41
10 Lys	121.1	8.11	56.19	4.73	34.77	1.77; 1.66	172.18	24.57	1.29; 1.05	CD 29.98, HD2 1.49, CE 42.10, HE2 2.89
11 Gly	111.6	8.47	44.14	4.48; 3.82			172.61			
12 Ala	125.7	9.05	55.51	4.06	18.52	1.47	178.74			
13 Glu	112.5	9.04	56.01	4.37	29.68	2.26; 1.78	174.22		2.33	
14 Gly	106.3	7.45	44.42	4.32;3.66			172.27			
15 Ala	122.4	8.15	51.27	4.83	20.53	1.38	176.51			
16 Met	117.2	8.32	56.31	4.06	27.21	2.54; 1.88	171.03	33.98	2.32	
17 Val	109.9	7.90	58.32	4.97	35.18	2.02	174.05	18.58	0.62	CG2 21.69, HG2 0.53
18 Phe	119.5	8.33	57.35	4.94	41.04	2.70	174.22			
19 Glu	120.1	9.05	53.16	4.78	34.32	2.03; 1.81	172.72	37.21	2.17	
20 Pro	-	-	63.76	4.84	n/a	2.54; 2.16	171.54	24.74	1.98; 1.77	CD 50.42, HD 3.56; 3.91
21 Ala	115.5	7.93	51.94	4.50	20.33	1.74	173.73			
22 Tyr	117.3	7.34	56.31	5.21	39.59	3.02; 2.74	172.85			CD 131.71, HD 6.91, CE 115.84, HE 6.60
23 Ile	129.0	8.76	60.64	3.95	40.46	1.56	171.19	28.95	1.07; 0.66	CG2 20.03, HG2 0.57, CD1 16.07, HD1 0.55

Table 2.1: Continued

Residue		^{15}N	^{1}H^N	C$^\alpha$	^{1}H$^\alpha$	C$^\beta$	^{1}H$^\beta$	CO	C$^\gamma$	^{1}H$^\gamma$	Others
24	Lys	127.0	8.05	55.16	4.86	33.15	1.82; 1.61	172.90	25.01	1.39	CE 42.47, HE 3.00
25	Ala	126.3	8.49	50.08	4.69	23.07	1.04	173.13			
26	Asn	119.4	9.32	50.84	5.12	39.54	2.54	170.69			ND 110.29, HD 8.30, 7.00
27	Pro	-	-	64.20	4.11	31.57	2.32; 2.05	175.85	26.48	1.98	CD 49.07, HD 3.40, 3.33
28	Gly	114.8	9.40	44.85	4.38; 3.40			172.70			
29	Asp	122.2	7.98	55.30	4.93	41.98	2.76; 2.69	172.99			
30	Thr	106.3	8.50	59.02	5.26	71.60	3.80	171.71	21.32	0.95	
31	Val	122.4	9.09	60.32	4.55	33.50	1.68	173.43	20.27	0.49	CG2 23.18, HG2 0.06
32	Thr	123.2	8.88	61.98	4.88	69.86	3.86	170.94	20.83	1.07	
33	Phe	126.3	9.64	57.32	4.95	40.16	3.18; 3.13	173.41			CD 131.04, HD 7.33
34	Ile	122.0	9.14	57.87	4.76	41.24	1.80	173.32	27.11	1.51; 1.00	CG2 16.36, HG2 0.75, CD 13.24, HD1 0.74
35	Pro	-	-	61.91	4.94	29.68	2.38; 2.05	173.05	27.24	2.04; 1.85	CD 51.13, HD 3.76
36	Val	114.1	8.25	65.79	3.64	32.26	1.92	175.53	20.71	0.84	CG2 22.46, HG2 0.74
37	Asp	115.2	7.12	52.71	5.06	44.05	2.84	173.12			
38	Lys	116.3	8.03	55.86	4.34	33.06	1.87; 1.71	176.24			
39	Gly	107.1	9.80	44.72	3.93; 3.33			170.67			
40	His	115.7	7.07	54.37	5.96	36.44	3.35; 2.53	173.10			ND2 106.87; HD 7.15; 6.81
41	Asn	124.9	9.47	52.15	4.82	40.71	2.87; 2.20	168.38			
42	Val	111.2	7.66	59.89	5.03	34.45	1.46	171.54			CG1 18.51; HG1 0.27; CG2 21.50; HG2 0.15
43	Glu	125.3	9.17	54.34	4.53	33.07	1.77; 1.59	173.35	35.42	2.31; 2.17	
44	Ser	118.7	7.91	57.81	3.80	63.40	3.61; 2.54	172.15			
45	Ile	123.0	7.68	62.17	3.81	38.14	1.55	175.00	29.12	1.46	CG2 17.72, HG2 0.94, CD 14.41, HD 0.74
46	Lys	n/a	n/a	n/a	n/a	n/a	n/a	n/a	n/a	n/a	n/a
47	Asp	n/a	n/a	56.79	4.47	39.51	3.08; 2.91	174.35			

^{1}H and ^{13}C and ^{15}N resonances assignment of pseudoazurin from *Al.faecalis* S-6

Table 2.1: Continued

Residue		^{15}N	^{1}H^N	C$^\alpha$	^{1}H$^\alpha$	C$^\beta$	^{1}H$^\beta$	CO	C$^\gamma$	^{1}H$^\gamma$	Others
48	Met	118.4	8.09	54.44	4.64	33.17	2.16; 1.94	171.12	33.94	2.50; 2.37	
49	Ile	107.9	6.83	58.21	4.85	38.81	1.66	174.60	18.71	0.99	CD 49.20, HD 2.60; 2.04
50	Pro	-	-	62.98	4.20	32.42	2.26; 1.45	175.78	29.19	1.30	
51	Glu	122.4	8.55	58.38	4.02	29.42	1.98; 1.94	172.69	36.28	2.27	
52	Gly	112.3	8.61	45.10	4.22; 3.67			174.71			
53	Ala	122.2	7.77	51.25	4.55	20.22	1.44	174.27			
54	Glu	120.9	8.39	55.77	4.41	31.44	2.15; 2.01	173.82	36.40	2.47; 2.43	CD 29.33, HD 1.62, CE 42.24, HE 2.96
55	Lys	121.4	8.05	56.11	4.17	32.83	1.70	171.98	24.35	1.40; 1.31	CD 132.23, HD 7.00
56	Phe	115.0	7.80	55.67	4.97	41.82	3.14; 3.02	172.63			
57	Lys	119.9	8.13	56.30	4.72	35.68	1.70; 1.69	173.03		1.05	HD 1.24
58	Ser	123.9	9.42	57.01	4.53	65.77	4.21; 2.95	175.82			
59	Lys	119.9	8.82	55.74	4.39	33.39	1.84; 1.68	174.92			
60	Ile	123.7	8.33	62.48	3.92	37.81	1.63	172.32	28.08	1.39; 0.99	CG2 16.14, HG2 0.77, CD 13.07, HD1 0.66
61	Asn	115.3	8.49	56.32	4.42	36.92	3.50; 3.11	171.36			ND 112.37, HD 7.63, 7.10
64	Tyr	124.3	8.78	58.57	4.78	43.06	2.93; 2.88	172.07			CD 130.74, HD1 6.94, CE 116.50, HE1 6.48
65	Val	127.4	7.66	61.52	4.44	32.47	1.70	173.83	20.72	0.83	CG2 20.71, HG2 0.60
66	Leu	111.0	9.16	53.00	4.28	45.54	1.97; 1.03	172.93	26.37	0.26	CD1 26.82, HD1 0.94; 0.26
67	Thr	123.2	8.38	62.42	4.59	68.66	3.88	174.05	20.72	0.93	
68	Val	120.7	8.15	59.71	4.32	32.40	1.74	172.47	19.20		
69	Thr	116.1	8.65	63.15	4.22	70.06	4.13	172.89	22.02	1.12	
70	Gln	120.4	7.82	52.99	4.79	28.78	2.06; 1.94	173.30	32.69	2.33	NE2 110.87, HE 7.44, 6.82
71	Pro	-	-	62.80	4.30	32.75	2.32; 2.04	173.33	27.62	2.15; 1.93	CD 51.40; HD 4.00, 3.76
72	Gly	106.7	8.82	43.87	4.60; 3.60			174.05			
73	Ala	123.0	9.84	49.92	5.78	21.08	1.15	172.32			
74	Tyr	118.9	9.51	55.79	5.23	40.43	3.34; 2.49	172.79			CD 131.17, HD 7.16, CE1 116.34, HE1 6.79
75	Leu	125.9	8.82	53.96	5.33	44.12	2.16; 1.13		27.97	1.68	CD1 25.60, HD1 1.06, CD2 26.40, HD2 0.92

Table 2.1: Continued

Residue		¹⁵N	¹Hᴺ	Cᵅ	¹Hᵅ	Cᵝ	¹Hᵝ	CO	Cᵞ	¹Hᵞ	Others
77	**Lys**	114.6	8.91	52.99	5.72	37.88	1.90; 1.54	172.16			
78	**Cys**	123.6	7.39	58.52	5.06;3.14	32.88	2.77	176.41			
79	**Thr**	125.3	9.58	64.83	4.32	70.48	3.73	174.14	22.58	1.20	
80	**Pro**	-	-	65.45	n/a	n/a	n/a	177.84			
81	**His**	116.1	8.23	56.88	5.15	32.63	3.87; 3.41	175.43			HD 6.99, HE 8.23
82	**Tyr**	128.0	8.20	60.86	4.40	39.07	3.71; 2.97	176.01			CD 131.51, HD 7.06, CE1 116.48, HE1 6.65
86	**Met**	121.9	7.34	58.79	3.98	31.40	2.41	171.42		2.41	
87	**Ile**	119.4	7.55	58.74	5.65	45.16	2.15	172.76	25.61	1.58; 1.29	CG2 21.67, HG2 1.23, CD1 15.22, HD1 0.87
88	**Ala**	119.8	8.36	51.00	4.77	21.22	0.69	172.00			
89	**Leu**	121.6	8.91	52.83	5.36	46.49	1.89; 1.08	172.52	27.72	1.41	CD1 24.23, HD1 0.83, CD2 26.15, HD2 0.76
90	**Ile**	124.4	9.34	59.46	4.79	39.25	1.74	173.01	27.33	1.57; 0.76	CG2 17.76, HG2 0.46, CD 14.55, HD 0.61
91	**Ala**	114.6	9.27	50.91	4.77	20.41	1.29	173.25			
92	**Val**	124.5	8.97	61.12	4.63	31.09	2.70	175.92	22.79	0.72	CG2 21.00, HG2 0.51
93	**Gly**	114.9	8.50	43.76	4.37;4.02			170.74			
94	**Asp**	116.9	8.20	54.94	4.55	42.22	2.66; 2.59	175.33			
95	**Ser**	113.3	8.69	56.77	4.25	63.01	3.74; 3.86				
96	**Pro**	-	-	62.99	4.44	31.93	2.56	178.12	27.97	2.09; 1.85	CD 49.75, HD 3.66
97	**Ala**	127.6	9.11	55.02	4.62	18.85	1.53	176.34			
98	**Asn**	111.7	8.66	52.98	5.00	36.81	3.16; 2.71	173.67			ND 114.15, HD 7.92, 7.81
99	**Leu**	121.6	7.25	58.80	3.84	42.36	1.96; 1.31	175.84	26.93	1.67	CD1 25.67, HD1 0.93, CD2 25.00, HD2 .88
100	**Asp**	117.2	8.59	57.77	4.27	39.94	2.62	177.26			
101	**Gln**	119.8	7.74	58.86	3.98	28.14	2.17	176.66	33.92	2.41	NE2 110.65, HE2 7.41, 6.80
102	**Ile**	119.2	7.53	64.81	3.77	38.30	2.05	177.21	29.16	1.80; 0.98	CG2 18.29, HG2 0.91, CD1 14.97, HD1 0.59
103	**Val**	120.5	8.55	67.94	3.36	31.68	2.16	175.82	23.69	0.99	CG2 21.99, HG2 0.88
104	**Ser**	111.3	7.92	60.02	4.25	64.00	3.92	173.09			
105	**Ala**	123.5	7.12	52.56	4.17	19.28	1.45	176.98			

^{1}H and ^{13}C and ^{15}N resonances assignment of pseudoazurin from *Al.faecalis* S-6

Table 2.1: Continued

Residue		^{15}N	^{1}H^N	C$^\alpha$	^{1}H$^\alpha$	C$^\beta$	^{1}H$^\beta$	CO	C$^\gamma$	^{1}H$^\gamma$	Others
106	Lys	124.7	8.72	58.17	4.21	31.95	1.79	174.26		1.48	
107	Lys	122.6	8.13	54.42	4.89	31.82	1.99; 1.66	170.69	21.05	1.50	CE 40.16, HE 2.78
108	Pro	-	-	n/a	n/a	n/a	n/a				
109	Lys	125.9	8.70	60.51	4.04	32.54	1.95; 1.84	176.66	24.73	1.52	CG2 17.89, HG2 0.74, CD1 13.77, HD1 0.92
110	Ile	116.1	8.55	63.54	4.07	37.89	1.74	175.58	29.74	1.54; 1.13	CG2 23.62, HG2 0.53
111	Val	119.9	6.58	66.25	3.43	31.50	2.09	174.94	21.86	1.01	
112	Gln	120.2	8.23	58.93	3.88	27.49	2.10	176.39	31.47	2.51	NE2 116.09, HE2 8.14, 6.82
113	Glu	116.9	8.52	59.56	4.03	29.74	2.13, 2.05	178.34	36.92	2.50; 2.24	
114	Arg	118.9	7.70	59.61	4.15	29.70	2.18; 1.92	176.83	28.06	2.03	CD 43.55, HD 3.63 3.32
115	Leu	120.3	8.85	57.92	3.95	42.00	2.17; 1.39	176.18	27.41	0.90	HD 1.57
116	Glu	116.6	8.60	60.16	3.85	29.25	2.12; 2.05	178.00	37.43	2.67; 2.20	
117	Lys	119.4	7.57	59.47	4.16	32.48	2.05	177.71	25.41	1.63; 1.53	CD 29.29, HD 1.75, CE 42.28, HE 3.02
118	Val	120.1	8.40	66.11	3.83	31.98	2.42	177.55	22.81	1.16	CG2 22.28, HG2 1.07
119	Ile	118.2	8.26	64.74	3.64	37.89	1.87	176.38	28.79	1.14	CG2 17.26, HG2 0.89, CD1 13.83, HD1 0.77
120	Ala	121.0	7.70	54.42	4.16	18.45	1.51	177.46			
121	Ser	111.4	7.67	59.29	4.40	63.93	3.99	172.18			
122	Ala	124.7	7.25	52.60	4.01	18.58	0.89	174.68			
123	Lys	124.6	7.36	57.73	4.11	33.87	1.83; 1.72	179.50	24.70	1.42	

Table 2.2: ^{1}H, ^{15}N assignment of PAZ Zn II from at 25°C, 20 mM sodium phosphate buffer pH 6.5

Residue		^{15}N	^{1}H^N	Residue		^{15}N	^{1}H^N
-1	Ala	n/a	n/a	51	Glu	122.93	8.579
0	Ser	110.72	8.313	52	Gly	112.71	8.602
1	Glu	126.75	8.667	53	Ala	122.47	7.678
2	Asn	117.31	8.273	54	Glu	121.69	8.437
3	Ile	129.03	8.709	55	Lys	121.56	8.016
4	Glu	126.17	8.336	56	Phe	114.62	7.664
5	Val	124.84	9.006	57	Lys	n/a	n/a
6	His	125.5	9.104	58	Ser	124.97	9.426
7	Met	121.37	8.285	59	Lys	119.67	8.819
8	Leu	121.81	7.714	60	Ile	124.5	8.414
9	Asn	119.95	10.568	61	Asn	116.08	8.575
10	Lys	122.44	8.083	62	Glu	119.29	7.556
11	Gly	111.3	8.425	63	Asn	124.17	8.752
12	Ala	126.83	8.923	64	Tyr	125.65	8.362
13	Glu	112.98	9.137	65	Val	127.79	7.753
14	Gly	106.52	7.441	66	Leu	131.69	9.049
15	Ala	122.64	8.341	67	Thr	123.59	8.375
16	Met	114.61	8.364	68	Val	120.26	7.974
17	Val	109.65	7.515	69	Thr	116.48	8.661
18	Phe	120.23	8.664	70	Gln	121.06	7.814
19	Glu	119.21	8.682	71	Pro	-	-
20	Pro	-	-	72	Gly	107.04	8.792
21	Ala	115.55	7.92	73	Ala	123.19	9.815
22	Tyr	117.55	7.219	74	Tyr	118.98	9.424
23	Ile	129.24	8.601	75	Leu	126.17	8.823
24	Lys	127.44	8.036	76	Val	118.6	8.676
25	Ala	126.97	8.46	77	Lys	114.14	8.965
26	Asn	119.39	9.207	78	Cys	121.54	7.545
27	Pro	-	-	79	Thr	127.79	9.75
28	Gly	115.25	9.45	80	Pro	-	-
29	Asp	122.79	7.893	81	His	114.06	7.316
30	Thr	105.35	8.46	82	Tyr	128.25	7.661
31	Val	121.99	9.019	83	Ala	116.42	8.525
32	Thr	123.23	8.78	84	Met	113.06	7.081
33	Phe	126.68	9.55	85	Gly	103.95	8.038
34	Ile	121.77	9.051	86	Met	121.58	7.476
35	Pro	-	-	87	Ile	120.6	7.761
36	Val	129.41	8.139	88	Ala	120.05	8.379
37	Asp	114.11	7.193	89	Leu	122.27	8.891

Table 2.2: Continued

Residue		^{15}N	^{1}H^{N}	Residue		^{15}N	^{1}H^{N}
38	Lys	118.22	8.292	90	Ile	124.84	9.279
39	Gly	106.6	9.554	91	Ala	131.54	9.193
40	His	116.5	8.36	92	Val	124.84	8.911
41	Asn	125.19	9.095	93	Gly	115.26	8.412
42	Val	111.65	7.681	94	Asp	117.29	8.239
43	Glu	125.53	8.986	95	Ser	113.67	8.769
44	Ser	120.56	7.934	96	Pro	-	-
45	Ile	123.1	7.534	97	Ala	128.04	9.107
46	Lys	n/a	n/a	98	Asn	112.04	8.605
47	Asp	n/a	n/a	99	Leu	121.67	7.09
48	Met	118.08	8.004	100	Asp	117.73	8.587
49	Ile	107.89	6.72	101	Gln	120.21	7.724
103	Val	121.02	8.554	114	Arg	119.1	7.772
104	Ser	111.58	7.87	115	Leu	120.82	8.729
105	Ala	123.9	6.994	116	Glu	116.99	8.602
106	Lys	124.78	8.747	117	Lys	119.53	7.501
107	Lys	123.04	8.141	118	Val	119.22	8.089
108	Pro	-	-	119	Ile	119.28	8.057
109	Lys	126.06	8.66	120	Ala	121.08	7.643
110	Ile	116.24	8.538	121	Ser	111.67	7.594
111	Val	119.75	6.375	122	Ala	124.85	7.113
112	Gln	120.47	8.189	123	Lys	124.8	7.286
113	Glu	117.26	8.47				

Chapter III

Redox state dependent binding between PAZ and NiR

Abstract

The redox state dependence of the binding between PAZ and NiR was studied by NMR spectroscopy. Reduced and oxidized PAZ interacts differently with NiR. Binding in the reduced state is characterized by the presence of two binding modes, a slow and a fast exchange mode with a K_d^{app} of $1x10^{-4}$ M. In the oxidized state of PAZ, binding occurs in a fast exchange mode with a K_d of $1x10^{-4}$ M as well. Metal substituted proteins have been used to clarify the redox state dependence of complex formation. It is concluded that the metal charge of NiR does not affect the mode of binding of its partner PAZ. A model is proposed to explain the characteristic behaviour of the complex in the reduced state.

3.1   Introduction

Electron transfer (ET) complexes are generally characterized by a high turnover rate, which is essential for their biological function. These complexes have a lifetime in the order of milliseconds and a dissociation constant (K_d) in the millimolar – micromolar range, hence the name 'transient complexes'.

Pseudoazurin (PAZ) and nitrite reductase (NiR) from *Alcaligenes faecalis* S-6 participate in the denitrification pathway reducing nitrate to nitric oxide (Kakutani, 1981b). PAZ (14 kDa) is a protein belonging to the group of blue copper proteins, characterized by a type 1 copper site (Messerschmidt, 2001). NiR is a trimeric enzyme (108 kDa) with each subunit containing two copper atoms: a type 1 copper site and a type 2 copper site (see Chapter I). During the denitrification process the type 1 copper site in PAZ acts as electron donor to the type 1 copper site on NiR. The electron is successively transferred to the catalytic site, the type 2 copper, in which nitrite reduction takes place (Suzuki, 2000; Suzuki, 1999; Suzuki, 1994).

In this chapter we analyze the oxidation state dependence of complex formation between PAZ and NiR. NMR titration experiments were performed with PAZ and NiR both in the reduced and oxidized states. To avoid paramagnetic effects of the Cu II state, as well as ET during the experiments, Zn II and Co II have been used as Cu II substitutes in PAZ and NiR, respectively. Structures of various metal substituted cupredoxins have been determined and it has been shown that there is very little change at the active site as a consequence of the metal replacement (Bonander, 2004; Moratal, 1995; Tsai, 1995; Blackwell, 1994; Nar, 1992; Church, 1986). Furthermore, it has been demonstrated that Zn-PAZ is structurally identical (RMSD of backbone atoms <0.3 Å) to Cu-PAZ (Prudêncio, 2004). NiR from which the Cu in the type 2 site had been removed (NiR Cu-T2D) has also been used to perform experiments described in this chapter to maintain the Cu in the type 1 site in the reduced state. Removal of the type 2 copper prevents rapid oxidation by trace amounts of dioxygen.

3.2   Materials and Methods

3.2.1   *Proteins preparation*

PAZ expression and purification
^{15}N labelled PAZ was prepared as described in Chapter II.

Unlabelled PAZ was expressed in *E. coli* strain BL21 (DE3) transformed with the plasmid pET-28a (+)-PAZwt. A 10 ml 2xYT/Kanamicyn (100 mg/L) preculture grown at 30°C at 250 rpm for 6 h was used to inoculate 1 L of 2xYT. Cultures were grown under the same conditions to $OD_{600} = 1.0$ and then induced by addition of 0.5 mM IPTG. At this point the temperature was reduced to 25°C and after 10 h cultures were harvested by centrifugation. The purification procedure was similar to that of ^{15}N labelled PAZ. The 277/595 absorbance ratio of PAZ was 1.9 indicating a purity > 95%. The yield amounted to ~ 1g/L of culture.

NiR expression and purification

The gene coding for *Al. faecalis* NiR has been subcloned previously in pET-28a creating a plasmid for cytoplasmic expression of the mature protein in *E. coli*. The vector, kindly provided by Dr. M.J. Boulanger and Prof. M.E.P. Murphy, contains a kanamycin resistance gene and allows for expression of recombinant genes under the control of the T7 promoter. The construct codes for a C-terminal His-tag, introduced to facilitate purification. For the protein interaction studies, this His-tag was considered as a possible source of interference. Therefore, the His-tag was removed by introducing a stop codon before the His-tag sequence by a three step PCR mutagenesis protocol, yielding pET28a(+)-NiRwt.

NiR Cu-Cu was produced in *E. coli* strain BL21 (DE3) transformed with the plasmid pET28a(+)-NiRwt. A 10 ml 2xYT/kanamicyn (100 mg/L) preculture grown at 30°C at 250 rpm for 6 h was used to inoculate 1 L of 2xYT/Kanamicyn (100 mg/L). Cultures were grown under the same conditions to an OD_{600} = 1.0 and then expression was induced by addition of 0.5 mM IPTG. At this point the temperature was lowered to 25°C and after 10 h cultures were harvested by centrifugation. Cell pellets were resuspended in 20 mM phosphate buffer pH 7.0 containing 500 mM NaCl, 1 mM phenyl-methyl-sulphonyl-fluoride (PMSF), DNase, 0.5 mM $CuCl_2$ and lysed using a French press cell (15.000 PSIG). After centrifugation for 15 min at 10.000 rpm the supernatant was dialysed against 20 mM phosphate buffer pH 7.0 and loaded onto a DEAE column pre-equilibrated with the same buffer. Under a gradient of 0 - 250 mM NaCl, NiR eluted at circa 140 mM. Fractions containing NiR were concentrated and purified further on a Superdex 75 FPLC gel filtration column. The 280/468 absorbance ratio of NiR was 16 and the yield was 150 mg/L of culture.

3.2.2 *Depletion of the Type 2 copper*

NiR Cu-T2D was obtained following the published procedure (Suzuki, 1997). Briefly, nitrogen gas (99.99%) was bubbled into a flask containing 300 ml of 0.1M Tris–HCl buffer pH 7 with a dialysis bag of NiR (3 ml) for 1 h at 4 ºC and then potassium hexacyanoferrate (II) (0.6 g) was added to the buffer solution. After the bubbling of nitrogen gas had continued for 0.5 h, EDTA (0.5 g) and dimethylglyoxime (0.12 g) were added to the solution and the flask was quickly sealed. The enzyme solution was dialyzed at 4 ºC under anaerobic conditions. After 5 days the enzyme solution was anaerobically washed overnight by dialysis against 0.1 M Tris-HCl buffer and then the dialysis was carried out in air for three times. Copper depletion was checked by EPR.

EPR spectroscopy was performed on a frozen solution using a 9 GHz ELEXSYS E680 spectrometer (Bruker, Rheinstetten, Germany). The spectra were acquired at a temperature of 40 K. The amplitude and the frequency of the modulation were respectively 0.5 mT and 100 KHz. The spectra were recorded using a power of 0.6 mW and the total measurement time was 21 min per spectrum. Thirty transients were accumulated per spectrum.

In Figure 3.1 the EPR spectrum of type 2 Cu depleted NiR (a) and of NiR with both type1 and type 2 copper sites (b) are reported, confirming type 2 copper depletion in the former.

Type 2 Cu

Type 1 Cu

a)

b)

Magnetic field (T)
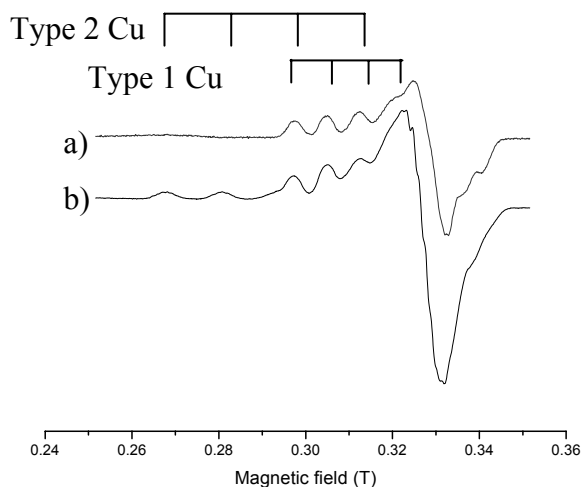
Figure 3.1: EPR spectra of NiR Cu-T2D (a) and NiR Cu II–Cu II (b).The hyperfine signals corresponding to the type 1 and the type 2 Cu centres are identified by stick diagrams. The *g* values for the type 1 centre are g_{xx} =2.025, g_{yy} =2.055 and g_{zz} = 2.195 (A_{zz} = 7.5 mT). The type 2 centre has *g* values of g_{xx} =2.076, g_{yy} =2.076 and g_{zz} = 2.358 (A_{zz} = 13 mT) (*g* and *A* values were kindly provided by M. Fittipaldi).

3.2.3 *Metal substitution*

PAZ Zn II
PAZ Zn II was prepared as described, (see Chapter II).

NiR Co II-Co II
Substitution of copper by cobalt for both the type 1 and the type 2 site in NiR was achieved following the published procedure (Suzuki, 1998). Apo-NiR was prepared by dialyzing the native enzyme against 0.1 M Tris-HCl buffer (pH 8.0) containing 10mM KCN at 4 ºC. The dialysis was carried out for 4 days, during which time the KCN buffer solution was renewed twice. The protein was then dialyzed 3 times against 0.1 M Tris-HCl buffer (pH 8.0) to remove excess of KCN and copper. Apo-NiR was incubated with $CoCl_2 \cdot 6H_2O$ in a ratio 1:1 under anaerobic conditions in 0.1 M Tris-HCl buffer (pH 8.0) for 4 days and successively dialysed against the same buffer 3 times to remove the excess of cobalt. Cobalt insertion was checked optically and by 1D-NMR.

3.2.4 *NMR samples*

NMR samples for direct titration (NiR titrated into PAZ) were prepared with 0.2 mM of ^{15}N-PAZ in 20 mM phosphate buffer pH 6.5. NiR 1.3 mM (trimer concentration) was prepared in the same buffer. For the inverse titration (PAZ titrated into NiR) NMR samples

were prepared with 0.4 mM (subunit concentration) of NiR Cu I-Cu I in 20 mM phosphate buffer pH 6.5 and ^{15}N-PAZ Cu I 3.9 mM was prepared in the same buffer. Protein concentrations were determined optically following the characteristic absorbance peaks: at 593 nm for PAZ Cu II ($\varepsilon = 2.9$ mM^{-1} cm^{-1}) (Kakutani, 1981b), at 277 nm for PAZ Zn II ($\varepsilon = 5.7$ mM^{-1} cm^{-1}) assuming that at that wavelength PAZ Cu II and PAZ Zn II have the same extinction coefficient. For NiR Cu II-Cu II the concentration was determined optically by measuring the absorbance at 589 nm ($\varepsilon = 2.9$ mM^{-1} cm^{-1} per subunit) (Kakutani, 1981c) and at 280 nm for NiR Co II-Co II ($\varepsilon = 44.5$ mM^{-1} cm^{-1} per subunit), assuming that at that wavelength NiR Cu II-Cu II and NiR Co II-Co II have the same extinction coefficient.

NMR samples in the reduced form contained 1.0 mM sodium ascorbate at pH 6.5 and were prepared in an anaerobic vial. All NMR samples contained 6-10% of D$_2$O for lock and the solutions were degassed by blowing argon over the surface.

For each titration, samples of PAZ and NiR were set at the same pH and the pH was checked again at the end of the titration.

3.2.5 NMR titration experiments

Two different NMR experiments were performed: "direct" titration and "inverse" titration. In the direct titration a sample containing ^{15}N-PAZ is titrated with microliter aliquots of unlabelled NiR. In the inverse titration a sample containing unlabelled NiR is titrated with microliter aliquots of ^{15}N-PAZ. The latter experiment allows the observation of ^{15}N-PAZ signals in a range of protein ratios, enabling the determination of binding constants. Both experiments were performed by recording [^{15}N-^{1}H] HSQC spectra after each addition and analysing the changes in intensity, line width and chemical shift of ^{15}N-PAZ resonances. For each titration experiment a reference spectrum of the free protein (^{15}N-PAZ Cu I or ^{15}N-PAZ Zn II) was recorded.

All NMR experiments were performed at 14.1 T on a Bruker DMX600 spectrometer operating at 293 K and equipped with TXI-Z-GRAD (^{1}H, ^{13}C and ^{15}N) probe. All spectra were processed in AZARA (available from http://www.bio.cam.ac.uk/azara/) and analyzed with the assignment programme ANSIG (Helgstrand, 2000; Kraulis, 1989).

3.2.6 Assignment of PAZ Cu I and PAZ Zn II

Assignments of the ^{15}N-PAZ Cu I and ^{15}N-PAZ Zn II HSQC spectra have been reported in Chapter II.

3.2.7 Binding Curves

Binding curves were obtained by plotting the signal intensities against the molar ratio of PAZ / NiR. Data were fitted to a one-site binding model using Origin version 6.0 (Microcal.). The equation used for the non-linear fitting was:

$$I = aP_f + b \qquad\qquad\qquad\qquad \text{(eq.3-1)}$$

where I is the intensity of free PAZ signal, a (in units of M^{-1}) representing the intensity coefficient of the observed nucleus, b a dimensionless correction term for baseline artefacts and P_f is the free PAZ concentration, with

$$P_f = (P_0^i - x_i)$$ (eq.3-2)

where P_0^i, the total PAZ concentration at titration step i, is related to the concentration of the stock solution of PAZ (P_0), the initial concentration of NiR (N_0) and the molar ratio R_i of the total PAZ and NiR (N_0^i) concentrations at step i ($R_i = P_0^i/N_0^i$):

$$P_0^i = \frac{R_i N_0 P_0}{N_0 R_i + P_0}$$ (eq.3-3)

Similarly, N_0^i is given by:

$$N_0^i = \frac{N_0 P_0}{N_0 R_i + P_0}$$ (eq.3-4)

In eq.3-2 x_i is the concentration of the complex between pseudoazurin and NiR which can be obtained by:

$$\frac{1}{K_d^{app}} = \frac{x_i}{(P_0^i - x_i)(N_0^i - x_i)}$$ (eq.3-5)

Substitution yields:

$$I = \frac{1}{2} a \left(\frac{N_0 P_0}{N_0 R_i + P_0}(R_i - 1) - K_d^{app} + \sqrt{\left(\frac{N_0 P_0}{N_0 R_i + P_0}(R_i + 1) + K_d^{app} \right)^2 - 4\frac{P_0 R_i N_0^2}{(N_0 R_i + P_0)^2}} \right) + b$$

(eq.3-6)

The experimental data were fitted with eq.3-6, using I and R_i as dependent and independent variables, respectively and a, b and K_d^{app} as fitted parameters.

3.2.8   Isothermal Titration Calorimetry

All calorimetric experiments were performed with an OMEGA titration calorimeter (Microcal.). The experiments were performed at 25ºC and with both PAZ and NiR in the oxidized state (PAZ Cu II and NiR Cu II-Cu II). 3.2 mM PAZ Cu II and 0.51 mM NiR Cu

II-Cu II (subunit concentration) were dialysed against 20 mM potassium phosphate buffer at pH 6.5 over-night to minimize artefacts due to minor differences in buffer composition. All solutions were thoroughly degassed by stirring under vacuum before use. The reaction cell contained 0.17 mM NiR Cu II–Cu II. The injection syringe was filled with 3.2 mM PAZ Cu II and was rotate at 300 rpm during equilibration and experiment. Injections were started after equilibration to baseline stability. The experiment consisted of 17 injections of 15 µl volumes and the time between injections was 460 s. The titration data were corrected for the small heat changes observed in control experiments of buffer into buffer and PAZ into buffer under the same experimental conditions.

The data analysis software provided with the calorimeter was used for analysis. Baseline and integration of the peaks was executed manually. The fitting procedure was performed using Origin Microcal. with a user-defined equation for a one-binding-site model.

3.3   Results

3.3.1   The complex of reduced ^{15}N- PAZ Cu I and NiR

For the complex in the reduced form, two types of experiments were performed: direct and inverse titrations. The direct titration was performed by recording [^{15}N, ^{1}H] HSQC spectra of ^{15}N-PAZ Cu I after addition of microliter aliquots of NiR Cu I-T2D. Changes in signal intensities, line width and chemical shifts were followed in order to determine the binding characteristics between PAZ Cu I and NiR Cu I-T2D. Upon addition of NiR Cu I-T2D up to 0.9 mol. eq. of subunit, the intensities of ^{15}N-PAZ Cu I resonances decreased (Figure 3.2) and exhibited a small increase in line width in the proton dimension (~5 Hz). This behaviour suggests that binding occurs with modest affinity and that binding and dissociation are slow on the NMR time scale (see Chapter I). On the other hand, small chemical shift perturbations were observed (Figure 3.3), suggesting a fast exchange regime for binding. In several experiments similar shifts were observed and these could be shown not to be caused by pH effects or temperature changes. Furthermore, they all map in an area around the proposed electron transfer port, His81 (see Chapter VI).

For a further confirmation of these observations, an inverse titration was performed: NiR Cu I-T2D 0.4 mM (subunit concentration) was titrated with ^{15}N-PAZ Cu I. Resonances of many PAZ residues became observable at 0.4 mol.eq. of ^{15}N-PAZ Cu I, corresponding to a concentration of 0.16 mM PAZ. Free PAZ is readily observable at a concentration of 0.1 mM under the same conditions. Thus, PAZ binds to NiR, but with modest affinity. In the case of tight binding, free PAZ would only be observable at molar ratios >1.

The curves of signal intensity versus molar ratio of PAZ/NiR have been plotted for several residues and are shown in Figure 3.4. The deviation from the line predicted for the absence of binding (dotted line) represents intensity loss due to binding to NiR. Global fitting to equation eq.3-6 yields a K_d^{app} of $1.0 \pm 0.1 \times 10^{-4}$ M (see Table 3.1).

In the inverse titration the increase in line width between the signals at a PAZ/NiR ratio of 0.4 and 1.75 is ~ 5 Hz, like in the direct titration, but when the same signal is compared

with the signal of the free form of PAZ the increase is more significant, ~ 20 Hz (Figure 3.5).

Moreover, the peaks that were shifting during direct titration showed the same chemical shift perturbations also in the inverse titration. The largest shift was observed in the ^{1}H dimension for Lys109 (0.25 ppm) and in the ^{15}N dimension for Met84 (0.8 ppm).

Thr 32 (^{15}N-PAZ Cu I)
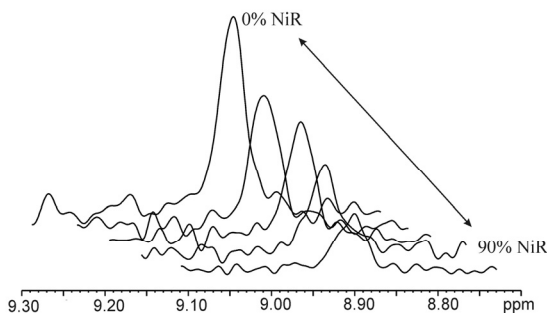
Figure 3.2: Cross-section along the F2 dimension through the ^{1}H^N resonance of Thr 32 (PAZ Cu I). The figure shows the decrease in the intensity on PAZ Cu I amide signal upon addition of NiR Cu I-T2D during direct titration. The signal becomes very weak when 0.9 mol.eq. of NiR Cu I-T2D (subunit equivalent) is added to the sample. Spectra are indicated in perspective for clarity.
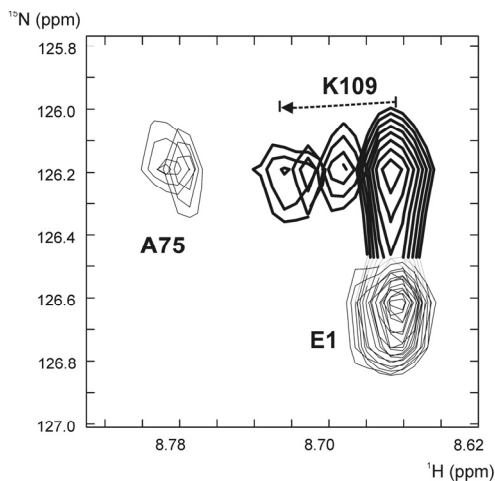
Figure 3.3: Overlay of a part of the [^{15}N-^{1}H] HSQC spectra of ^{15}N-PAZ Cu I in the free form and in the complex with NiR Cu I-T2D. The cross peak of residue K109 (dark line) shifts upon direct titration with NiR Cu I-T2D from right to left, as indicated by the arrow (0%, 20%, 40% and 60%). Residues E1 and A75 do not shift during the titration.

50
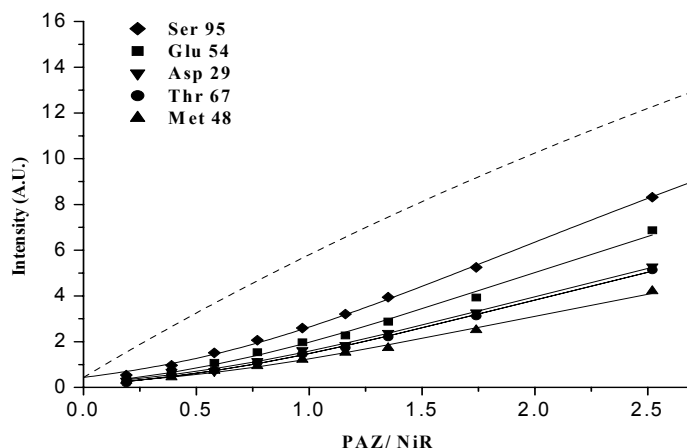
Figure 3.4: Binding curves for the interaction of ^{15}N-PAZ Cu I with NiR Cu I-T2D. The intensity of several PAZ amide resonances (arbitrary units, A.U.), measured during indirect titration, are plotted against the PAZ/NiR (subunit) ratio. Solid lines represent global fits to a model describing one PAZ binding site per NiR Cu I-T2D subunit (eq.3-6), yielding a K_d^{app} of $1.0 \pm 0.1 \times 10^{-4}$ M. The dashed line represents a simulation of the intensity for S95 in the absence of binding.

Table 3.1: Value of *a* (intensity coefficient in M^{-1}) and *b* (dimensionless correction term for the baseline artefact) resulting from the fitting with eq.3-6 of the intensities of the residues Glu54, Tyr67, Met48, Asp29 and Ser95, with K_d^{app} as shared parameter fitted to be $1.0 \pm 0.1 \times 10^{-4}$M.

Residue	a (10^3 M^{-1})	b
Ser 95	14.8 ± 0.2	0.44 ± 0.07
Glu 54	12.2 ± 0.2	0.15 ± 0.06
Asp 29	9.5 ± 0.2	0.17 ± 0.06
Tyr 67	9.3 ± 0.2	0.09 ± 0.06
Met 48	7.4 ± 0.2	0.15 ± 0.06

Ser 95 (^{15}N-PAZ)

8.70   8.60   8.50   8.40   8.30 ppm
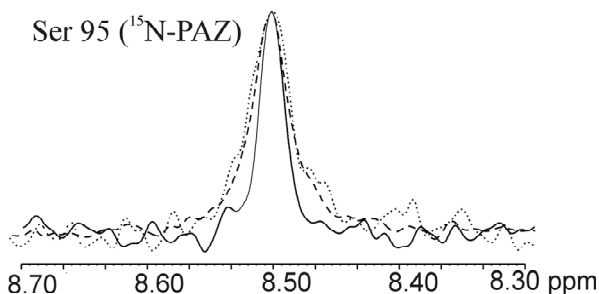
Figure 3.5: Cross-section through the $^1H^N$ resonance of Ser95 of ^{15}N-PAZ Cu I, in the absence of NiR (solid line, 22 Hz), and at PAZ/NiR ratios of 0.4 (dashed line, 37 Hz) and 1.75 (dotted line, 41Hz).

The direct titration was repeated with NiR Cu I-Cu I (under rigorously anaerobic conditions) and the spectra showed the same behaviour as with NiR Cu I-T2D indicating that the depletion of Cu in the type 2 site does not affect the binding between the two proteins. It can be concluded that reduced PAZ in the complex with reduced NiR experiences two binding modes: a slow exchange mode characterized by intensity loss without large line broadening and a fast exchange mode characterized by chemical shift perturbations. The fact that the shifts are small and accompanied by a limited increase in line width suggests that the dissociation constant of this process is much larger than the protein concentration used in the NMR experiment ($K_d > 1$ mM). The presence of only one mode can not explain the complexity of the phenomena observed. A slow exchange mode can not explain the presence of the chemical shift perturbations. On the other hand, a fast exchange mode with a $K_d > 1$ mM can not explain the combination of weak signals (significant binding) and only limited line width increase. The fact that the chemical shift perturbations (Figure 3.3) are confined to a specific region on ^{15}N-PAZ Cu I surface which is known to be involved in the binding interface with NiR Cu I-T2D (see Chapter IV), also suggests that these perturbations represent the binding process.

To establish the effect of the NiR metal charge state on the binding, a direct titration of ^{15}N-PAZ Cu I into a solution of NiR with its coppers replaced by Co II (mimicking NiR Cu II-Cu II) was performed. The effect of the complex formation on the [^{15}N-^{1}H] HSQC spectrum of ^{15}N-PAZ Cu I upon addition of NiR Co II- Co II was the same as described for the complex between ^{15}N-PAZ Cu I and NiR Cu I-T2D, where the presence of two simultaneous exchange regimes was suggested by the decrease of PAZ intensity signals, small line broadening and small chemical shift perturbations.

3.3.2   *The complex in the oxidized form: ^{15}N-PAZ Cu II / Zn II and NiR*

^{15}N-PAZ Cu II (0.2 mM) was titrated with NiR Cu II-Cu II and NiR Cu II-T2D (3.8 mM stock solutions). Although the presence of the paramagnetic Cu II in ^{15}N-PAZ precludes the observation of resonances from residues close to the metal site of ^{15}N-PAZ, it is possible to identify changes in the spectral features: increases of ~ 20 Hz in the line width in the proton dimension of the amide signals of ^{15}N-PAZ Cu II were observed upon interaction with 0.15 mol.eq. of NiR Cu-Cu subunits. Upon addition of 0.2 mol.eq. of NiR Cu–Cu subunits to

^{15}N-PAZ Cu II, resonances were no longer detectable due to line broadening. The same was observed in a titration of ^{15}N-PAZ Cu II with cobalt substituted NiR (NiR Co II-Co II). When the copper atom of ^{15}N-PAZ was replaced by Zn II to create a redox inactive and diamagnetic protein with the same charge as the copper in the oxidized form, the behaviour of the residues around the metal centre could be followed. ^{15}N-PAZ Zn II was titrated with NiR Cu-Cu and NiR Cu-T2D in either the reduced or oxidized state. Increases of ~ 20 Hz in the line width at half height in the proton dimension on the amide signals of ^{15}N-PAZ Zn II were observed upon interaction with 0.2 mol. eq. of NiR Cu-T2D subunits (Figure 3.6). At a ratio NiR Cu-T2D / ^{15}N-PAZ Zn II of 0.2, ^{15}N-PAZ Zn II residues resonances were not longer detectable due to line broadening (Figure 3.7), both with reduced and oxidized NiR Cu-T2D.

During direct titration of ^{15}N-PAZ Zn II with NiR Cu-Cu and NiR Cu-T2D, a number of peaks showed chemical shift perturbations (Figure 3.8). At 0.15 mol.eq. of reduced NiR the largest shift was observed in the ^{1}H dimension for Lys109 (0.17 ppm) and in the ^{15}N dimension for Met84 (0.43 ppm), similar to the titration with PAZ Cu I at high NiR/PAZ ratios. Both line width increase and chemical shift perturbations are characteristics of a fast exchange regime on the NMR time scale ($k_{off} > 300$ s^{-1}).
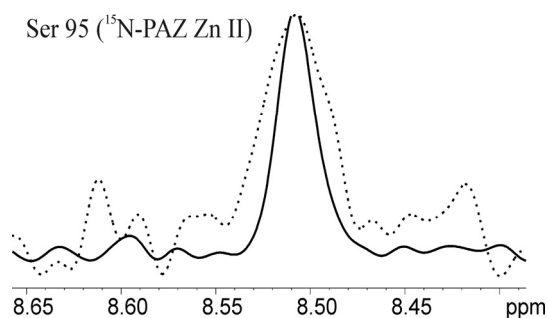
Ser 95 (^{15}N-PAZ Zn II)

Figure 3.6: Cross-section through the ^{1}H^{N} resonance of Ser95 of ^{15}N-PAZ Zn II. The solid line represents the signal of the free protein. The signal with the dotted line was taken when the ratio NiR Cu I-T2D / PAZ Zn II is 0.15. The line width at half-height is 22 Hz and 41 Hz, respectively.

Asn 26 (^{15}N-PAZ)   0% NiR

15% NiR
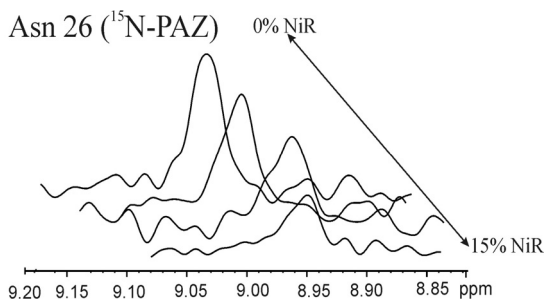
Figure 3.7: Cross-section along the F$_2$ dimension through the ^{1}H^{N} resonance of Asn26 (^{15}N- PAZ Zn II). The figure shows the decrease in the intensity of the amide signal upon addition of NiR Cu I-T2D. ^{15}N-PAZ Zn II amide signal becomes undetectable at the experimental conditions when 0.2 mol.eq. of NiR Cu I-T2D subunit is added
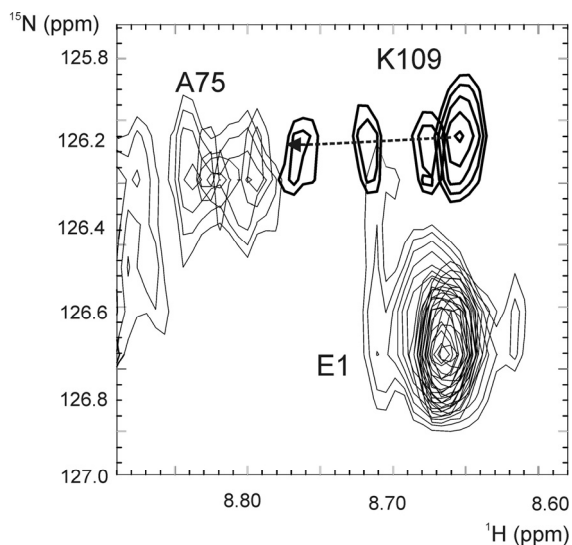
Figure 3.8: Overlay of a part of the [^{15}N-^{1}H] HSQC spectra of ^{15}N-PAZ Zn II in the free form and in the complex with NiR Cu I-T2D. The resonance of residue K109 (dark line) shifts upon addition of NiR Cu I-T2D and the signal is depicted at different percentage of NiR Cu I-T2D from right to left, as indicated by the arrow: 0%, 5%, 10% and 15%. Residues E1 and A75 do not shift upon NiR Cu I-T2D titration.

3.3.3 Isothermal Titration Calorimetry

Binding affinities between PAZ and NiR or NiR Cu-T2D, both in the oxidized state, were monitored using isothermal titration calorimetry (ITC).
In Figure 3.9 the data from the ITC titration experiments between PAZ Cu II - NiR Cu II-Cu II (right) and PAZ Cu II – NiR Cu II-T2D (left) are reported. The upper halves of each of the panels in the figures show the row data obtained for each PAZ injection into NiR, while the binding isotherm is plotted in the bottom part of the panels. The data were fitted using a one-site binding model; a two-site binding model did not result in significant improvement of the fit and neither did a cooperative binding model. The stoichiometry (N) and dissociation constant (K_d) are reported in Table 3.2.
Titration of PAZ Cu II into NiR Cu II-Cu II yielded a $K_d = 1.6 \pm 0.2 \times 10^{-4}$ M (with a stoichiometry of PAZ and NiR of N = 0.82) while the titration of PAZ Cu II into NiR Cu II-T2D produced $K_d = 1.1 \pm 0.1 \times 10^{-4}$ M (with a stoichiometry of PAZ and NiR of N = 1.1).
Titration of the reduced proteins (PAZ Cu I and NiR Cu I-T2D) required the presence of ascorbate in all solutions. Reactions of ascorbate with small quantities of dioxygen upon mixing resulted in irreproducible results, and reliable binding data could not be obtained.
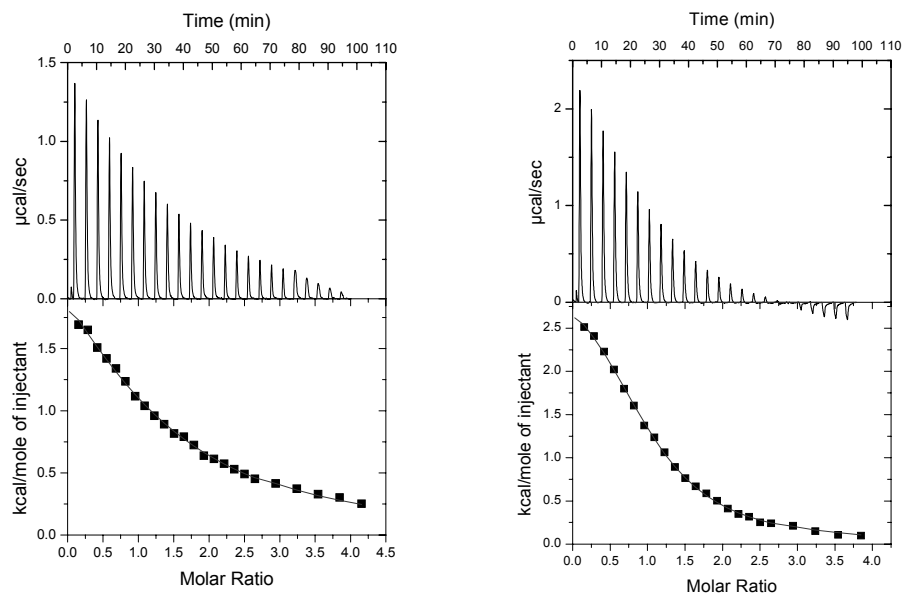
Figure 3.9: Isothermal titration calorimetric profile of the association of PAZ Cu II with NiR Cu II-Cu II (right) and NiR Cu II-T2D (left) at pH 6.5, 25ºC in 20 mM sodium-phosphate buffer. The top panel shows the incremental heat liberation upon titration of 3.2 mM of PAZ into 0.17 mM of NIR. Seventeen 15 µl injections were performed into NiR. The bottom panel shows the integrated area for the above peaks plotted against the molar ratio of PAZ/NiR. The solid line represents a fit to a single-site binding model.

Table 3.2: Calorimetric data derived from association reaction between PAZ Cu II and NiR Cu II-Cu II and PAZ Cu II and NiR Cu II-T2D in the oxidized form.

	$K_d(M)$	N
PAZ ox -NiR ox	$1.6 \pm 0.2 \times 10^{-4}$	0.82 ± 0.1
PAZ ox –NiRT2D ox	$1.1 \pm 0.1 \times 10^{-4}$	1.1 ± 0.1

3.4 Discussion

3.4.1 Different binding modes for PAZ Cu I and PAZ Cu II / Zn II

The binding of PAZ to NiR with both partners in different oxidation states has been studied by NMR spectroscopy. Direct and inverse titration experiments of PAZ Cu I with NiR Cu I-Cu I or NiR Cu I-T2D reveal two exchange modes occurring simultaneously: a slow exchange mode evidenced by the decrease of signal intensities without extensive line broadening, and a fast exchange mode represented by chemical shift perturbations of amide resonances located in a specific area on the PAZ surface. In the inverse titration (^{15}N-PAZ Cu I titrated into NiR Cu I-T2D), ^{15}N-PAZ Cu I signals appear already at a molar ratio of 2.5 (NiR subunits/PAZ), so with NiR still in excess, indicating that the binding related to the slow exchange mode is not very tight (Figure 3.4). Yet, a comparison with signal intensities of a spectrum of free PAZ at the same concentration readily indicates that binding occurs. This is also borne out by the simulated curve for the signal intensity in the absence of binding (dashed line in Figure 3.4).

Small chemical shift perturbations for ^{15}N-PAZ Cu I were observed upon mixing of PAZ with NiR, both in direct and inverse titrations. The perturbations were largest at the higher ratios of NiR/PAZ but decreased only little with decreasing ratios. Similarly, line broadening was observed for PAZ Cu I due to the presence of NiR, which decreased only marginally with increasing PAZ concentrations in the inverse titration. These observations suggest that PAZ interacts with NiR in a fast exchange mode, with very weak affinity. For a K_d that is similar or larger than the highest PAZ and NiR concentrations, only small changes in chemical shift perturbations and line broadening are expected in the inverse and direct titrations. A comparison with the effects observed for oxidized PAZ suggests that, for example, at concentrations of NiR and PAZ Cu I of 0.4 and 0.2 mM, respectively, circa 15% of available PAZ is in the bound state in the fast exchange mode.

Similar behaviour is observed when PAZ Cu I is titrated with NiR Co II-Co II, indicating that the metal charge on NiR does not affect the mode of binding to its redox partner, PAZ.

A different binding behaviour is observed when the same direct titration is performed with NiR Cu-Cu or NiR Cu-T2D either in the oxidized or reduced form and ^{15}N-PAZ Cu II /Zn II. The effect of NiR binding on the ^{15}N-PAZ Zn II spectra is dramatically different: already at a ratio NiR / PAZ of 0.2, ^{15}N-PAZ Zn II amide signals are not longer detectable due to line broadening. The difference in line width of the signal between free PAZ and its bound form at a ratio of 0.15 was ~20 Hz, which is similar to that of the reduced form at a ratio of 1.7. Chemical shift perturbations are observed for resonances of residues located on the same surface area around the metal centre as in the reduced form.

Similar line broadening effects are observed for ^{15}N-PAZ Cu II with NiR Cu II-Cu II and NiR Co II-Co II. These results suggest that PAZ Zn II/Cu II binds to NiR in a fast exchange mode with a K_d on the order of 10^{-4} M or less. This is confirmed by the K_d values obtained via ITC. There is no evidence for a dual binding mode in the case of PAZ Cu II/ Zn II.

Redox state dependent binding, as the one described here for PAZ and NiR, has been studied for other transient complexes before through different techniques.

The binding of plastocyanin to photosystem I (PSI) has been analyzed by the technique of perturbed angular correlation of γ-rays (PAC) as a function of the charge state of the copper ion (Danielsen, 1999). From previous work, the dissociation constant was shown to be dependent on the charge of the metal ion of plastocyanin (K_d^{CuII}/ K_d^{CuI} at least 24) (Drepper, 1996). By comparing the structures of Cd and Ag plastocyanin and their complex with PSI, it was suggested that the metal site structure, involving the His87 metal ligand, is involved in regulating the dissociation constant of the complex and, more specifically, that binding of Ag-plastocyanin to PSI stabilizes the Ag metal centre structure. It is also important to notice that the structural change of the metal centre was not attributed to a protonation of the N^δ of His 87.

In work of Zhu et al., the molecular basis for the effect of complex formation of amicyanin with its partner methylamine dehydrogenase (MADH) (Zhu, 1998) is described. Protonation of the His95 copper ligand in amicyanin has been shown to be responsible for the pH dependence of its E_m value. However, when amicyanin is in complex with its redox partner, MADH, its E_m is not pH dependent. By comparing the crystal structures of free and bound amicyanin, it was observed that the conformational change of His95, responsible for the described phenomena, would be sterically hindered in the complex. Consequently, His95 is prevented from dissociating from the copper upon reduction, maintaining the E_m value suitable for the ET to occur. The complex formation between MADH and amicyanin has been shown to decrease by 73 mV the redox potential of amicyanin, facilitating its ET to cytochrome *c*-551i (Davidson, 1995; Gray, 1986).

From these studies the conclusion arises that conformational changes in the metal centre due to the metal oxidation state can change the binding characteristics and that complex formation itself can affect the metal centre structure of the proteins.

3.4.2   *Modelling of PAZ Cu I binding mode*

The redox state dependence of the binding modes suggest that the reduced form of PAZ exists in two forms, PAZ Cu I and PAZ*Cu I, while the oxidized form, PAZ Cu II, exists only in one. In the HSQC spectrum of PAZ, single resonances are observed for each amide, indicating that in the case of two forms, either they exist in fast exchange or one is dominant. To explain all the observations, the model in Scheme 3.1 is proposed. PAZ and PAZ* are in equilibrium (**a**) and PAZ* is assumed to be the dominant conformation while the reaction is slow on the NMR time scale ($k_{ex} \leq 100$ s^{-1}). Furthermore, PAZ binds NiR with high affinity (**d**), while PAZ* does so with low affinity (**b**, $K_d \geq 0.5$ mM). Equilibrium (**c**, PAZ-NiR $\rightleftarrows$ PAZ*-NiR) is shifted to the left relative to (**a**) to match the equilibrium ratio of (**d**) and (**b**) and close a thermodynamic cycle. In this scheme, slow exchange binding of PAZ* (the observed form of PAZ) occurs via (**a**) and (**d**), because the step from PAZ* to PAZ is slow. Fast exchange binding occurs via (**b**). The K_d^{app} determined from the inverse titration was of $1.0 \pm 0.1 \times 10^{-4}$ M. This value is based on the decrease of the intensity due to the binding, assuming that bound PAZ does not contribute to the intensity of the HSQC signals. Thus, it represents the apparent K_d^{app} for both (**b**) and (**d**). Modelling shows that for PAZ*/PAZ>10 and PAZ*-NiR/PAZ-NiR<0.07, at [PAZ] = 200 μM and [NiR] = 400 μM, a binding fraction of PAZ*/PAZ*-NiR (fast exchange mode) of 0.15 is

obtained, in line with the sizes of the observed chemical shift perturbations for this equilibrium, with $K_d^{(d)}$ = 10 μM, $K_d^{(b)}$ = 1.4 mM and K_d^{app} = 100 μM, respectively. Increasing the concentration of PAZ to twice that of NiR, reduces the PAZ*/PAZ*-NiR to 0.05, thus, it is possible to reproduce all experimental observations with the model in Scheme 1 assuming a high PAZ*/PAZ ratio, and it yields a surprisingly large imbalance in the equilibria, $K_d^{(b)}/K_d^{(d)}$ = $K^{(a)}/K^{(c)} \geq 100$. Another possibility that should be taken into consideration is that the equilibrium **a** might not be in slow but in fast exchange. Consequently, to yield a K_d^{app} = 100 μM, equilibrium **d** needs to be in a slow exchange with a K_d in the order of 1-10 μM.

The binding of the oxidized PAZ can be described with a single binding mode in fast exchange, similar to (**b**), with a K_d of circa 100 μM. Remarkably, this K_d and the K_d^{app} for the reduced state are similar, suggesting that both redox states bind with a similar effective affinity. An explanation for the two forms of PAZ is the subject of next chapter.

Scheme 3.1: Possible equilibria involved in the interaction between PAZ Cu I and NiR where two simultaneous binding mode are involved.
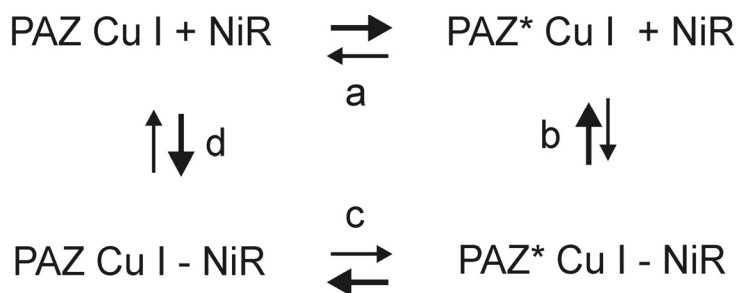
Chapter IV

Protonation of histidine residues in pseudoazurin: effect on NiR binding

Abstract

In this chapter the pH behaviour of PAZ was investigated by NMR spectroscopy in order to investigate histidine protonation effects on NiR binding. The pK_a values of the surface exposed His6 and of the His81 copper ligand have been determined to be 7.2 and 4.8, respectively. PAZ titration into NiR has been performed at two different pHs (5.5 and 8.0). At pH 8.0 the K_d^{app} is six times larger than at pH 6.5, indicating a weaker binding. However, the spectral characteristics show that His6 is unlikely to be responsible for the occurrence of a dual binding mode of PAZ and NiR in the reduced state. The experiments still leave open the possibility that protonation of His81 is connected to the occurrence of two binding modes for the reduced complex.

4.1 Introduction

In previous studies it has been demonstrated that the titration behaviour of amino acid residues whose pK_a values are in the physiological range, can have a significant effect on the reactivity of cupredoxins. For example, in several crystal studies conformational changes were observed for cupredoxins as a function of pH (Zhu, 1998; Vakoufari, 1994; Guss, 1986). The protonation of the exposed histidine ligand was shown to a have large effect on the reduction potential of plastocyanin (Katoh, 1962). Studies on amicyanin demonstrated that protonation of the copper ligand His95 affects the reorganization energy of the ET reaction (Lommen, 2004). Later it was also shown that a pH dependent conformational change of the same His95 plays an important role in the function of the protein itself (Zhu, 1998). The pK_a value of His95 in the reduced form of amicyanin has been determined as 6.7 (Lommen, 1988). Through crystallography it has been confirmed that in the reduced form amicyanin under goes a pH dependent conformational change. Protonated His95 in reduced amicyanin dissociates from the copper changing the E_m. This conformational change, called "flipping", is hindered when amicyanin is in the complex with MADH and, consequently, His95 in the complex is prevented to dissociate from the copper coordination, thus maintaining the right E_m.

A second example is provided by *Ps. aeruginosa* azurin, where protonation / deprotonation of His35 causes conformational changes and influences the driving force of electron transfer reaction with protein redox partners (Jeuken, 2000; Kalverda, 1999; Van de Kamp, 1993). Thirdly, the surface exposed histidine (His6) in pseudoazurin from *Ac. cycloclastes* has been shown to have similar features (Sato, 2002). His6 exhibits a redox state dependent pK_a (7.1 ± 0.1 for PAZ Cu I and 6.5 ± 0.1 for PAZ Cu II). Given the distance between this residue and the copper (14.8 Å) it was suggested that the effect is mainly electrostatic in nature. Hence, surface exposed histidines can affect cupredoxin properties. Nevertheless, this effect is subtle when compared with the histidine (His81) copper ligand protonation / deprotonation effect (Dennison, 1994). In PAZ, His6 is conserved but the structural effects of its protonation in the different redox states are less pronounced (Vakoufari, 1994) due to a difference in residue 36 Thr in *Ac. cycloclastes* and Val36 in *Al. faecalis* (Inoue, 1999).

In Chapter III, the redox state dependent binding of PAZ to NiR was described. It was found that the reduced PAZ has two binding modes, which were ascribed to two conformations of PAZ. In this chapter, the pH dependence of the NMR signal of free PAZ and of PAZ in the complex with NiR is investigated, in order to establish whether His81 or His6 could be the cause of the conformational heterogeneity of PAZ.

On the basis of what has been previously described for PAZ from *Ac. cycloclastes*, it was assumed that His6 in *Al. faecalis* PAZ has a redox state dependent pK_a. Thus, His6 represents a potential candidate to cause redox state dependent conformational modes: two populations of PAZ His6 could give different binding modes when interacting with NiR, the unprotonated might be in fast exchange for instance, with low affinity, while the protonated form might be in slow exchange and exhibit a stronger binding. Although the pK_a of His81 is much lower, it is also redox state dependent and, as well as His6, it could be the cause of the redox state dependent binding of PAZ to NiR.

First the pH behaviour of PAZ was studied in detail. The pK_a values of His6 and His81 in *Al. faecalis* PAZ were determined on the basis of the pH dependence of amide NMR resonances. Then, inverse titrations at pH values of 5.5 and 8.0 were performed between ^{15}N-PAZ Cu I and NiR Cu I-T2D.

4.2   Materials and methods

Protein solutions were prepared using Ultrafree centrifugal ultrafiltration tubes (5 kDa molecular weight cut-off) and exchanged into 20 mM sodium-phosphate buffer, 1 mM sodium ascorbate and 10% of D_2O. For the pH titration of free PAZ 1mM of ^{15}N labelled protein was prepared. The pH was adjusted by adding microliter aliquots of 1 M NaOH and 1 M HCl, and spectra were recorded over a range of pH 4.0 - 8.1. To study the pH effect on complex formation a sample containing 0.4 mM NiR Cu I–T2D and a stock solution of 3.9 mM ^{15}N-PAZ Cu I was prepared in the same buffer as above and the pH adjusted according to the desired value. All ^{15}N-HSQC spectra were acquired at 293 K on a Bruker DMX 600 NMR spectrometer. The chemical shift perturbations arising from complex formation between PAZ and NiR were determined with respect to free PAZ at the same pH.

4.2.1   pH titration curves

Titration curves were obtained by plotting the chemical shift change as a function of the pH for backbone PAZ amide protons ($^1H^N$) and nitrogens (^{15}N), and fitting to a model which describes a single protonation event:

$$\delta = \frac{\left(K_a \delta_H + [H^+] \delta_L\right)}{K_a + [H^+]} \qquad \text{(eq. 4-1)}$$

where δ_H and δ_L are the ^{15}N or ^1H amide chemical shift at high and low pH respectively. For resonances which were sensitive to more than one titrating group, the titration curves were fitted to a two-pK_a model:

$$\delta = \frac{\left([H^+]^2 \delta_L + [H^+] K_{a1} \delta_M + K_{a1} K_{a2} \delta_H\right)}{\left(K_{a1} K_{a2} + [H^+] K_{a1} + [H^+]^2\right)} \qquad \text{(eq. 4-2)}$$

where δ_M is the ^{15}N or ^1H amide chemical shift at intermediate pH and K_{a1} and K_{a2} the association constants at low and high pH, respectively . Fits were obtained by non-linear curve fitting of the respective models with $[H^+]$ and δ as the independent and dependent variables, respectively, and δ_H, δ_M, δ_L, K_a, K_{a1} and K_{a2} as the fitted parameters.

4.3   Results

4.3.1   PAZ pH titration

During the pH titration of reduced ^{15}N-PAZ Cu I over the range of pH 4.0-8.1 more than 85 % of the signals shifted. Depending on the residue type and position, various curve shapes and pK_a values were observed for the backbone amide resonances (Figure 4.1). PAZ contains 3 histidines, His6, 40 and 81. His6 is a surface exposed histidine while His40 and 81 are involved in copper coordination. His6 and 81 are available for protonation, while, His40 is unlikely to protonate as it is buried and strongly H-bonded. Some of the titration curves for residues affected by protonation of His6 or 81 could be fitted with a single pK_a while others, sensitive to more than one titrating group, were fitted with two pK_a values. These pK_a values are reported in Table 4.1. A global fitting of the titration curves of the residues strongly affected by protonation of His 6 is presented in 4. 2. These fittings yield a pK_a of His6 of 7.2 ± 0.1.

Around pH 5 several acidic residues start to become protonated. For this reason, it is difficult to determine which region of the protein is affected by protonation of His81.

However, a global fitting for titration curves of the residues more affected by protonation of His 81 is shown in Figure 4.3. These fittings yield a pK_a of His81 of 4.8 ± 0.1.

Both the signals of His81 and His40 disappear below pH 6.0, probably because their shifts, due to His81 protonation, are so large that they are no longer in fast exchange on the NMR time scale.

Figure 4.1: Representative pK_a curves arising from the pH dependence of the chemical shift of backbone amides in ^{15}N-PAZ Cu I. For each residue, in the left column is plotted the ^{15}N amide chemical shift and in the right column the ^{1}H one.
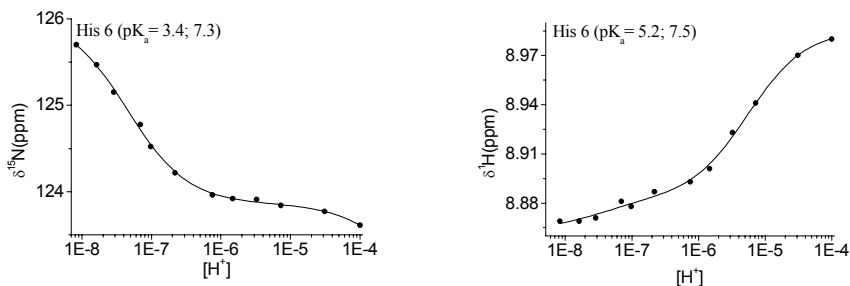
Figure 4.1: Continued
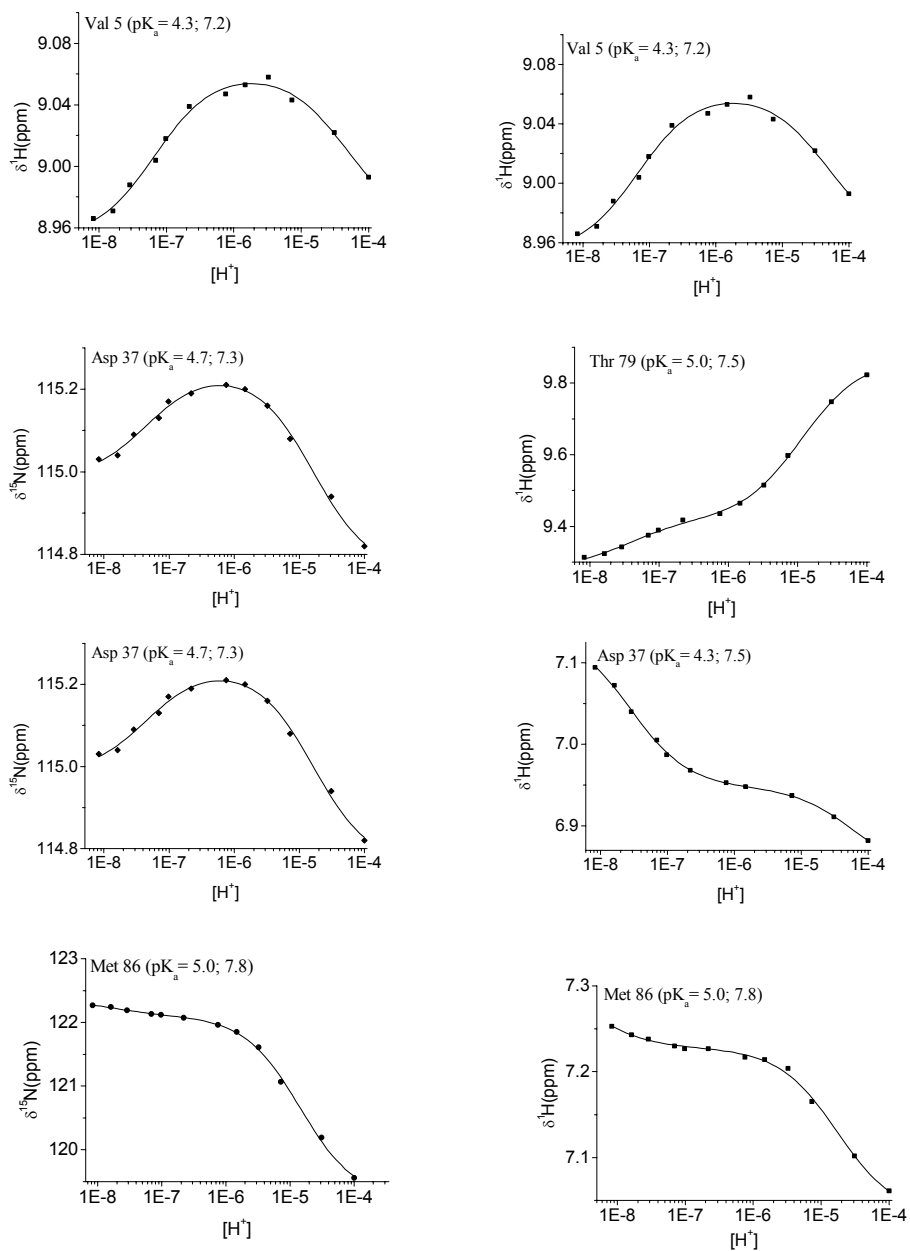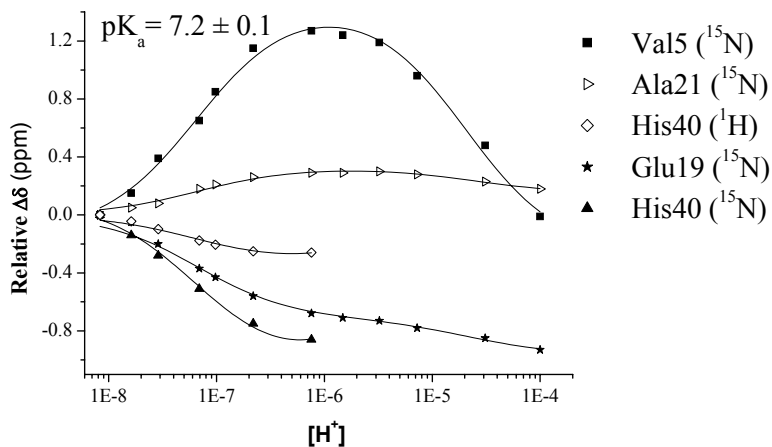
Figure 4.2: Global fitting of pK_a curves for several residues influenced by protonation of His6. The chemical shift changes ($\Delta\delta$) for the indicated nuclei are plotted as a function of pH relative to the δ at pH 8.1.
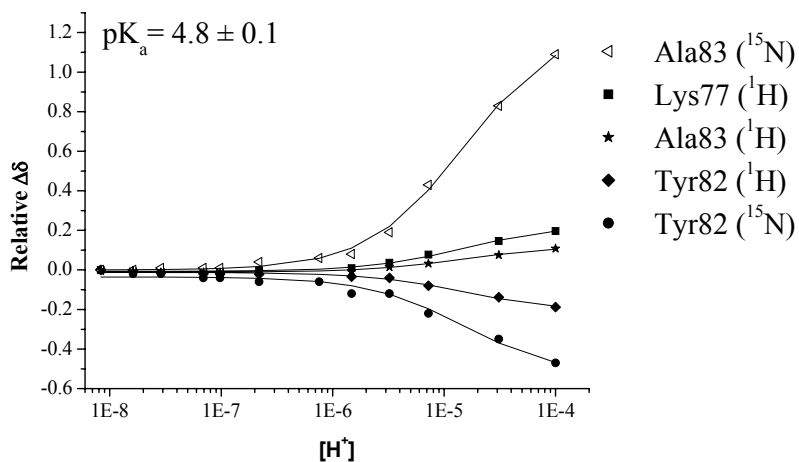
Figure 4.3: Global fitting of pK_a curves for several residues influenced by protonation of His81. The chemical shift changes ($\Delta\delta$) for the indicated nuclei are plotted as a function of pH relative to the δ at pH 8.1.

Table 4.1: PK$_a$ values obtained by fitting with eq. 4-1 or eq. 4-2 the chemical shift changes of residues (in ^{15}N or ^{1}H dimension) affected during a pH titration between pH 8.0 - 4.0.

Residue	(^{15}N) pK$_{a1}$	(^{15}N) pK$_{a2}$	(^{1}H) pK$_{a1}$	(^{1}H) pK$_{a2}$
Glu 1	5.0 ± 0.1	7.2 ± 0.1	4.7 ± 0.1	7.2 ± 0.1
Glu 4	5.0 ± 0.1	7.2 ± 0.1		
His 6	-	7.3 ± 0.2	5.2 ± 0.1	7.5 ± 0.5
Val 5	5.4 ± 0.2	7.3 ± 0.1	4.3 ± 0.1	7.2 ± 0.1
Leu 8	5.9 ± 0.1		4.7 ± 0.1	
Lys 10	4.7 ± 0.1		5.0 ± 0.1	
Gly 11	4.7 ± 0.1			
G;u 13	4.5 ± 0.1		4.7 ± 0.1	
Val 17	5.0 ± 0.1		5.0 ± 0.1	7.7 ± 0.2
Glu19	4.5 ± 0.1	7.3 ± 0.1	5.0 ± 0.1	7.7 ± 0.2
Ala21	4.4 ± 0.2	7.4± 0.2		
Asn 26	5.0 ± 0.1		4.7 ± 0.1	
Asp 29	4.4 ± 0.1		5.0 ± 0.1	
Thr 30	5.6 ± 0.1		5.0 ± 0.1	7.0 ± 0.1
Val 36	5.0 ± 0.1			
Ile 34		7.6 ± 0.2		7.5 ± 0.2
Asp 37	4.7 ± 0.2	7.3 ± 0.1	4.3 ± 0.1	7.5 ± 0.2
Gly39	4.7± 0.2	7.3± 0.1	4.4 ± 0.2	7.2 ± 0.1
His 40	n.o.	7.4 ± 0.1	n.o.	7.5 ± 0.1
Lys 77	5.0 ± 0.1	-	5.0 ± 0.1	-
Cys 78	5.0 ± 0.1			
Thr 79	5.0 ± 0.1	7.5 ± 0.3	5.0 ± 0.1	7.5 ± 0.1
His 81	n.o		n.o.	
Tyr 82	5.0 ± 0.1	-	4.7 ± 0.2	
Ala 83	4.7 ± 0.3	-	5.0 ± 0.1	-
Met 84	4.7 ± 0.1		5.0 ± 0.1	
Met 86	5.0 ± 0.1	7.8 ± 0.1	4.7 ± 0.1	8.4 ± 0.2
Ala 88	5.0 ± 0.1	7.7 ± 0.1	5.0 ± 0.1	7.6 ± 0.1

n.o.: not observed due to broadening at pH < 6.0
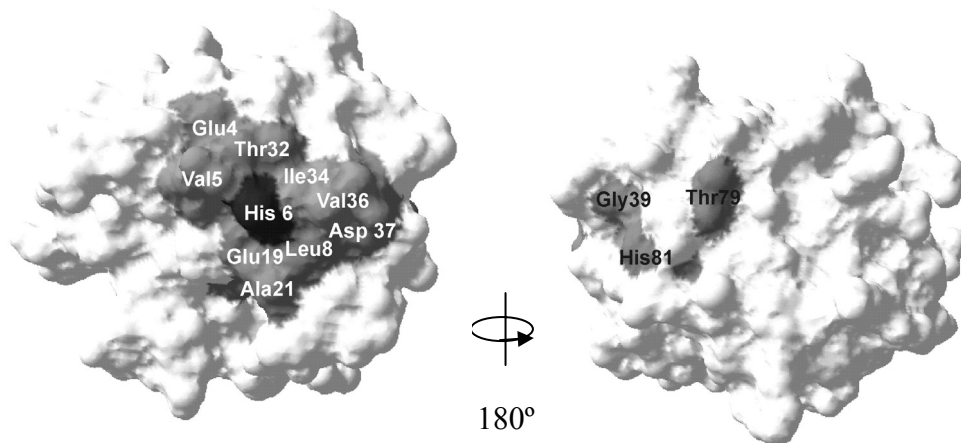
Figure 4.4: Surface representation of PAZ facing His6 (front and back). Residues affected by His6 protonation are depicted in grey while His6 in black. Some residues (V17, F18, V31, T32, F33, G39 and H40) affected by His6 protonation are buried beneath the surface.
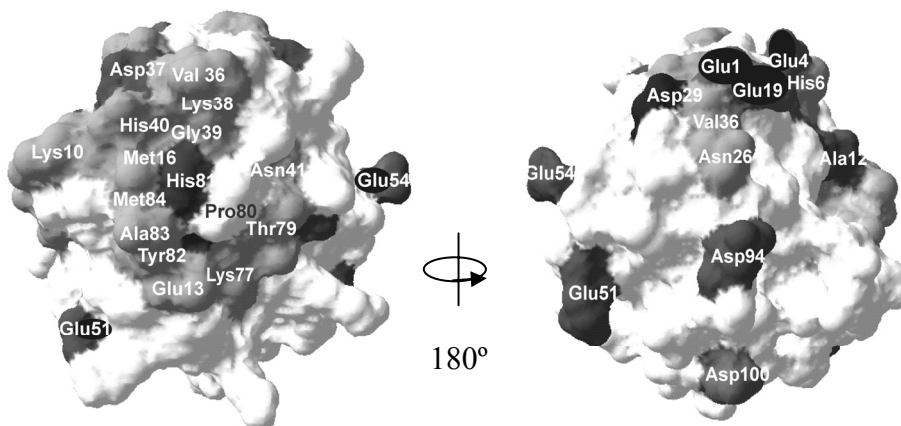
Figure 4.5: Surface representation of PAZ facing His81 (left) and after 180˚ turn (right). Residues affected by low pH are depicted in grey while His81 and acidic residues are depicted in black.

The protonation of His6 results in a strong perturbation of the resonances of 22 residues, all located around His6 (Figure 4.4). It is remarkable that the protonation of an exposed residue has such large effects.

Between pH 6.6 and 5.3, in the pH range closer to His81 pK_a, ca. 30 residues were affected. Their locations are more spread on the protein surface (Figure 4.5), related in part to the possible simultaneous protonation of acidic residues.

Residues K10, M16, V36, G39, N41, K77, T79, Y82, A83 and M84 are probably affected predominantly by protonation of His 81.

4.3.2   pH effect on PAZ/NiR complex

To investigate the pH dependence on complex formation between PAZ Cu I and NiR Cu I-T2D, inverse titrations, like the one described in Chapter III at pH 6.5, were performed at pH values 5.5 and 8.0. At pH 5.5 NiR was unstable making it impossible to define a binding constant. However, chemical shift perturbations (Figure 4.6a, b and c) were generally smaller when compared to the same titration at pH 6.5 but still involving the same residues (His40 and 81, which are copper ligands, and Met84, Ala15 and Arg114). The small size of the chemical shift perturbations can be explained by NiR precipitation, which hindered the determination of the concentration of the proteins.

The line width did not increase during the titration and was only a little larger compared to the free pseudoazurin (Figure 4.6d). Charge neutralization of the acidic residues on NiR at pH 5.5 could also result in diminished affinity for PAZ.

At pH 8.0 the spectral features caused by complex formation are also similar to those at pH 6.5. The inverse titration was accompanied by chemical shift perturbations of residues K109, H81, H40, M84, V17, R114 and K10 (Figure 4.7a, b and c). Those residues also exhibited perturbations in the experiment performed at pH 6.5. The line broadening (Figure 4.7d) upon complex formation results less compare with the experiment at pH 5.5 in agreement with a lower binding constant.

Inverse titration pH=5.5
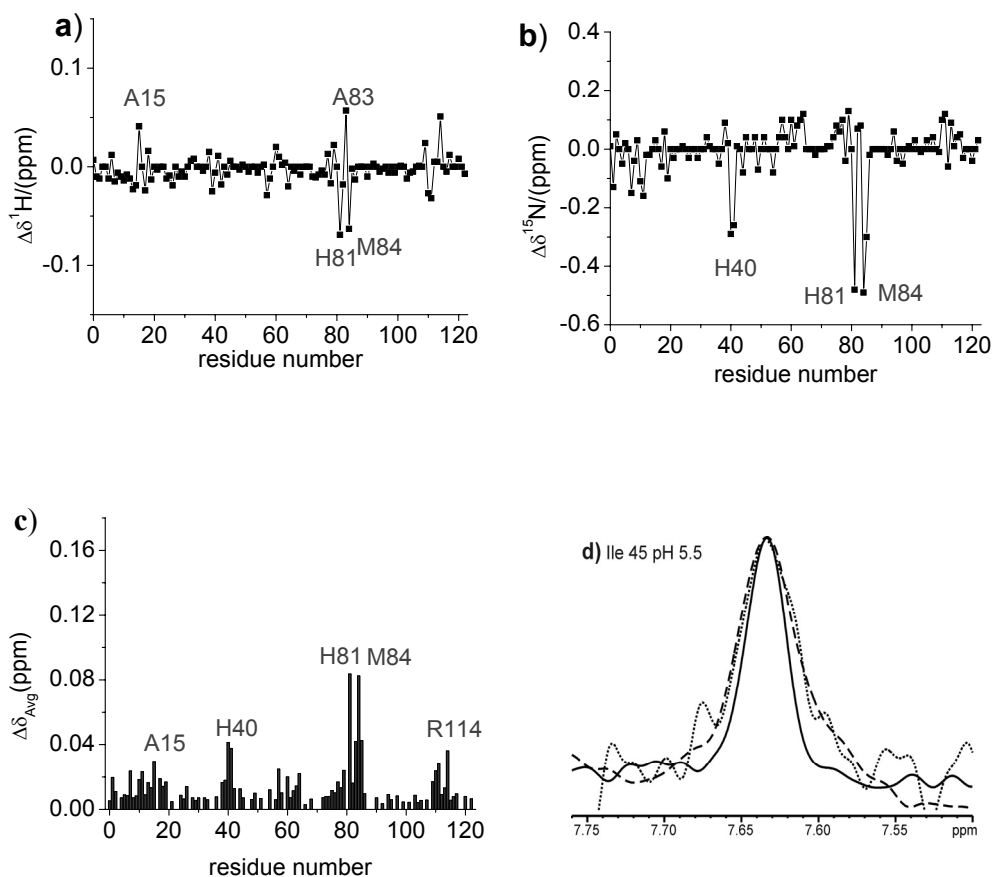
Figure 4.6: Changes in ^1H (a) and ^{15}N (b) chemical shift upon complex formation between ^{15}N-PAZ Cu I and NiR Cu I-T2D at a ratio of 0.58 at pH 5.5. c) Changes in the average chemical shift ($\Delta\delta_{avg}$) upon complex formation between ^{15}N-PAZ Cu I and NiR Cu I-T2D at a ratio of 0.58. d) Cross-section through the $^1H^N$ resonance of Ile45 of ^{15}N-PAZ Cu I. The resonances with the solid line represent the signal of free PAZ. Dotted line is the signal observed at a ratio ^{15}N-PAZ/NiR Cu I T2D of 0.25 and dashed line at ratio 2.6 during the inverse titration at pH 5.5.

Inverse titration pH=8.0
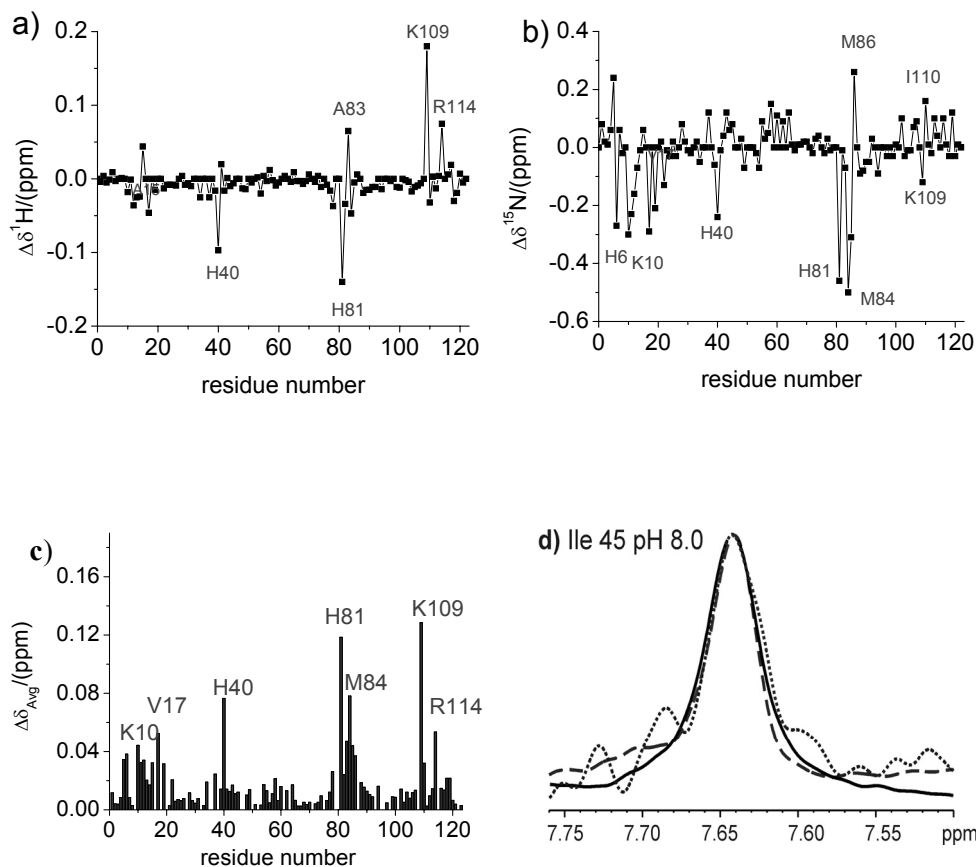
Figure 4.7: Changes in [1]H (a) and [15]N (b) chemical shift upon complex formation between ^{15}N-PAZ Cu I and NiR Cu I-T2D at a ratio of 0.58 at pH 8.0. c) Changes in the average chemical shift ($\Delta\delta_{avg}$) upon complex formation between ^{15}N-PAZ Cu I and NiR Cu I-T2D at a ratio of 0.58. d) Cross-section through the [1]H[N] resonance of Ile45 of ^{15}N-PAZ Cu I. The resonances with the solid line represent the signal of free PAZ. Dotted line is the signal observed at a ratio ^{15}N-PAZ/NiR Cu I T2D of 0.25 and dashed line at ratio 2.6 during the inverse titration at pH 8.0.

At pH 8 it was possible to determine the binding constant for the inverse titration on the basis of signal intensities, as described in Chapter III. The global fitting, shown in Figure 4.8, yields a the dissociation constant of $6.0 \pm 0.2 \times 10^{-4}$ M indicating a six fold weaker binding at pH 8.0 as compared to pH 6.5. However, the deviation from the line predicted in the absence of binding for residue T67, (dotted line, Figure 4.8) demonstrates that the proteins are binding.
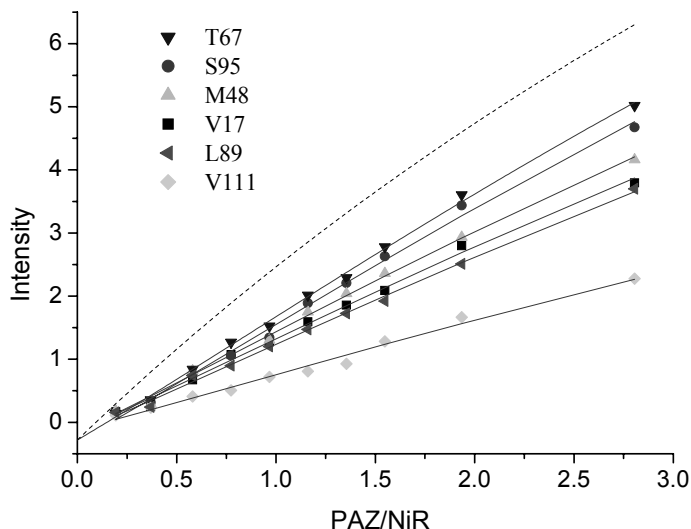
Figure 4.8: Binding curves for the interaction of ^{15}N-PAZ Cu I with NiR Cu I-T2D at pH 8.0. The intensity of several PAZ amide resonances (arbitrary units, A.U.) are plotted against the PAZ/NiR (subunit) ratio. Solid lines represent global fits to a model describing one PAZ binding site per NiR Cu I-T2D (eq.3-6, Chapter III) for residues T67, S95, M84, V17, L89 and V111, yielding a K_d^{app} of $6.0 \pm 0.1 \times 10^{-4}$ M. The dotted line represents the predicted line in the absence of binding for T67 using the *a* and *b* values obtained from the fit.

4.4   Discussion

A pK_a of 7.2 has been determined for the surface exposed His6 and a pK_a of 4.8 for His81 copper ligand in *Al. faecalis* S-6 in PAZ Cu I. These values are close to those determined for *Ac. cycloclastes* pseudoazurin (pK_a = 7.1 for His6 (Sato, 2002) and pK_a = 5.2 for His81(Dennison, 1994).

On the basis of a comparison with the pH titration of free PAZ, it is clear that the observed spectral perturbations upon addition of NiR can be attributed to complex formation and not to small pH effects. Although many of the residues involved in the complex interface also experience shifts during the pH titration, there are essential differences. For example Lys10, Ala83, Met84 and Asp114, which shift upon NiR binding, are unaffected by the pH titration between pH 8 and 5. On the other hand, residues like Thr79, Asp37 and 56 are affected during pH titration but unaffected upon NiR binding. For other residues, the direction of the shift in the nitrogen and in the proton dimension differs between the pH titration and complex formation.

His6 protonation is the most obvious candidate to cause the two binding modes between PAZ Cu I and NiR Cu I–T2D described in Chapter III. The pK_a of His6 has been shown to be redox state dependent in *Ac. cycloclastes* pseudoazurin (Sato, 2002).The pK_a (7.2) of His6 in *Al. faecalis* PAZ is close to the pH (6.5) of the binding experiments, and thus, two possible populations of PAZ, one with His6 protonated and one with it deprotonated, could be responsible for this phenomenon. According to this hypothesis, we expected to observe a single binding behaviour when repeating the titration experiments at pH 5.5 and 8.0, because the equilibrium (His6 protonation/deprotonation) would be pushed to one side.

However, the typical combination of limited line broadening, intensities decrease and chemical shift perturbations was also observed at both pH 5.5 and 8.0, comparable to the data at pH 6.5 (Chapter III), although that the perturbations at pH 5.5 and 8.0 are smaller than at pH 6.5. It is concluded that His6 is unlikely to be the cause of the dual mode of binding to NiR.

The possibility of a PAZ alkaline transition has been also considered. In *Ac. cycloclastes* pseudoazurin, deprotonation of Lys surface residues situated close to the copper site have been found to result in a structural change of the copper site. Also deprotonation of lysine residues surrounding the hydrophobic patch around His81 (as Lys38 and 77) at $pK_a \sim 10.3$, change the copper position moving it away from the axial Met ligand. This has been observed on pseudoazurin Cu II and Ni II but not on the reduced form (Sato, 2002; Dennison, 2002; Dennison, 1999). Due to the high pH at which the alkaline transition occurs ($pK_a \sim 10.3$), it is unlikely that this can be the explanation for the conformational difference between PAZ and PAZ* which has been suggested at pH 6.5. At pH 6.5 the ratio of deprotonated / protonated lysines would be < 0.001, and the amount of the deprotonated form would be less than the 5-15% of PAZ* estimated to be in fast exchange (see Scheme 1, Chapter III). Furthermore, for the alkaline transition to be the cause of the different binding modes between oxidized and reduced form of PAZ, such modification should have been present only in the reduced form and not in the oxidized one. Such difference has not been reported.

Another explanation for the double binding modes of reduced PAZ might arise from dimer formation in solution. However, a monomer-dimer equilibrium has been found only for *Paracoccus pantotrophus* PAZ in the oxidized not in the reduced form (Pauleta, 2004). Also for PAZ from other organisms the reduced and oxidized forms occur only as monomer (Thompson, 2000; Inoue, 1999; Vakoufari, 1994). In our case, no indication of dimer formation is observed during purification procedures; hence, dimer formation also does not appear to be a plausible explanation for the occurrence of two binding modes of reduced PAZ.

The other residue that could explain the dual binding mode is His81. Voukofari et al. (Vakoufari, 1994) studied the PAZ structure at different oxidation states or pH values. It was shown that upon protonation of the copper coordinating histidine (His 81) at pH 4.4, the copper ion Cu I is displaced towards the plane of the remaining ligands (S^γ(Cys), N^δ(His) and S^δ(Met). This conformational change results in a trigonal planar geometry with His 81 no longer acting as a copper ligand.

The pK_a of His81 is much lower than that of His6. Under any of the experimental conditions (pH 5.5, 6.5 or 8), the deprotonated form would be in excess and in Scheme 1 in Chapter III would represent the PAZ* form. Given the low pK_a it can be expected that in the pH range 5.5-8, the exchange regimes would not change dramatically. At increased pH, the K_d^{app} would increase due to a shift in equilibrium a in Scheme 1, Chapter III. This is in accordance with the observation that K_d^{app} at pH 8 is six-fold larger than at pH 6.5.

The Scheme 1 in Chapter III further proposes that either equilibrium a or d or a combination of both is slow on the NMR time scale. The observation that some resonances (His40, His81) disappear from the HSQC spectrum at pH < 6 could indicate that His81 protonation is the slow event. However, more evidence would be needed to ascertain that His81 protonation is the cause of the dual binding phenomenon.

Other residues might also be candidates to explain this observation. In the work of Libeu et all. (Libeu, 1997), structural differences, not related to histidine protonations, between PAZ in the reduced and oxidized form were described: Met7 and Pro35 move co-ordinately closer to His 40 upon reduction which is unique for cupredoxin.

It is possible that such changes could represent the cause of dual binding to NiR. Mutagenesis of these residues may shed more light on this issue.

Chapter V

Mapping of the binding site of reduced pseudoazurin in complex with nitrite reductase by cross saturation transfer

Abstract

Nitrite reductase (NiR) catalyzes the reduction of nitrite to nitrite oxide as a part of the denitrification process. In *Alcaligenes faecalis* S-6, the copper protein pseudoazurin acts as electron donor to NiR. The binding surface of pseudoazurin involved in the formation of the 152 kDa complex with NiR has been determined by NMR using cross-saturation from NiR to perdeuterated PAZ. Due to the transient nature of the complex, saturation effects can be observed on the resonances of the unbound protein. The binding site comprises the hydrophobic area surrounding the exposed copper ligand His81 suggesting that this residue is important for efficient electron transfer.

5.1 Introduction

The peculiar interaction between the reduced forms of PAZ and NiR, discussed in Chapter III, suggests that PAZ exists in two forms. One form binds with moderate to high affinity to NiR and results in a binding process that is slow on the NMR time scale. The second form leads to a fast exchange mode, but with very low affinity. It can be estimated that this form represents only a few percent of bound PAZ under the experimental conditions. To probe the binding site of NiR in the slow-exchange form, chemical shift perturbation analysis cannot be used. In the slow exchange regime, binding results in a reduction of the intensity of the signals of free PAZ (see Chapter I). Thus, the chemical shift of the resonance does not contain information about the bound form. However, if the exchange rate between bound and free states is in the order of the $1/T_2$ or $1/T_1$ relaxation rates, it is possible to obtain this information by methods relying on relaxation rate differences (e.g. line broadening in the bound state) or saturation transfer. The latter has been applied here.

For this purpose, a recently developed method, cross saturation transfer (c.s.t.) (Nakanishi, 2002; Takahashi, 2000), has been applied to identify the binding area of reduced PAZ in the complex with reduced NiR.

In Figure 5.1 the principle of the method is schematically illustrated. To map the binding site of PAZ, this protein was uniformly labeled with ^{2}H and ^{15}N and complexed with unlabeled NiR. In this way it is possible to non-selectively irradiate, using an appropriate radio frequency (R.F.), the aliphatic proton resonances of NiR without irradiating PAZ resonances. Through spin diffusion (Takahashi, 2000; Akasaka, 1981; Kalk, 1976), which refers to the transfer of magnetization by means of dipolar interactions between spins, not only NiR aliphatic proton resonances will be saturated but also its aromatic and amide ones. Due to the lack of aliphatic protons in the deuterated PAZ, the amide protons of PAZ can only experience magnetization saturation if located close to NiR protons. The low proton density of the deuterated PAZ will guarantee that the effect of the cross saturation transfer derives from NiR and not from protons within PAZ itself. To avoid intramolecular transfer of saturation between amide protons within PAZ, the experiment is performed in 90% D_2O / 10% H_2O solution, rendering most amides deuterated. This also helps to prevent saturation transfer via solvent molecules.

The cross saturation transfer will result in a selective intensity decrease of the resonances of PAZ amide nuclei close to the interface. By observing the reduction of the peak intensities in ^{15}N-^{1}H PAZ TROSY spectra (Pervushin, 1998), it is possible to identify the complex interface. Furthermore, the saturation effect on the resonances of the bound PAZ Cu I can be observed on the resonances of the free protein provided the exchange rate is at least on the order of the longitudinal relaxation rate of the amide resonances (~ 0.3 s^{-1}). A binding ratio of 3:1 between PAZ and NiR has been demonstrated via ITC (see Chapter III), therefore the complex has a molecular weight of 152 kDa.

5.2 Materials and Methods

5.2.1 Protocol for the production of deuterium labeled PAZ in E. coli

Part of the PAZ gene coding for the mature protein was subcloned in pET-28a (+), creating a plasmid for expression in the cytoplasm of *E. coli*. Protein was produced in *E. coli* strain HMS174 in a M9 minimal medium containing 0.7 g/L $^{15}NH_4Cl$ and 5 g/L Na-acetate-d_3, as sole nitrogen and carbon sources, respectively. Cultures were incubated at 37°C with a shaking speed of 250 rpm. *E. coli* was adapted for growth in D_2O by increasing the percentage of D_2O in consecutive 5 ml cultures from 0% to 50%, 80%, 95% and 99.9%. The cultures were used for inoculation at a ratio 1:5 when their OD_{600} was 0.4. In this way cells slowly adapted first to the deuterated carbon source and then to the deuterated medium. The final preculture was diluted several times to a ratio 1:5 and cultured each time to $OD_{600} = 0.4$. The final volume was 1 liter. In this way, the bacteria remained in the exponential growth phase during the dilution steps. In the final culture, expression was induced at $OD_{600} = 0.6$ with 0.5 mM IPTG, and 100 μM copper citrate was added. Cultures were harvested at $OD_{600} = 0.9$ by centrifugation, 10 h after induction. From the first dilution step in the final medium until harvest it took 7 days. Purification was performed as described in Chapter II. The yield was 7.5 mg/L and the deuteration level of the aliphatic protons was determined by mass spectrometry to be 93%.
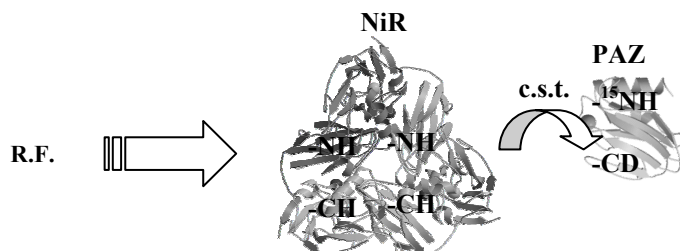
Figure 5.1: Principle of the cross-saturation transfer method. PAZ with residues to be identified in the complex interface, is uniformly labeled with ^2H (D) and ^{15}N. The saturation caused by the irradiation (R.F.) of the non labeled NiR (trimer) is transferred to PAZ.

5.2.2 Sample preparation and NMR experiment

In these experiments, type 2 copper depleted NiR (NiR Cu I T2D was used (for its preparation see Chapter III) to avoid oxidation during the experiment. Both NiR and PAZ were in the Cu I state.

Two NMR samples containing 1 mM ^2H-^{15}N-PAZ Cu I ($^{15}N > 98\%$ and $^2H > 93\%$) with or without 0.2 mM (trimeric) NiR Cu I T2D, respectively, were left for 8 h at room temperature and 2 days at 4 °C with 8 mM sodium ascorbate in a buffer solution (20 mM

potassium phosphate pH 6.5) of 90% D_2O / 10% H_2O to allow for equilibration of the amide exchange process.

To determine the degree of saturation, for each sample one spectrum was acquired with saturation of the aliphatic region and one without. It was critical to record these spectra in an interleaved fashion, i.e. for each t_1 increment in the 2D experiment the two FIDs were recorded consecutively. Afterwards, the combined data set was deconvoluted into the spectra with and without saturation and the intensity ratios of the amide resonances were determined. NMR spectra were acquired at 293 K on a Bruker AV 750 MHz wide-bore system with 5 mm BBI-2 Grad probe. The saturation transfer experiment (Takahashi, 2000) consisted of a TROSY (Pervushin, 1997) experiment preceded by a 3 s selective saturation period using the WURST-20 saturation scheme (Kupce, 1995) and ^1H decoupling at 0.13 kHz with the offset at -1.2 ppm. The total duration of each scan was 4.2 s. The number of scans and increments was 80 and 410, respectively. The total experiment for the two interleaved experiments took 77 h.

All spectra were processed in AZARA (http://www.bio.cam.ac.uk/azara/) and analyzed with the assignment program ANSIG (Helgstrand, 2000; Kraulis, 1989).

5.3   Results and discussion

The binding site for NiR on PAZ was determined by analyzing the effect of the saturation transfer from NiR to PAZ. The results are plotted for all PAZ residues in Figure 5.2
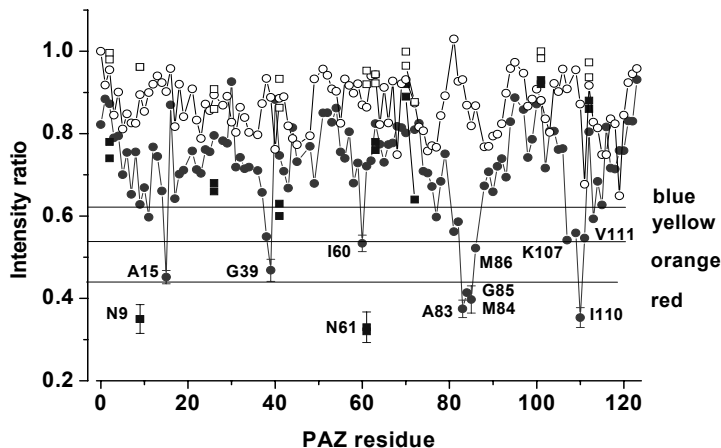
Figure 5.2: The intensity ratio of the resonances of the amide protons in the cross saturation experiments with and without irradiation of the aliphatic region in the spectrum are plotted against the PAZ Cu I residue number. The open and solid symbols represent PAZ Cu I in the absence and presence of NiR Cu I-T2D, respectively. Circles represent backbone amide protons; squares represent side-chain amide protons. Errors are <0.05 and are indicated for the most affected residues only. The horizontal lines indicate the colour classification of the intensity ratios used in Figure 5.3.

The open symbols indicate the intensity ratios of amide resonances of PAZ Cu I in the experiment with and without irradiation in the absence of NiR Cu I-T2D. The circles and squares represent backbone and side-chain amide resonances, respectively. A small uniform decrease of the intensities of the amide protons is observed, probably due to the saturation transfer from the residual 7% aliphatic protons in the deuterated PAZ Cu I. The solid symbols in Figure 5.2 give the intensity ratios for the mixture of PAZ Cu I and NiR Cu I-T2D, with circles and squares representing backbone and side-chain amide protons, respectively. A larger general decrease is observed and a number of residues show substantially smaller ratios due to saturation transfer from NiR Cu I-T2D.

The residues that exhibit the strongest intensity reduction due to the c.s.t. are indicated below the horizontal line assigned with red colour. The intensity ratios reported in Figure 5.2 have been mapped onto a surface representation of the PAZ crystal structure (Petratos, 1988) in Figure 5.3, using the colour code according to the classification shown in Figure 5.2 (horizontal lines). Remarkably, the affected residues all map near to the exposed copper ligand His81. The equivalent His residue has been shown to be involved in ET in other blue copper proteins (Ubbink, 1998; Chen, 1998; Van de Kamp, 1993). The results strongly suggest that also in the PAZ:NiR complex ET proceeds through the exposed His ligand.

To illustrate the decrease in intensities of the residues affected by c.s.t., TROSY spectra without and with irradiation are shown in Figure 5.4 and 5.5, respectively.

It should be noted that saturation effects can only be observed for amide protons located close to NiR. Interface residues with exposed side chains but buried amide protons may remain unaffected. The residues indicated in Figure 5.3A thus represent the minimal binding interface.

In previous studies (Kukimoto, 1996; Kukimoto, 1995) mutagenesis of PAZ and NiR was used to identify the region of PAZ involved in binding with NiR. Lysine residues surrounding the hydrophobic patch around the copper center in PAZ and some negatively charged residues on NiR surface around its type 1 copper centre were replaced by uncharged residues. While all the PAZ mutants retained the ability to transfer electrons (k_{cat} did not change significantly upon mutation), an increase of the K_m value for PAZ mutants involving K38, K77, K10 and K57 indicated that the affinity for NiR was affected. Mutations of negatively charged residues on NiR (E118, E197, D201, E204 and D205) also affected the binding affinity for PAZ, suggesting that electrostatic interactions are of importance for complex formation.

In the experiment described in this chapter, 7 of the 13 residues identified as affected most by the c.s.t., (G39, I60, M84, A15, I110, A83 and Y82) are non-polar residues. K38, K109 and K107 represent the charged residues involved in the complex formation. Furthermore, the solvent exposed side chain amides of N9 and N61 are affected. The results demonstrate that the interface is at least partially of a hydrophobic nature.

Given the effects of charge mutations on the affinity observed in the kinetic studies, it can be concluded that both electrostatic and hydrophobic interactions contribute to complex formation and clearly, the kinetic studies and NMR results provide complementary information on the nature of the complex interface.
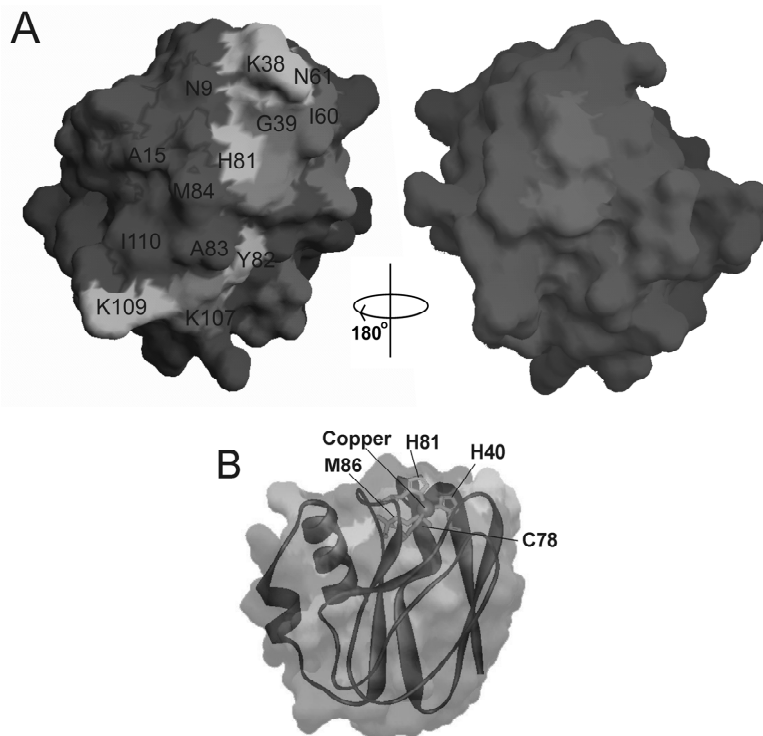
Figure 5.3.: Binding map. A) Surface representation of the PAZ Cu I structure using the colour code according to the classification shown in Figure 5.2; with intensity ratios <0.41 in red, 0.41-0.51 in orange, 0.52-0.55 in yellow and >0.54 in blue. Residues for which no data are available (prolines, K46, D47) are shown in grey. Relevant residues are indicated. B) Semi-transparent representation, tilted relative to A) to show the location of the copper site. The figure was produced using GRASP (Nicholls, 1991). (For a color picture see Appendix).

Figure 5.4: ^{1}H/^{15}N TROSY spectrum without irradiation of ^{2}H/^{15}N PAZ Cu I 1mM in complex with NiR Cu I-T2D (0.2mM in trimer) in 20 mM potassium phosphate buffer pH 6.5 and in 10% H_2O / 90% ^2H_2O.

Figure 5.5: ^{1}H/^{15}N TROSY spectrum with irradiation of ^{2}H/^{15}N-PAZ Cu I 1 mM in complex with NiR Cu I-T2D (0.2mM in trimer) in 20 mM potassium phosphate buffer pH 6.5 and in 10% H$_2$O / 90% 2H$_2$O. The most strongly affected residues are encircled.

Chapter VI

Mapping the binding site of pseudoazurin for nitrite reductase using NMR chemical shift perturbations

Abstract

Through NMR chemical shift perturbations the binding area on the pseudoazurin surface for NiR has been determined. The experiment has been performed with PAZ and NiR in different oxidation states. The results show that the binding area is similar for all the oxidation states, despite differences in binding mode. In all cases binding is localized at the hydrophobic patch, close to the copper centre. Both polar and non-polar residues are involved in the binding, suggesting that both hydrophobic and electrostatic interactions are important for complex formation. Furthermore, the size of the shifts characterizes the PAZ-NiR complex as a 'single-orientation' complex rather than a dynamic ensemble.

6.1 Introduction

NMR titration experiments provide, under some conditions, a useful tool to describe the interaction area between proteins (Zuiderweg, 2002). Provided the complex dissociation is fast on the NMR time scale, changes in the ^{15}N-^{1}H HSQC spectra of the ^{15}N-labelled protein (e.g. PAZ) upon titration with the partner protein (NiR) can be related to the binding interface on the observed protein. In the fast exchange regime, the line width increases due to the larger correlation time of the complex as compared with the free protein, and at the same time the resonances of the nuclei that are affected by the presence of the binding partner, exhibit a chemical shift perturbation. A single set of resonances, representing the average between free and bound ^{15}N-labelled PAZ, as described in Chapter I, is observed. By following the residues that shift the most during the titration and mapping this information onto the protein surface, it is possible to localize the area involved in complex formation. Furthermore, the identification of specific residues involved in the binding sheds light on the kind of forces involved in complex formation.

Pseudoazurin (PAZ) and nitrite reductase (NiR) from *Al. faecalis* S-6 show different interaction modes according to the PAZ redox state (see Chapter III). For PAZ in the oxidized state, binding and dissociation occurs in the fast exchange regime while in the reduced state there are two binding modes, one slow and the other fast, occurring simultaneously. Hence, the chemical shift perturbation method can be applied to study the interaction in the oxidized form of the complex and also partially the one in the reduced form. To localize the binding area of PAZ and NiR in the slow exchange reduced form, cross saturation transfer has been used (Chapter V). The comparison of the binding maps obtained in the different redox states, taking into consideration the differences in the applied methods, can give a complete overview of the interactions involved.

6.2 Materials and method

Proteins purification and sample preparation as well as the NMR experiments were performed as described in Chapter III.

The average chemical shift perturbation ($\Delta\delta_{avg}$) was calculated by using the equation below (Grzesiek, S., 1996):

$$\Delta\delta_{avg} = \sqrt{\frac{(\Delta\delta N / 5)^2 + \Delta\delta H^2}{2}} \qquad \text{(eq. 6-1)}$$

in which $\Delta\delta N$ and $\Delta\delta H$ represent the changes in the chemical shifts of the amide nitrogen and proton of a given residue, respectively.

6.3 Results

6.3.1 The complex between PAZ Cu I and NiR Cu I-T2D

In an inverse titration experiment (see Chapter III) [^{15}N, ^{1}H] HSQC spectra have been recorded starting from a ratio NiR Cu I-T2D/ ^{15}N-PAZ of 5.2 and after addition of microliter aliquots of PAZ to a ratio of 0.4. Chemical shifts were followed in order to determine the residues involved in the binding with NiR and the characteristics of the binding itself. The backbone amide chemical shift perturbations for PAZ at a ratio NiR Cu I-T2D / PAZ of 1.7 compared to the spectra of the free ^{15}N-PAZ Cu I are plotted in Figure 6.1a (^{15}N on the left and ^{1}H on the right). $\Delta\delta_{avg}$ values at the same ratio (Figure 6.2a) were calculated using equation eq.6-1 reported in Materials and methods. The chemical shift perturbations identify the region of PAZ Cu I involved in the binding interface with NiR Cu I-T2D in the fast exchange mode. Figure 6.3a shows the location of the affected residues mapped on the crystal structure of PAZ (Petratos, 1988), coloured according to the colour classification indicated in Figure 6.2a. The majority of the affected residues lie in a region close to copper ligand His81. The residues strongly involved in the binding are hydrophobic (Met84 and Gly85) as well as polar (His40, His81 and Lys109). Other residues (Arg114, Ala83, Met7, Ile110 and Lys10) are also contributing to the complex formation with a smaller chemical shift perturbation upon complex formation.

6.3.2 The complex between PAZ Zn II and NiR Cu-Cu

In order to identify the binding surface of the complex between PAZ in the oxidized form and NiR, the copper atom of PAZ was replaced by Zn II. Zn II is redox inactive, enabling the analysis of the interaction with both reduced and oxidized NiR without interference of ET events. Zn II is also diamagnetic, contrary to Cu II. The paramagnetic cupric state causes severe broadening of the proton resonances in the vicinity of the metal, hindering their detection in standard NMR experiments. Structures of various metal substituted cupredoxins have been determined and have shown that there is very little change at the active site as a consequence of the metal replacement (Bonander, 2004; Moratal, 1995; Tsai, 1995; Blackwell, 1994; Nar, 1992; Church, 1986). More recent crystallographic structures shows no change between PAZ Cu and PAZ Zn (Prudêncio, 2004).

The backbone amide chemical shift perturbations were calculated from the difference between free PAZ Zn II and in the complex with NiR Cu I T2D and NiR Cu II-Cu II (Figure 6.1b and 6.1c, with ^{15}N and ^{1}H perturbation on the left and right, respectively). The average amide chemical shifts ($\Delta\delta_{avg}$) at a molar ratio of 0.15 of either NiR Cu I-T2D or NiR Cu II-Cu II over PAZ were calculated from equation eq.6-1 reported in Materials and methods, and were plotted for all PAZ residues (Figure 6.2b and 6.2c respectively).
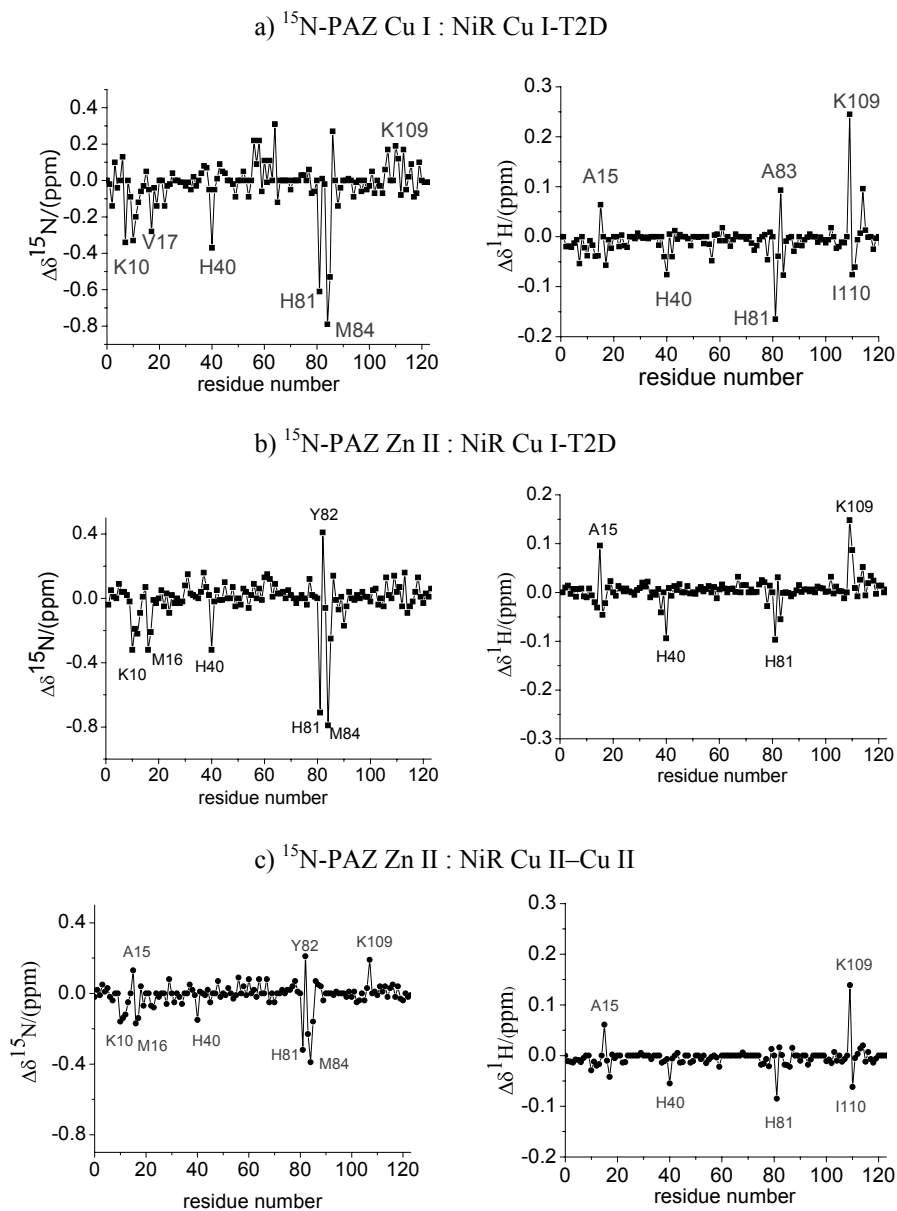
Figure 6.1: Changes in the chemical shift (Δδ) in the nitrogen dimension (left) and in the proton dimension (right) upon complex formation between a) NiR Cu I-T2D : ^{15}N-PAZ Cu I at a ratio of 1.7 and b) NiR Cu I-T2D : ^{15}N-PAZ Zn II at a ratio of 0.15. c) NiR Cu II-Cu II: ^{15}N-PAZ Zn II at a ratio of 0.10.

In Figure 6.2b and 6.2c, $\Delta\delta_{avg}$ values for ^{15}N-PAZ Zn II upon interaction with NiR Cu I-T2D and NiR Cu II-Cu II, respectively, have been mapped onto a surface representation of PAZ, colour – coded according to the size of their shift indicated with the horizontal lines of Figure 6.2b and 6.2c.

Comparing the binding maps of Figure 6.3b and 6.3c, it can be concluded that the same patch on the PAZ surface is involved in complex formation between PAZ Zn II and NiR Cu I-T2D and NiR Cu II-Cu II. As in the complex between PAZ Cu I and NiR Cu I-T2D (Figure 6.3a), the largest effects are found in the hydrophobic patch around the copper centre. Met84, Ala15 together with His40, His81 and Lys109 are strongly affected from the binding. Lys10, Met16, Val17, Tyr82, Ala83, Gly85, Lys107, Ile110 and Arg114 are also involved in the binding but show smaller perturbations.

2a) ^{15}N-PAZ Cu I : NiR Cu I-T2D

2b) ^{15}N-PAZ Zn II : NiR Cu I-T2D

2c) ^{15}N-PAZ Zn II : NiR Cu II-Cu II
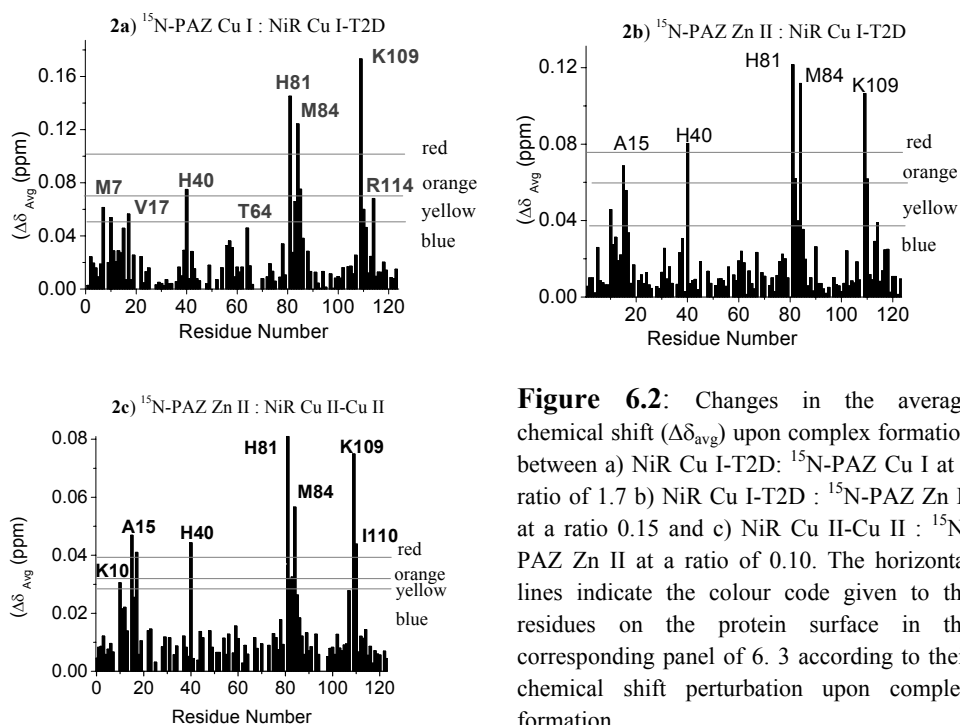
Figure 6.2: Changes in the average chemical shift ($\Delta\delta_{avg}$) upon complex formation between a) NiR Cu I-T2D: ^{15}N-PAZ Cu I at a ratio of 1.7 b) NiR Cu I-T2D : ^{15}N-PAZ Zn II at a ratio 0.15 and c) NiR Cu II-Cu II : ^{15}N-PAZ Zn II at a ratio of 0.10. The horizontal lines indicate the colour code given to the residues on the protein surface in the corresponding panel of 6. 3 according to their chemical shift perturbation upon complex formation

85

**a) PAZ Cu I : NiR Cu I-T2D
(inverse titration)**
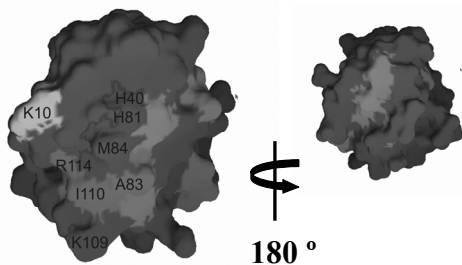
**b) PAZ Zn II : NiR CuI-T2D
(direct titration)**
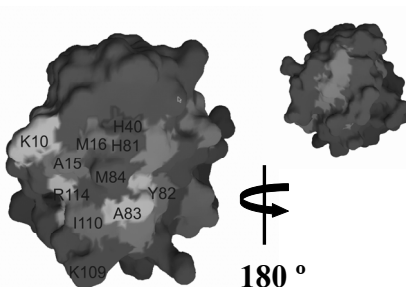
c) PAZ Zn II : NiR Cu II-Cu II

(direct titration)

3) PAZ Cu I : NiR Cu I-T2D

(cross saturation transfer method)

Figure 6.3: Mapping of the $\Delta\delta_{avg}$ on the surface of PAZ (front side on the left and back side on the right) for the complexes a) NiR Cu I-T2D : ^{15}N-PAZ Cu I at a ratio of 1.7 in the inverse titration; b) NiR Cu I-T2D :[15]N-PAZ Zn II at a ratio 0.15 in the direct titration; c) NiR Cu II-Cu II :[15]N-PAZ Zn II at a ratio of 0.10 in the direct titration and d) map obtained with cross saturation transfer for complex formation between NiR Cu I-T2D and ^{15}N-PAZ Cu I at a ratio of 0.7. Residues are colour-coded according with the horizontal line in Figure 6.2a, b and c (for Figure 6.3a, b and c respectively). In figure 6.3d the colour code according to the classification shown in Figure 5.2 in Chapter 5 has been used. (For a color picture see Appendix).

6.4 Docking calculations

Docking calculations were carried out with the programme Bigger (Bimolecular Complex Generation with Global Evaluation and Ranking) (Morelli, 2001; Palma, 2000) which requires as input a 3D structure for each of the two interacting proteins. The structure of the complex is then calculated through a soft docking approach. The algorithm used for calculation procedure consists in two steps called "searching and filtering" and "scoring" In the first step the programme generates a population of docked geometries with a maximal surface matching. Each protein is converted into a matrix of cubic cells of $1A^3$ size; the largest protein is used as target and the smallest as the probe. First the probe is translated with respect to the target to obtain optimal surface matching. The probe is then rotated in steps of 15˚. The process is repeated to achieve a complete search of the interaction space.

Experimental results derived from NMR chemical shift perturbation have been used as constraints. The algorithm recently in use is meant to restrict the docking search from the start so that all models generated fit the constraints. The result of this procedure is an ensemble of 5000 possible model structures for the complex, selected on the basis of best surface matching.

For subsequent analysis, the 5000 model structures in the above ensemble are ranked based on computational score functions. To this end, a so called "global scoring function" defined from the combination of several terms is computed by the program. The scoring function combines several interaction terms: geometric packing of the surfaces, electrostatic interactions, desolvation energy, and pair-wise propensities of the amino-acid side chains to contact across the molecular interface. The simulation was carried out with and without experimental constraints.

In the present calculation the following residues on PAZ surface were used as constraints for docking calculation because they are the most affected during chemical shift perturbation experiments: Lys109, His 81, His 40, Ala15, Met84, Ile110, Met16, Tyr82.

Inspection of the 200 highest ranking complexes provides very similar results either with or without experimental constraints. Considering more than 200 ranking solutions does not change the results.

Since the results were obtained for docking at just one side of the NiR trimer, a symmetry operation was performed in order to obtain the same results for the other two NiR subunits. The process simply consists of saving the first 200 solutions as water molecules in a pdb format (the spheres in Figure 6.4) plus one subunit of the NiR, then use the structure alignment tool of Chemera (http://www.dq.fct.unl.pt/bioin/chemera/) to align this subunits with each of the three monomers in NiR. The results obtained are presented in Figure 6.4. The experimentally ranked docking calculations suggest a unique binding site of PAZ for each NiR monomer with a Cu (PAZ)-Cu (type1 NiR) distance of ~14 Å. The distance between the copper ligands His81 of PAZ and His of NiR is ~8 Å.

In Figure 6.5 is depicted the interface of the complex between PAZ and a NiR subunit of the top ranking solution, showing that the interaction between the two proteins occurs through the hydrophobic patch around the type 1 copper site on both PAZ and NiR. The hydrophobic patch around type1 copper site of NiR is indicated as the binding site for PAZ.

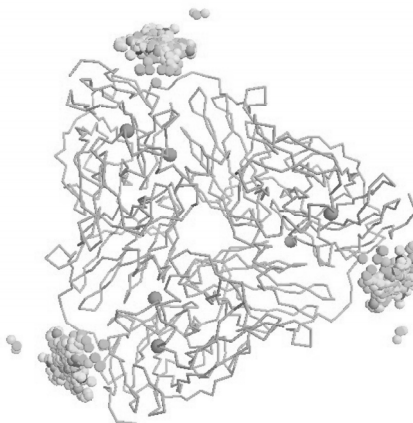These results clearly suggest that hydrophobic interactions are important in complex formation.

Figure 6.4: The experimentally ranked docking geometries generated by BIGGER programme. NiR is depicted as C^α trace with the type1 and type2 coppers shown as green spheres. The geometric centre of PAZ is represented by spheres in each of the top 200 orientations. The colour indicates the ranking position on a scale from blue to red with red indicating the highest ranking. (For a color picture see Appendix).
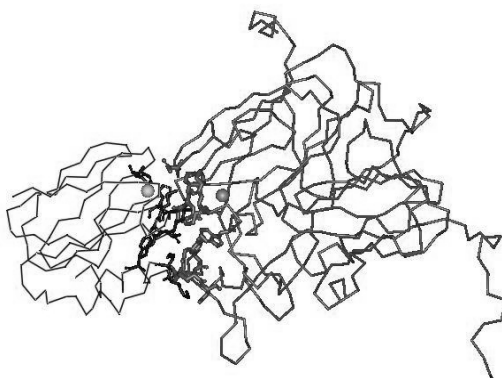
Figure 6.5: Top ranking orientation of PAZ to NiR subunit. PAZ and NiR are depicted as C^α trace with the residues at the interface in sticks. Copper atoms are indicated as spheres in blue on PAZ and orange on NiR.

The minimum distance between any atom on the probe (PAZ) and the selected atoms on the target (NiR) have been identified from the top ranking structure. The histograms in Figure 6.6 present for each NiR residue in the interface the distribution of distances between that residue and PAZ for the 200 best docking solutions. The histograms reported here are for those NiR residues for which the distance from PAZ surface, for at least 30% of the 200 structures considered, is within 4 Å from PAZ. From the reported histograms it is possible to notice that for the corresponding residues (Thr92, Leu93, Met94, Asn115, Pro116, Met141, Trp144, Glu197, Gly200, Asp201, Tyr203, Glu204, Asp205) the majority of the solutions are within a limited distance from the target NiR residue, thus identifying a unique binding site for PAZ on the NiR surface a result of the docking calculation. It is important to notice that Glu197, Glu204 Asp201 and Asp205 have been indicated in previous mutagenesis/kinetics experiments as those involved in the binding with PAZ together with E118 (Kukimoto, 1996). The importance of tryptophane in the binding area has been demonstrated for nitrite reductase from *Al. xiylosoxidans* in complex with its partner azurin (Barrett, 2004). Mutation of Trp138 to His has little effect on the overall structure of nitrite reductase while the enzymatic activity with its physiological electron donor azurin significantly decreases. Trp138 occupies a strategic position between His139, Type 1 Cu ligand and Tyr197, identified in a docking model (Murphy, 2002), as a residue involved in the binding interface. The intramolecular electron transfer is proposed to occur from azurin the His117 Cu ligand, via a trough-space process between the two aromatic side chains of Trp138 and Tyr197, to His139 type 1 Cu ligand of nitrite reductase, suggesting that Trp138 plays a key role in the electron transfer between the two proteins. The docking model presented here suggests that Trp144 and Tyr203 of NiR might play the same role as described above.

The binding site is depicted in Figure 6.7 for one of the three NiR subunits

The closest contacts in the top ranking solution between PAZ and NiR are listed in Table 1. A possible electron transfer pathway from PAZ to NiR, identified on the basis on the smallest distance between residues close to the copper centre, might involve His81 or Pro80 on PAZ side and Met94 and His95 on NiR side.

Distance between Asp205 (NiR) and PAZ
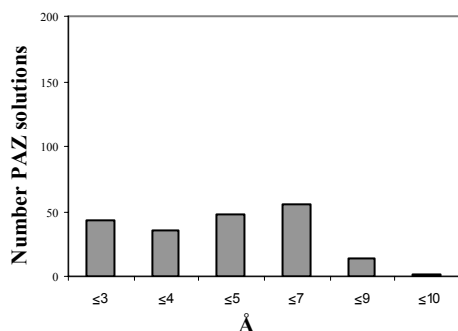
Figure 6.6: The histograms indicate NiR residues (Thr92, Leu93, Met94, Asn115, Pro116, Met141, Trp144, Glu197, Gly200, Asp201, Tyr203, Glu204, Asp205 indicated on the figure title) which are within 4 Å from PAZ surface at least in 30% of the 200 structures. The histograms indicate the number of structures and their corresponding minimum distances from any atom on the probe (PAZ) and the selected residue on the target (NiR).
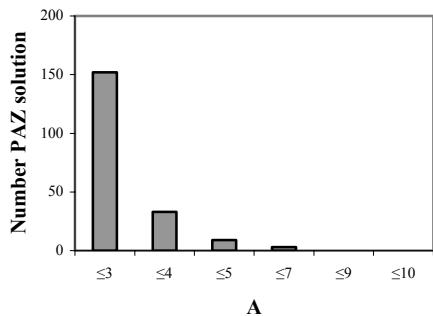
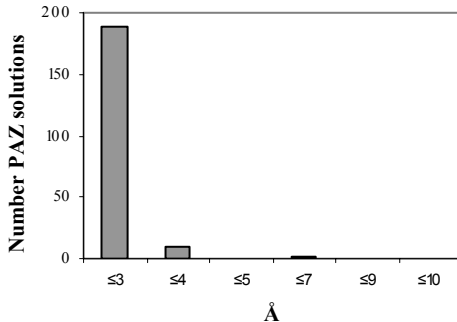**Figure 6.6**: Continued
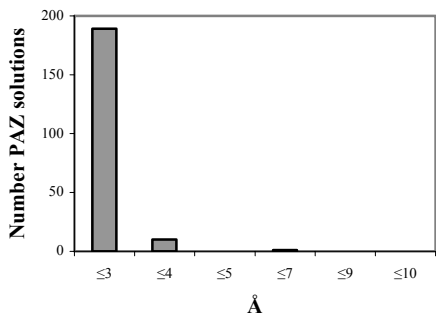
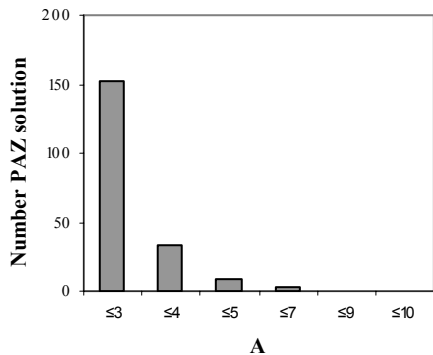**Distance between Asn115 (NiR) and PAZ** **Distance between Gly200 (NiR) and PAZ**
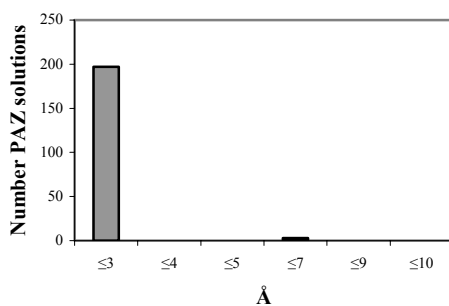
Distance between Met141 (NiR) and PAZ **Distance between Asn115 (NiR) and PAZ**

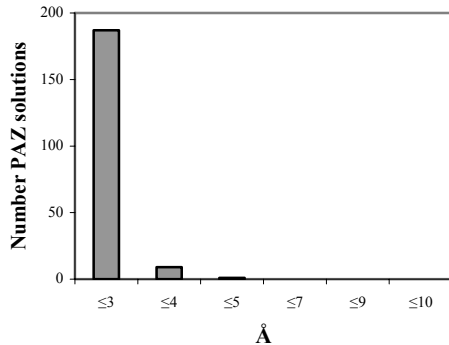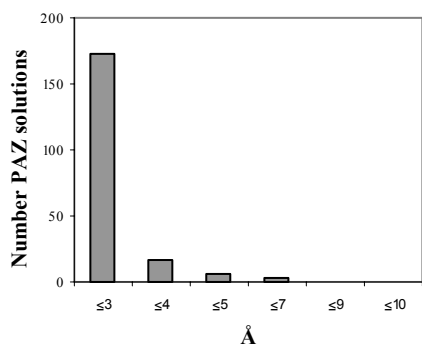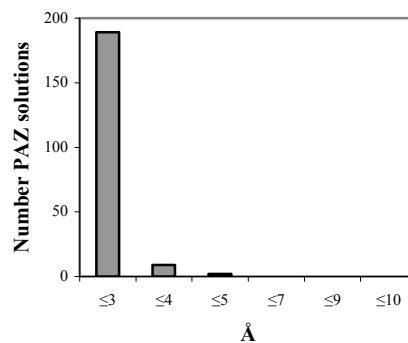**Distance between Asp 201 (NiR) and PAZ** **Distance between Gly200 (NiR) and PAZ**
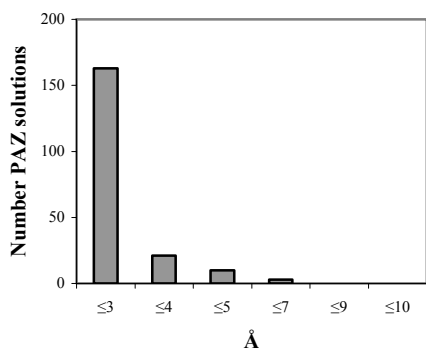
Figure 6.6: Continued
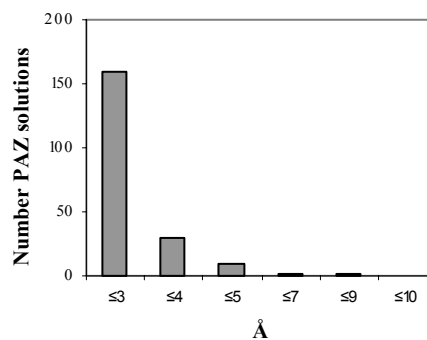
Distance between Glu204 (NiR) and PAZ

Distance between Met94 (NiR) and PAZ

Distance between Thr92 (NiR) and PAZ

Distance between Pro116 (NiR) and PAZ

Distance between Pro139 (NiR) and PAZ
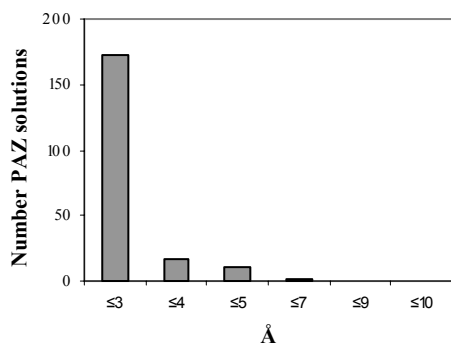
Distance between Glu197 (NiR) and PAZ
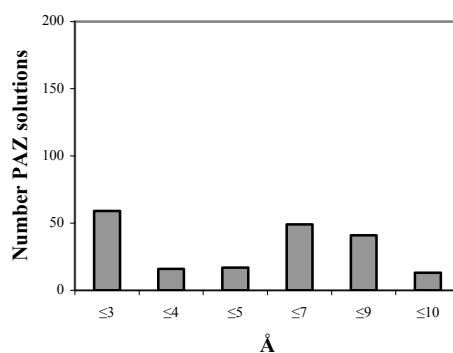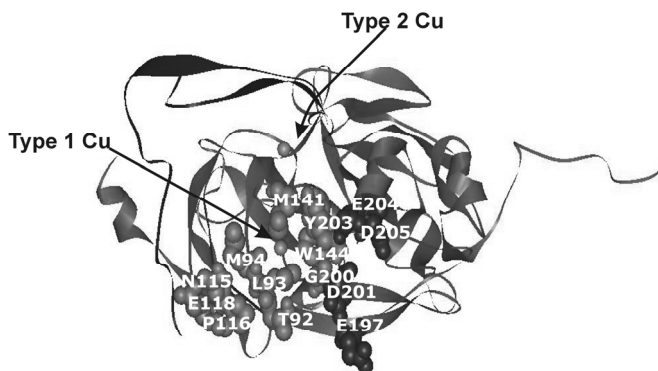
Figure 6.7: Binding site on the surface of NiR subunit surface. The residues involved in the interaction are depicted as green spheres and labelled, the dark green spheres indicate those residues that have been also identified as involved in the binding in the mutagenesis and kinetic studies (Kukimoto, 1996). E118 which also results involved in the binding in the mutagenesis and kinetic studies is depicted as blue spheres. The remaining protein is depicted in ribbons (one monomer in green and the tail of the adjacent monomer in blue) and the two copper atoms as orange spheres. (For a color picture see Appendix).

Table 6.1: List of the distances between residues on the binding surface of PAZ and those on NiR, observed for the top ranking docking solution.

NiR	2-3 Å (PAZ)	4-5 Å (PAZ)	<7Å (PAZ)
Thr92	Pro80	Thr79, His81, Tyr82	Lys77,Cys78, Ala83, Met84
Leu93		Pro80, Ala83, Met84	Thr79, His81, Tyr82, Gly85
Met94		Met16, Pro80, His81	Asn9, Gly39, Thr79, Met84
Asn115		Lys38, Gly39, His40, Ile60, Pro80, His81	Asn61, Cys78
Pro116		Ile60, Pro80	Gly39, Thr79, His 81
Met141	Met 84	Ala15, Met16, Ala83	His81, Ala83, Gly85, Met86
Trp144		Ala83, Met84	Ile110
Glu197	Lys106		Lys107
Gly200	Ala83, Pro108	Met84, Lys109, Ile110	Tyr82, Gly85, Lys107, Val111
Asp201	Pro108, Lys109	Lys106, Lys107, Ile110	Tyr82, Ala83, Val111
Tyr203		Ala83, Lys109, Ile110	Ala15, Met84, Gly85, Pro108, Val111, Glu113, Arg114
Glu204	Lys109, Ile110	Pro108, Val111, Glu113	Ala83, Gly85, Lys107, Gln112, Arg114
Asp205	Lys109		Ile110, Glu113

Among the 11 most affected residues in the chemical shift perturbation experiments, 4 hydrophobic residues on PAZ (Ala15, Met16, Met84, Ala83) are close to hydrophobic residues on NiR, 4 polar residues on PAZ (His81, Asp114, His40, Tyr82) are close to polar residues on NiR while K109 positively charged seems to be very close to the negatively charged residue of NiR E204,.

In conclusion, docking results seem to confirm that the complex between PAZ and NiR occurs via hydrophobic as well as electrostatic interactions.

6.5   Discussion

The $[^{15}N\text{-}^{1}H]$-HSQC spectra of ^{15}N-PAZ in both redox states have been monitored during titration with the unlabeled interaction partner (NiR), also in two redox states. The interaction with NiR causes changes on PAZ binding interface; hence it affects the chemical shifts of the nuclei in this area. The identification of the affected residues and the quantification of the chemical shift perturbations allow to discern not only the interface of the complex on the PAZ surface but also the type of the interaction (hydrophobic or electrostatic) between the two proteins.

Determination of the binding surface through chemical shift perturbations has been possible for PAZ in the oxidized state in complex with NiR Cu-Cu or NiR Cu-T2D either oxidized or reduced and for one of the two binding modes (see Chapter III) between PAZ Cu I and NiR Cu I-Cu I or NiR Cu I-T2D.

It is important to note that the chemical shift perturbations are caused in both reduced and oxidized states by the complex formation. This is confirmed by the fact that the direction of the shift in the nitrogen and proton dimension for both reduced and oxidized PAZ is very similar (Figure 6.1a and 6.1b). Chemical shift perturbations can also arise from pHs effects but, as discussed in Chapter IV, the effect of pH on the PAZ spectrum are unrelated to those observed for complex formation.

Comparing the binding maps between PAZ and NiR in different redox states, it is evident that the binding area is located around the His81 copper ligand. Ala15, Met16, Tyr82, Ala83, Met84 and Ile110 are the apolar residues involved in the binding while His 40 and His 81 (both copper ligands) together with Lys10, Lys107, Lys109 and Arg114 are the polar ones. The binding surface in the oxidized form of the complex is larger compared with the reduced one, because of the involvement of Ala15, Met16 and Tyr82.

Observing the binding map obtained via cross saturation transfer, which corresponds to the slow exchange binding mode between PAZ Cu I and NiR Cu I-T2D, it is possible to notice a more extended area involved in the binding compared with the one obtained via the chemical shift perturbations. The differences in binding maps may be attributable to differences in the applied methods. For example, amide groups which are not on the protein surface will be less affected by cross saturation transfer although the corresponding side-chain may be involved in binding, like residue His 81. However, it may also be that the larger binding area is a consequence of the tighter binding in the slow exchange mode observed with the c.s.t. method.

Previous studies on electron transfer complexes have shown the importance of electrostatic and hydrophobic interactions as well as their balance for the characteristics of the complex (Worrall, 2003; Worrall, 2002; Murphy, 2002; Crowley, 2002a; Crowley, 2002b; Crowley, 2002c; Bergkvist, 2001; Crowley, 2001; Worrall, 2001; Ejdebäck, 2000; Morelli, 2000a; Morelli, 2000b; Pettigrew, 1999; Goodfellow, 1999; Ubbink, 1998; Ubbink, 1997; Gray, 1988). It has been established that some complexes exist largely in a single conformation, for example the complexes of cyt f and plastocyanin from higher plants and the cyanobacterium *Phormidium laminosum* (Crowley, 2001; Ubbink, 1998) and the complex of yeast cytochrome c peroxidase and cytochrome c (Worrall, 2001). In those cases, a specific orientation is maintained for a large part of the lifetime of the complex by both electrostatic and hydrophobic interactions. A consequence of this type of interaction is the occurrence of relatively large chemical shift perturbations in a localized area of the surface ($\Delta\delta_{avg} \approx 0.3$ ppm extrapolated to the 100% bound state) upon complex formation. Other complexes seem to occur in a dynamic ensemble of conformations, like the complex of myoglobin and cytochrome b_5 (Worrall, 2001). In these complexes, there is not a single specific orientation, but rather numerous conformations exist with similar energies. In this case the interaction is predominantly electrostatic. Consequently, chemical shift perturbations are smaller ($\Delta\delta_{avg} \approx 0.019$ ppm extrapolated to the 100% bound state) and the binding area is less localized.

In the case of PAZ and NiR the $\Delta\delta_{avg}$ could not be extrapolated to 100% binding. However, in the complex between NiR Cu I T2D and PAZ Zn II at a ratio of 0.15 in which only 15% of PAZ can be in the bound state, a $\Delta\delta_{avg}$ of 0.12 ppm is observed for His81. This would translate into a $\Delta\delta_{avg}$ of ~ 0.7 ppm at 100% bound, which represents a large shift. The same is true also for the complex between PAZ Zn II and NiR Cu II-Cu II. In the case of PAZ Cu I and NiR Cu I-T2D, two binding modes are involved, one tighter and the other weaker. On the basis of Scheme 1 in Chapter III, it can be estimated that the chemical shift perturbation represents about 20% bound state in fast exchange with the free protein. Thus, the $\Delta\delta_{avg}$ of 0.16 ppm observed for Lys 109 would translate in a $\Delta\delta_{avg}$ of 0.8 ppm in the 100% bound state (fast exchange mode). These data suggest a well-defined orientation in all cases for PAZ in complex with NiR.

As suggested already for other ET complexes, charged residues through long range interactions may play a pivotal role in the formation of the encounter complex, while the hydrophobic interactions help to orient the proteins into a single orientation suitable for the ET reaction. Our results clearly suggest that a combination of electrostatic and hydrophobic forces enable fast and specific binding, essential for efficient electron transfer from PAZ to NiR as well as rapid turnover of the complex.

Chapter VII

Interaction between azurin and nitrite reductase from *Neisseria gonorrhoeae* by NMR

Abstract

It has been suggested that azurin and nitrite reductase are physiological ET partners in Neisseria gonorrhoeae (Boulanger, 2002). The possibility of complex formation between these two proteins was tested by NMR spectroscopy experiments. These proteins have crystal structures similar to PAZ and NiR from *Al. faecalis*, but the azurin surface charge distribution is different from that of PAZ. The experiments show no evidence for complex formation. The absence of any detectable interaction is attributed to their membrane location. Consequently, the proteins may interact via a different mechanism for example in a collisional fashion.

7.1 Introduction

The gene for nitrite reductase (AniA) of the obligate pathogen *Neisseria gonorrhoeae* (Mellies, 1997) is a component of a denitrification system which is strongly induced when grown anaerobically *in vitro* in the presence of nitrite (Knapp, 1984).

The sequence of AniA (Hoehn, 1992a) reveals a lipoprotein consensus sequence similar to those of other proteins present in the gonococcal outer membrane. Via mutagenesis it has been shown that an oxygen-depleted environment was necessary for AniA growth and that aniA expression was higher under anaerobic conditions in presence of nitrite, suggesting AniA as a nitrite reductase.

Database searches revealed significant homologies between AniA and copper-containing nitrite reductases from several denitrifying bacteria. Type 1 and type 2 ligands are conserved, as are the active site residues Asp97 and His 240 (see Chapter I). AniA shares 45% sequence identity with *Haloarcula marismortui* nitrite reductase but only 26% with NiRs from *Al. faecalis* S-6 and *Al. xylosoxidans. S*till, the 3D structure of AniA is similar to those of the latter NiRs (Boulanger, 2002).

A small blue copper protein has also been identified in *N. gonorrhoeae,* called azurin (Laz) (Woods, 1989). It contains a pentapeptide repeat typical of outer membrane proteins. It has been suggested that this azurin acts as electron donor for AniA, with both proteins tethered to the outer membrane via palmityl fatty acid chains (Boulanger, 2002).

To find support for this hypothesis, the interaction between Laz and AniA was studied by NMR spectroscopy using chemical shift perturbation analysis.

7.2   Materials and Methods

7.2.1   *Proteins preparation*

Azurin expression and purification
Part of the azurin gene, coding for the mature protein without the palmitoylation sequence and the linker peptide, has been subcloned in pET-28a (+), creating a plasmid for expression in the cytoplasm of *E. coli*. The gene contains a His-tag and a thrombin protease cleavage site for His tag removal. The plasmid was kindly provided by Prof. M.E.P. Murphy and Dr. M. Boulanger (Univ. of Br. Columbia, Vancouver, Canada). The protein was produced in *E. coli* strain HMS174, cultured on minimal medium containing $^{15}NH_4Cl$. Cultures were incubated at 37°C with 250 rpm shaking to an OD_{600} of 0.7. Expression was induced with 0.5 mM IPTG, and 100 μM copper citrate was added. Ten hours after induction cultures were harvested by centrifugation. Cell pellets were resuspended in 20 mM phosphate buffer pH 7.0 containing 500 mM NaCl, 1 mM PMSF, DNase and 0.5 mM $CuCl_2$ and lysed using a French press cell (15.000 PSIG). After centrifugation for 15 min at 10.000 rpm the supernatant was dialysed against 20 mM phosphate buffer pH 7.0 and loaded onto a nickel affinity column for protein purification. Azurin eluted at 250 mM imidazole. This yielded a protein with a purity of >95% as determined by SDS-PAGE. The His-tag was removed by thrombin digestion overnight at 4˚C. A final dialysis step against

phosphate buffer 20 mM pH 7.0 supplemented with 10mM copper chloride yielded 35 mg L^{-1} of culture of pure protein.

The amino acid sequence of the recombinant protein, based on the DNA sequence was (132 amino acid with a molecular weight of 13903.6 Da for the apo protein)

G S H M A S N C A A T V E S N D N M Q F N T K D I Q V S K A C K E
F T I T L K H T G T Q P K A S M G H N L V I A K A E D M D G V F K
D G V G A A D T D Y V K P D D A R V V A H T K L I G G G E E S S L
T L D P A K L A D G D Y K F A C T F P G H G A L M N G K V T L V D

AniA expression and purification

Part of the AniA gene, coding for the mature protein, has been subcloned in pET-28a (+), creating a plasmid for expression in the cytoplasm of *E. coli*. The gene lacks the palmitoylation signal and contains a thrombin protease cleavage site in front of a C-terminal His-tag. The plasmid was kindly provided by Prof. M.E.P. Murphy and Dr. M. Boulanger (Univ. of Br. Columbia, Vancouver, Canada).

AniA was expressed in *E.coli* strain BL21 (DE3) transformed with the plasmid pET28a (+)Ania. A 10 ml 2xYT/kanamycin (100 mg/L) preculture grown at 30°C at 250 rpm for 6 h was used to inoculate 1 L of 2xYT/Kanamicyn (100 mg/L). Cultures were grown under the same conditions to an OD_{600} = 1.0 and then expression was induced by addition of 0.5 mM IPTG. At this point temperature was reduced to 25°C and, after 10 h, cultures were harvested by centrifugation. Cell pellets were resuspended in 20 mM phosphate buffer pH 7.0 containing 500 mM NaCl, 1 mM phenyl-methyl-sulphonyl-fluoride (PMSF), DNase, 0.5 mM $CuCl_2$ and lysed using a French press cell (15.000 PSIG).

After centrifugation for 15 min at 10.000 rpm the supernatant was dialysed against 20 mM phosphate buffer pH 7.0 and loaded onto a nickel affinity column to purify the protein. The protein purity was > 95% as determined by SDS-PAGE. The His-tag was removed with a thrombin digestion overnight at 4˚C. A final dialysis step was done against phosphate buffer 20 mM pH 7.0 supplemented with 10 mM copper chloride. The procedure yielded 20 mg/L of culture of pure protein.

7.2.2   *NMR samples and experiments*

NMR samples for direct titration (AniA titrated into Laz) were prepared with 0.3 mM of ^{15}N-Laz Cu I in 20 mM Na$^+$ phosphate. AniA Cu I-Cu I at 1.3 mM subunit concentration was prepared in the same buffer and 1.0 mM sodium ascorbate and 10% D_2O for lock. Protein concentrations were determined optically following the characteristic absorbance peaks: at 624 nm for Laz Cu II (ε = 5.9 mM^{-1} cm^{-1}). For AniA Cu II-CuII monomer the concentration was determined optically following the absorbance at 598 nm (ε = 6.0 mM^{-1} cm^{-1} per subunit).

The solutions were degassed by blowing argon over the surface.

[^{15}N-^{1}H] HSQC spectra of Laz were recorded after addition of microliter aliquots of AniA. The effects on peak intensities, line widths and chemical shifts were analysed. Titrations were performed at 313 K and 293 K at pH 6 and 7. All NMR experiments were performed

at 14.1 T on a Bruker DMX600 spectrometer equipped with TXI-Z-GRAD (^{1}H, ^{13}C and ^{15}N) probe.

Spectra were processed in AZARA (available from http://www.bio.cam.ac.uk/azara/) and analyzed with the assignment programme ANSIG (Helgstrand, 2000; Kraulis, 1989).

7.3   Results

7.3.1   [^{15}N-^{1}H] HSQC of Laz

The [^{15}N-^{1}H]-HSQC spectra of Laz (Figure 7.1) has the characteristics of a folded protein with dispersed cross peaks. The number of expected resonances from LAZ sequence is 145 (132 residues minus the presence of 4 Pro and the N-terminal amino group which are not detectable in these spectra, as well as the side chain amide signals of six Asn and three Gln). However, ~ 200 peaks are observed in the spectrum and some of them seem to belong to the same residue (double peaks), suggesting that LAZ it exists in two forms. The reason for this is unclear; it could be due to incomplete removal of the His-tag or the presence of Zn containing LAZ.

7.3.2   The complex of ^{15}N- Laz Cu I and AniA

Reduced AniA Cu I-Cu I was titrated into reduced ^{15}N-Laz Cu I and the effects of possible complex formation were analyzed by recording [^{15}N-^{1}H] HSQC spectra and following the effects on intensity, line width and chemical shift of the amide resonances of Laz. Titrations were performed at 20°C and 40°C and at pH 6 and 7. In all titrations even at 0.8 mol.eq. of AniA subunits, the signal intensities of ^{15}N-Laz Cu I showed only a small decrease caused by dilution (Figure 7.2). Signals did not show an increase in the line width and no chemical shift perturbations were observed.

7.4   Discussion

The NMR titration experiments present no evidence for complex formation between Laz and AniA from *N. gonorrhoeae*. The absence of any spectral changes upon AniA additions into a Laz solution indicates that, under the experimental conditions described above, the two proteins do not interact. Any complex formation would have to exhibit a very low affinity ($K_d \gg 1$mM) to remain unobservable in these experiments.

In previous work the surface characteristics of AniA described in Chapter I have been suggested to be a requirement for Laz binding. More precisely, the absence of two loops close to the supposed docking site, which are present in NiR from *Al. faecalis,* have been suggested to promote an intimate interaction between Laz and AniA (Boulanger, 2002).

The model of the structure of Laz (Figure 1.5b, Chapter I) shows many negative residues on the surface and, moreover, its pI of 4.7 is low compared with that of other azurins (*Ps. Aeruginosa,*

pI 5.7). Also AniA has many negative surface residues (pI 5.3), resembling NiR from *Al. faecalis* (pI 5.6).

Thus, while PAZ and NiR from *Al. faecalis* have an opposite net charge, Laz and AniA are both negatively charged. Hence, the electrostatic repulsion is the likely cause for the absence of high affinity complex formation between the two proteins.

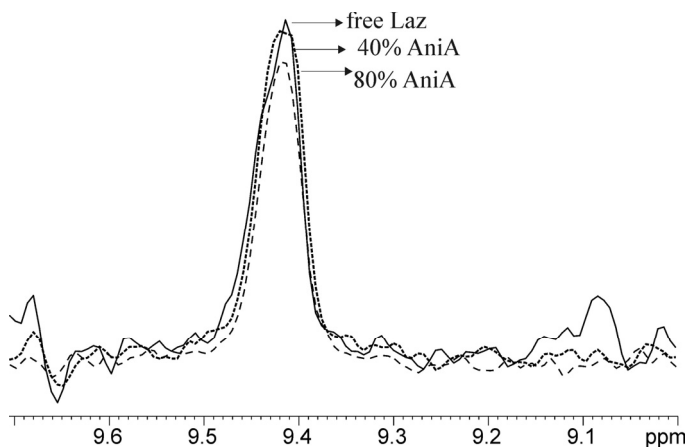**Figure 7.1**. ^{1}H-^{15}N-HSQC spectrum of Laz Cu I (20 mM potassium phosphate pH 6.5, 25ºC).
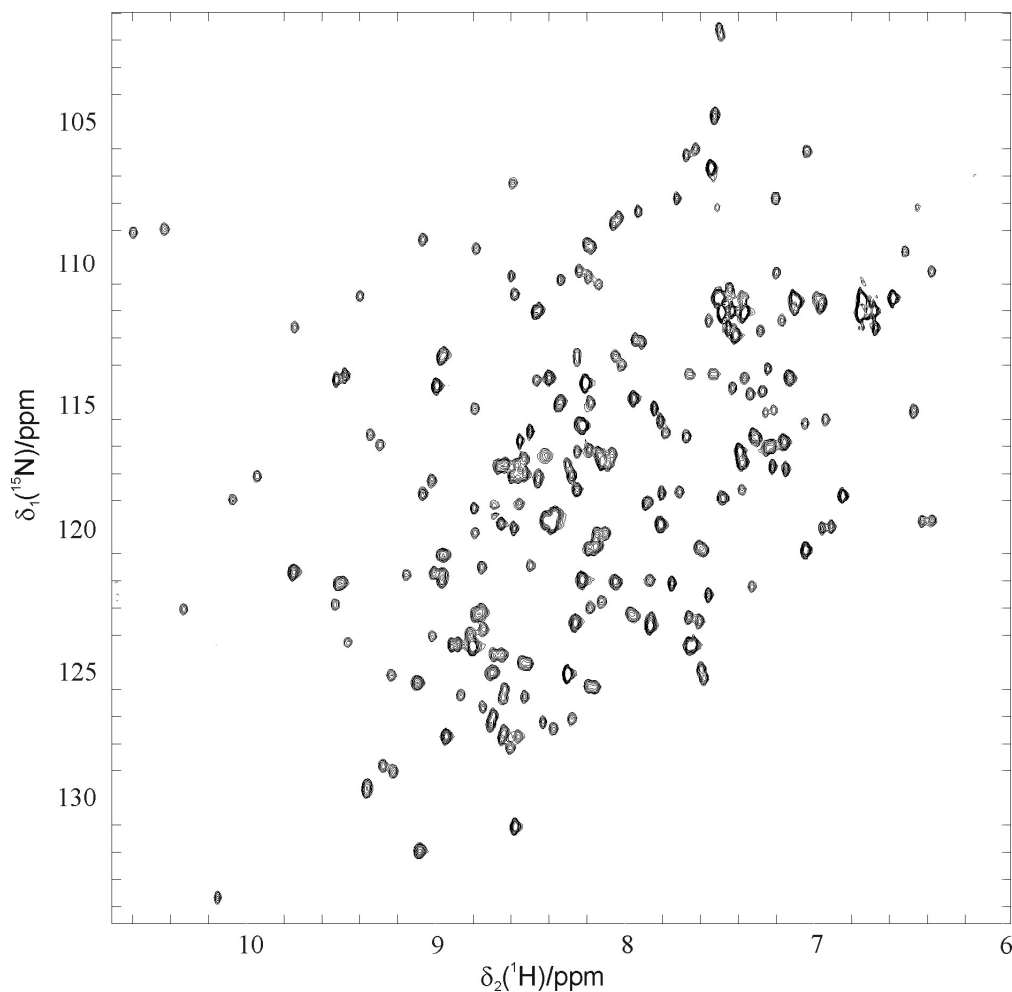
Figure 7.2: Cross-section along the F2 ^{1}H (F1 ^{15}N 111.5 ppm) dimension through a Laz amide resonance. The solid line represents the resonance of free Laz, dotted and dashed peaks represent the same resonance in the presence of 0.4 and 0.8 mol.eq. AniA subunits, respectively. The small decrease in the intensity during direct titration can be attributed to dilution.

This does not imply that Laz and AniA cannot be physiological redox partners. Fast ET can also occur via a collisional mechanism (Hervas, 1995) in which the proteins only form a very transient, low affinity but ET effective complex. The fact that both Laz and AniA are membrane bound may help to ensure high local concentrations and thus fast ET.

However, on the basis of the reported results, it can be concluded that the mechanism of ET between this nitrite reductase and its proposed partner must be very different from that of PAZ and NiR of *Al. faecalis*.

Chapter VIII

General discussion

8.1   Introduction

In this work the interaction between pseudoazurin and nitrite reductase from the denitrifying bacteria *Alcaligenes faecalis* S-6 has been characterized. The aim of the work was to analyze the nature of the interface of the complex to understand the molecular details of transient complex formation and how an appropriate compromise between specificity and affinity can be achieved. Various NMR spectroscopy techniques such as chemical shift perturbation analysis and cross saturation transfer have been used as tools for this investigation. For this purpose, first the assignment of the NMR spectra of PAZ Cu I (^{1}H, ^{13}C, ^{15}N) and Zn II (^{1}H, ^{15}N) was obtained (Chapter II).

8.2   Redox dependent binding between PAZ and NiR

Perhaps the most remarkable finding of the work was the redox state dependent binding modes of PAZ for NiR (Chapter III). NMR titration experiments demonstrate that PAZ in the reduced state interacts with NiR in a slow exchange mode with relatively high affinity. However, the results also present evidence for a simultaneous binding mode that has the characteristics of a fast exchange interaction. The dissociation constant for the combined interaction is ~100 μM, which has to be interpreted as an apparent dissociation constant, because it represents more than one equilibrium (Chapter III, Scheme 1). At equilibrium a large fraction of PAZ is bound to NiR in the slow exchange mode, while only 5-15% of the remaining free PAZ associates with NiR in a fast exchange mode. In the oxidized form of PAZ the results can be described by a single fast exchange mode.

In Chapter III a model is presented (Scheme 1) to describe the simultaneous occurrence of two binding modes of PAZ Cu I. It is proposed that PAZ exists in two forms, PAZ and PAZ* which possibly are in slow exchange with each other. The physical difference between the two is the subject of Chapter IV. The protonation/deprotonation of a His residue (His6 or His81) represents a plausible cause for this phenomenon because it is known that protonation of His Cu ligands (Zhu, 1998) as well as surface exposed His residues is redox state dependent.

On the basis of previous work (Sato, 2002) on pseudoazurin from *Ac. cycloclastes* (65% sequence identity with *Al. faecalis* PAZ)*,* it was assumed that also His6 in *Al. faecalis* PAZ would have a similar redox state dependent pK_a values (6.5 and 7.1 for the oxidized and reduced state in *Ac. cycloclastes* pseudoazurin, respectively). Thus, PAZ His6 presented a likely candidate to cause the redox state dependent conformational modes. Alternatively, His81, which is a copper ligand, could cause such effect although the pK_a is known to be well below the pH of the experiments (pH 6.5). By determining the pH dependence of PAZ Cu I resonances in the ^{15}N-HSQC spectra, the pK_a values of His6 and His81 were determined to be 7.2 and 4.8, respectively.

Experiments to establish the pH dependence of complex formation showed no evidence for a change in binding mechanism at pH 5.5 or 8.0 compared to pH 6.5. The only effect that was observed was a six-fold decrease in the apparent dissociation constant at pH 8. At pH 5.5 NiR was too unstable to obtain an accurate dissociation constant. It was concluded that

protonation of His6 could not be the determinant factor in the different binding mode of reduced and oxidized PAZ to NiR.

Hence, His81 remains as a candidate. At the pH range tested (5.5 – 8.0), it would not be expected that the spectral features are affected much, because the pK_a of His81 is 4.8. Furthermore, the pH titration indicates that His81 protonation is either slow or intermediate on the NMR time scale, contrary to His 6 protonation, which is fast. The same has been observed for the His 'flip' in amicyanin (Lommen, 1990)

It should be noted, that the redox-induced conformational changes at the copper site in terms of distances and angles are more limited for PAZ from *Al. faecalis* than for PAZ from *Ac. cycloclastes* (Table 8.1). Nevertheless, shifts around the copper ion were observed at pH 6.8 as structural responses to reduction in *Al. faecalis*: the copper moves to a more trigonal position and consequently, Met7 and Pro35 change their position (Libeu, 1997).

Table 8.1: Distance and angles parameter of the metal centre in pseudoazurin in *Ac. cycloclastes* and *Al. faecalis.*

PAZ	PDB entry	Distance from the Cu (Å)				Angle parameters (Å)					
		N-δ of His40 1	S-γ of Cys78 2	N-δ of His81 3	S-γ of Met84 4	Cu 1-2	Cu 1-3	Cu 1-4	Cu 2-3	Cu 2-4	Cu 3-4
Ac. cycloclastes oxidized pH 6.0	**1BQK** Resolution 1.35 Å (Inoue, T.)	1.95	2.13	1.92	2.71	107	135	100	87	114	107
Ac. cycloclastes reduced pH 6.0	**1BQR** Resolution 1.6 Å (Inoue, T.)	2.04	2.19	2.11	2.85	132	102	90	116	107	104
Al. faecalis oxidized pH 6.8	**8PAZ** Resolution 1.6 Å (Libeu)	2.20	2.14	2.27	2.67	138	100	86	111	107	109
Al. faecalis reduced pH 7.8	**1PAZA** Resolution 1.8 Å (Vakoufari,E.)	2.16	2.17	2.29	2.91	140	102	85	108	107	110
Al. faecalis reduced pH 4.4	**1PAZB** Resolution 1.8 Å (Vakoufari,E.)	2.19	2.16	3.09	2.42	138	94	97	83	122	116

Thus, there are more structural differences between the oxidized and reduced form of PAZ than the fact that His 81 is titratable in the latter only. Met7, Phe17 and Pro35 could exist in two forms in the reduced PAZ, thus representing the PAZ / PAZ* equilibrium. However, no evidence for a slow exchange in this region in the form of resonances of a second species has been observed. Furthermore, these residues are located outside the binding interface, so it is difficult to understand how they could affect the affinity for NiR so dramatically.

The K_d^{app} for PAZ Cu I and the K_d for PAZ Cu II are similar, ~ 100 µM, despite the difference in binding modes. At least under equilibrium conditions a change in the ΔE_m upon binding, which would accompany such an affinity difference, is thus not expected. Preliminary cyclic voltammetry measurements on PAZ and PAZ:NiR support this conclusion (results not shown).

8.3   Binding interface of pseudoazurin in the complex with NiR

In previous studies (Kukimoto, 1996; Kukimoto, 1995) mutagenesis of PAZ and NiR was used to identify the region of PAZ involved in binding with NiR. Lysine residues surrounding the hydrophobic patch around the copper center in PAZ and several negatively charged residues on NiR surface around its type 1 copper centre have been replaced independently with uncharged residues. While all the PAZ mutants retain the ability to transfer electrons (k_{cat} does not change significantly upon mutation), an increase of the K_m value for mutants involving K38, K77, K10 and K57 indicates that the affinity for NiR is affected. Also, mutations of negatively charged residues on NiR (E118, E197, D201, E204 and D205) decrease the binding affinity with PAZ, suggesting that the recognition of positively charged residues of PAZ by negatively charged ones from NiR is important for complex formation.

Furthermore, the presence of negatively charged residues on PAZ opposite the hydrophobic patch creates a dipole on PAZ. This dipole has been suggested to contribute to the optimal orientation of PAZ towards NiR (Murphy, 2002).

The identification of the binding interface in the reduced and in the oxidized forms of PAZ was performed by various NMR techniques and is reported in Chapters V and VI. In the reduced form of the complex, 7 of the 12 residues identified by cross-saturation transfer as those nearest to NiR in the interface are hydrophobic or aromatic residues (G39, I60, M84, A15, I110, A83 and Y82). K38, K109 and K107 represent the charged residues involved in the complex formation. Also the amide side chains of N9 and N61 are affected, and thus are close to NiR.

The fast exchange binding mode of reduced PAZ as well as the oxidized state have been studied via chemical shift perturbation analysis. Both states show very similar binding interfaces with the binding area located around the His81 copper ligand. Ala15, Met16, Tyr 82, Ala83, Met84, Ile110 are the hydrophobic and aromatic residues involved in the binding while His40 and His81 (both copper ligands) together with Arg114 and Lys residues 10, 107 and 109 are the polar ones. The binding surface in the oxidized form of the complex is larger than the reduced one with Ala15, Met16 and Tyr82 being unaffected in the latter.

Given the effects of charge mutations on the affinity observed in the kinetic studies, it can be concluded that both electrostatic and hydrophobic interactions contribute to complex formation and clearly, the kinetic studies and NMR results provide complementary information on the process of complex formation.

On the basis of these results, conclusions about the nature of the complex can be drawn. Previous structural studies on electron transfer complexes have shown the importance of both electrostatic and hydrophobic interactions and established their role in complex formation (Worrall, 2003; Worrall, 2002; Murphy, 2002; Crowley, 2002a; Crowley, 2002b; Crowley, 2002c; Bergkvist, 2001; Crowley, 2001; Worrall, 2001; Ejdebäck, 2000; Morelli, 2000a; Morelli, 2000b; Pettigrew, 1999; Goodfellow, 1999; Ubbink, 1998; Ubbink, 1997; Gray, 1988). A transient complex can be defined as a single-orientation complex or a dynamic ensemble of orientations. A single-orientation complex has been suggested to exist for the complex of cyt *f* and plastocyanin, from higher plants as well as *Phormidium laminosum* (Crowley, 2001; Ubbink, 1998) and for yeast cytochrome *c* peroxidase and cytochrome *c* (Worrall, 2001). In those cases, a specific orientation is maintained for a large part of the lifetime of the complex, stabilized by both electrostatic and hydrophobic interactions. In a dynamic ensemble, as suggested for myoglobin and cytochrome b_5, there is no specific orientation, but more orientations are possible with the same energy (Worrall, 2002; Liang, 2002). In this case, the interaction is predominantly electrostatic and not specific enough to determine a well-defined binding site. In this context the complex between PAZ and NiR appears to be characterized by a single orientation as concluded from the nature of the affected residues as well as the sizes of the chemical shift perturbations. A combination of electrostatic and hydrophobic forces, localized around the copper site, provides an optimization of the binding which on the one hand guarantees rapid electron transfer from PAZ to NiR and on the other ensures a high turnover rate essential for an electron transfer complex. As suggested already for other ET complexes, charged residues, through long-range interactions contribute to a first recognition between proteins, while the hydrophobic interactions guide the complex into a single orientation suitable for the ET reaction.

Remarkably, it was found that a system similar in its physiological function, that of azurin and nitrite reductase from *N. gonorrhoeae*, behaves differently, showing no evidence for complex formation in NMR experiments. The absence of binding suggests that these proteins interact via a collisional mechanism.

The finding suggests that different organisms have adapted the interaction between proteins according to the requirements set by the environment. Cupredoxins and in general metallo-proteins seem to offer a system with many variables in terms of surface charge, hydrophobic residues, metal charge and the structure of the metal centre with which to achieve such optimization in every situation.

Reference List

Abraham, Z.; Lowe, D.J. and Smith, B.E. Purification and characterization of the dissimilatory nitrite reductase from *Alcaligenes xylosoxidans* subsp. *xylosidans* (N.C.I.M.B. 11015): evidence for the presence of both type 1 and type 2 copper center. *Biochem J.* **295**, 587-593. **1993**.

(1968) *Reduction of dimensionality in biological diffusion process* Adam, G. and Delbrück, M. Rich A. and Davidson N. San Francisco

Adman, E.T.; Copper protein structures. *Adv. Protein Chem.* **42**, 145-197. **1991**.

Adman, E.T.; Godden, J.W. and Turley, S. The structure of copper-nitrite reductase from *Achromobacter cycloclastes* at five pH values, with NO_2^- bound and with type II copper depleted. *J. Biol. Chem.* **270**, 27458-27474. **1995**.

(2001) *Copper nitrite reductase* Adman, E.T. and Murphy, M.E.P. Messerschmidt, A., Huber, R., Poulos, T. L., and Wieghardt, K. Sussex, UK.

Akasaka, K. Longitudinal relaxation of protons under cross saturation and spin diffusion. *J. Magn. Reson.* **45**, 337-343. **1981**.

Ambler, R.P. and Tobari, J. The primary structure of *Pseudomonas* AM1 amicyanin and pseudoazurin. *J. Biochem. (Tokyo)* **232**, 451-457. **1985**.

Averill, B.A. Dissimilatory nitrite and nitric oxide reductases. *Chem. Rev.* **96**, 2951-2964. **1996**.

Back, E.; Burkhart, W.; Moyer, M.; Privalle, L. and Rothstein, S. Isolation of cDNA clones coding for spinach nitrite reductase: complete sequence and nitrate induction. *Mol. Gen. Genet.* **212**, 20-26. **1988**.

Baker, E.N. Structure of azurin from *Alcaligenes denitrificans* refinement at 1.8 A resolution and comparison of the two crystallographically independent molecules. *J. Mol. Biol.* **203**, 1071-1095. **1988**.

Bange, H.W. Global change. It's not a gas. *Nature* **408**, 301-302. **2000**.

Barrett, M.L.; Harris, R.L.; Antonyuk, S.; Hough, M.A.; Ellis, M.J.; Sawers, G.; Eady, R.R. and Hasnain, S.S. Insights into redox partner interactions and substrate binding in nitrite reductase from *Alcaligenes xylosoxidans*: crystal structures of the Trp138His and His313Gln mutants. *Biochemestry* **43**, 16311-16319. **2004**.

Bergkvist, A.; Ejdebäck, M.; Ubbink, M. and Karlsson, B.G. Surface interactions in the complex between cytochrome *f* and the E43Q/D44N and E59K/E60Q plastocyanin double mutants as determined by (1)H-NMR chemical shift analysis. *Protein Sci.* **10**, 2623-2626. **2001**.

Blackwell, K.A.; Anderson, B.F. and Baker, E.N. Metal substitution in a blue-copper protein: the crystal structure of cadmium-azurin at 1.8 Å resolution. *Acta Crystallogr. D Biol. Crystallogr.* **50**, 263-270. **1994**.

Bonander, N.; Vanngard, T.; Tsai, L.-C.; Langer, V. and Sjolin, L. The metal site of *Pseudomonas aeruginosa* azurin, revealed by a crystal structure determination of the Co(II) derivative and Co-EPR spectroscopy. *Proteins* **27**, 385-394. **2004**.

Boulanger, M.J.; Kukimoto, M.; Nishiyama, M.; Horinouchi, S. and Murphy, M.E.P. Catalytic roles of the two water bridged residues (Asp 98 and His 255) in the active site of copper-containing nitrite reductase. *J. Biol. Chem.* **275**, 23957. **2000**.

Boulanger, M.J. and Murphy, M.E. Crystal structure of the soluble domain of the major anaerobically induced outer membrane protein (AniA) from pathogenic

Neisseria: a new class of copper-containing nitrite reductases. *J. Mol. Biol.* **315**, 1111-1127. **2002**.

Chen, Z.W.; Barber, M.J.; McIntire, W.S. and Mathews, F.S. Crystallographic study of azurin from *Pseudomonas putida*. *Acta Crystallogr. D Biol. Crystallogr.* **54**, 253-268. **1998**.

Chothia, C. and Janin, J. Principles of protein-protein recognition. *Nature* **256**, 705. **1975**.

Church, W.B.; Guss, J.M.; Potter, J.J. and Freeman, H.C. The crystal structure of mercury-substituted poplar plastocyanin at 1.9-Å resolution. *J. Biol. Chem.* **261**, 234-237. **1986**.

Cole, J.A. and Brown, C.M. Nitrite reduction to ammonia by fermentative bacteria: A short circuit in the biological nitrogen cycle. *FEMS Microbiol. Lett.* **7**, 65-72. **1980**.

Crane, B.R. and Getzoff, E.D. The relationship between structure and function for the sulfite reductases. *Curr. Opin. Struc. Biol.* **6**, 744-756. **1996**.

Crowley, P.B. and Carrondo, M.A. The architecture of the binding site in redox protein complexes: implications for fast dissociation. *Proteins* **55**, 603-612. **2004**.

Crowley, P.B.; Diaz-Quintana, A.; Molina-Heredia, F.P.; Nieto, P.; Sutter, M.; Haehnel, W.; De La Rosa, M.A. and Ubbink, M. The interactions of cyanobacterial cytochrome *c*6 and cytochrome *f*, characterized by NMR. *J. Biol. Chem.* **277**, 48685-48689. **2002a**.

Crowley, P.B.; Otting, G.; Schlarb-Ridley, B.G.; Canters, G.W. and Ubbink, M. Hydrophobic interactions in a cyanobacterial plastocyanin-cytochrome *f* complex. *J. Am. Chem. Soc.* **123**, 10444-10453. **2001**.

Crowley, P.B.; Rabe, K.S.; Worrall, J.A.; Canters, G.W. and Ubbink, M. The ternary complex of cytochrome *f* and cytochrome *c*: identification of a second binding site and competition for plastocyanin binding. *Chembiochem* **3**, 526-533. **2002b**.

Crowley, P.B. and Ubbink, M. Close encounters of the transient kind: protein interactions in the photosynthetic redox chain investigated by NMR spectroscopy. *Acc. Chem Res.* **36**, 723-730. **2003**.

Crowley, P.B.; Vintonenko, N.; Bullerjahn, G.S. and Ubbink, M. Plastocyanin-cytochrome *f* interactions: the influence of hydrophobic patch mutations studied by NMR spectroscopy. *Biochemistry* **41**, 15698-15705. **2002c**.

Cutruzzola, F.; Brown, K.; Wilson, E.K.; Bellelli, A.; Arese, M.; Tegoni, M.; Cambillau, C. and Brunori, M. The nitrite reductase from *Pseudomonas aeruginosa*: essential role of two active-site histidines in the catalytic and structural properties. *Proc. Natl. Acad. Sci. USA* **98**, 2232-2237. **2001**.

Danielsen, E.; Sheller, H.V.; Bauer, R.; Hemmingsen, L.; Bjerrum, M.J. and Hansson, Ö. Plastocyanin binding to photosystem I as a function of the charge state of the metal ion: effect of the metal site conformation. *Biochemestry* **38**, 11531-11540. **1999**.

Davidson, V.L. and Jones, L.H. Complex formation with methylamine dehydrogenase affect the pathway of electron thansfer from amicyanin to cytochrome *c*-551i*. *J. Biol. Chem.* **270**, 23941-23943. **1995**.

Dennison, C. and Kohzuma, T. The alkaline transition of pseudoazurin from *Achromobacter cycloclastes* studied by paramagnetic NMR and its effect on electron transfer. *Inorg. Chem.* **38**, 1497. **1999**.

Dennison, C.; Kohzuma, T.; McFarlane, W.; Suzuki, S. and Sykes, A.G. Reactivity of pseudoazurin from *Achromobacter cycloclastes* with inorganic redox partners

and related NMR and electrochemical studies. *Inorg. Chem.* **33**, 3299-3305. **1994**.

Dennison, C.; Oda, K. and Kohzuma, T. Paramagnetic NMR studies of copper-containing nitrite reductase. *Chem. Commun.* 751-752. **2000**.

Dennison, C. and Sato, K. The paramagnetic ^{1}H NMR spectrum of Ni (II) pseudoazurin: investigation of the active site structure and the acid and alkaline transitions. *Inorg. Chem.* **41**, 6662-6672. **2002**.

Dodd, F.E.; Hasnain, S.S.; Hunter, W.N.; Abraham, Z.H.; Debenham, M.; Kanzler, H.; Eldridge, M.; Eady, R.R. Evidence for two distinct azurins in *Alcaligenes xylosoxidans* (NCIMB 11015): potential electron donors to nitrite reductase. *Biochemistry* **34**, 10180-10186. **1995**.

Dodd, F.E.; Van Beeumen, J.; Eady, R.R. and Hasnain, S.S. X-ray structure of a blue-copper nitrite reductase in two crystal forms. The nature of the copper sites, mode of substrate binding and recognition by redox partner. *J. Mol. Biol.* **282**, 369-382. **1998**.

Dose, M.M.; Hirasawa, M.; Kleis-SanFrancisco, S.; Lew, E.L. and Knaff, D.B. The ferredoxin-binding site of ferredoxin: Nitrite oxidoreductase. Differential chemical modification of the free enzyme and its complex with ferredoxin. *Plant Physiol.* **114**, 1047-1053. **1997**.

Drepper, F.; Hippler, M.; Nitschke, W. and Haehnel, W. Binding dynamics and electron transfer between plastocyanin and photosystem I. *Biochemistry* **35**, 1282-1295. **1996**.

Einsle, O.; Messerschmidt, A.; Huber, R.; Kroneck, P.M. and Neese, F. Mechanism of the six-electron reduction of nitrite to ammonia by cytochrome c nitrite reductase. *J. Am. Chem. Soc.* **124**, 11737-11745. **2002**.

Einsle, O.; Messerschmidt, A.; Stach, P.; Bourenkov, G.P.; Bartunik, H.D.; Huber, R. and Kroneck, P.M. Structure of cytochrome *c* nitrite reductase. *Nature* **400**, 476-480. **1999**.

Einsle, O.; Stach, P.; Messerschmidt, A.; Simon, J.; Kroger, A.; Huber, R. and Kroneck, P.M. Cytochrome *c* nitrite reductase from *Wolinella succinogenes*. Structure at 1.6 A resolution, inhibitor binding, and heme-packing motifs. *J. Biol. Chem.* **275**, 39608-39616. **2000**.

Ejdebäck; Bergkvist, A.; Karlsson, B.G. and Ubbink, M. Side-chain interactions in the plastocyanin-cytochrome *f* complex. *Biochemistry* **39**, 5022-5027. **2000**.

Exley, G.E.; Colandene, J.D. and Garrett, R.H. Molecular cloning, characterization, and nucleotide sequence of nit-6, the structural gene for nitrite reductase in *Neurospora crassa*. *J. Bacteriol.* **175**, 1379-2392. **1993**.

Fenderson, F.F.; Kumar, S.; Liu, M.-Y.; Payne, W.J. and Le Gall, J. Amino acid sequence of Nitrite reductase: a copper protein from *Achromobacter cycloclastes*. *Biochemistry* **30**, 7180-7185. **1991**.

Ferretti, S.; Lee, S.K.; MacCraith, B.D.; Oliva, A.G.; Richardson, D.J.; Russell, D.A.; Sapsford, K.E. and Vidal, M. Optical biosensing of nitrite ions using cytochrome *cd*1 nitrite reductase encapsulated in a sol-gel matrix. *Analyst* **125**, 1993-1999. **2000**.

Fleischmann, R.D.; Adams, M.D.; White, O.; Clayton, R.A.; Kirkness, E.F.; Kerlavage, A.R.; Bult, C.J.; Tomb, J.F. Whole-genome random sequencing and assembly of *Haemophilus influenzae* Rd. *Science* **269**, 496-512. **1995**.

Friemann, A.; Brinkmann, K. and Hachtel, W. Sequence of a cDNA encoding nitrite reductase from the tree *Betula pendula* and identification of conserved protein regions. *Mol. Gen. Genet.* **231**, 411-416. **1992**.

Garrett, D.S.; Seok, Y.-J.; Peterkofsky, A.; Clore, G.M. and Gronenborn, A.M. Identification by NMR of the binding surface for the histidine-containing phosphocarrier protein HPr on the N-terminal domain of enzyme I of the *Escherichia coli* phosphotransferase system. *Biochemestry* **36**, 4393-4398. **1997**.

Garrett, T.P.J.; Clingeleffer, D.J.; Guss, J.M.; Rogers, S.J. and Freeman, H.C. The crystal structure of poplar apoplastocyanin at 1.8-A resolution. The geometry of the copper-binding site is created by the polypeptide. *J. Biol. Chem.* **259**, 2822-2825. **1984**.

Grzesiek, S., Bax, A., Clore, G.M., Gronenborn, A.M., Hu, J.S., Kaufman, J., Palmer, I., Stahl, S.J., and Wingfield, P.T.. The solution structure of HIV-1 Nef reveals an unexpected fold and permits delineation of the binding surface for the SH3 domain of Hck tyrosine protein kinase. *Nat. Struc. Biol*. **3**, 340-345. **1996**

Glockner, A.B.; Jungst, A. and Zumft, W.G. Copper-containing nitrite reductase from *Pseudomonas aureofaciens* is functional in a mutationally cytochrome cd_1-free background (NirS-) of *Pseudomonas stutzeri*. *Arch. Microbiol.* **160**, 18-26. **1993**.

Goodfellow, B.J.; Macedo, A.L.; Rodrigues, P.; Moura, I.; Wray, V. and Moura, J.J.G. The solution structure of a [3Fe-4S] ferredoxin: oxidised ferredoxin II from *Desulfovibrio gigas*. *J. Biol. Inorg. Chem.* **4**, 421-430. **1999**.

Gray, H.B.; Malmström, B.G. and Williams, R.J.P. Copper coordination in blue proteins. *J. Biol. Inorg. Chem.* **5**, 559. **2000**.

Gray, K.A.; Davidson, V.L. and Knaff, D.B. Complex formation between methylamine dehydrogenase and amicyanin from *Paracoccus denitrificans*. *J. Biol. Chem.* **263**, 1387-13990. **1988**.

Gray, K.A.; Knaff, D.B.; Husain, M. and Devidson, V.L. Measurement of the oxidation-reduction potentials of amicyanin and *c*-type cytochromes from Paracoccus denitrificans. *FEBS Lett.* **207**, 239-242. **1986**.

Guex, N. and Peitsch, M.C. SWISS-MODEL and the Swiss-PdbViewer: an environment for comparative protein modeling. *Electrophoresis* **18**, 2714-2723. **1997a**.

Guex, N. and Peitsch, M.C. SWISS-MODEL: an environment for comparative protein modelling. *Electrophoresis* **18**, 2714-2723. **1997b**.

Guillet, V.; Lapthorn, A.; Fourniat, J.; Benoit, J.P.; Hartley, R.W. and Mauguen, Y. Crystallization and preliminary-X-ray investigation of barstar, the intracellular inhibitor of barnase. *Prot. Struc. Funct. Genet.* **17**, 325-328. **1993**.

Guss, J.M.; Harrowell, P.R.; Murata, M.; Norris, V.A. and Freeman, H.C. Crystal structure analyses of reduced (CuI) poplar plastocyanin at six pH values. *J. Mol. Biol.* **192**, 361-387. **1986**.

Helgstrand, M.; Kraulis, P.; Allard, P. and Hard, T. Ansig for Windows: an interactive computer program for semiautomatic assignment of protein NMR spectra. *J. Biomol. NMR* **18**, 329-336. **2000**.

Hervas, M.; Navarro, J.A.; Diaz, A.; Bottin, H. and De La Rosa, M.A. Laser-flash kinetic analysis of the fast electron transfer from plastocyanin and cytochrome *c*6 to photosystem I. Experimental evidence on the evolution of the reaction mechanism. *Biochemestry* **34**, 11321-11326. **1995**.

Hoehn, G.T. and Clark, V.L. Isolation and nucleotide sequence of the gene (aniA) encoding the major anaerobically induced outer membrane protein of *Nesseria gonorrhoeae*. *Infect. Immun.* **60**, 4695-4703. **1992a**.

Hoehn, G.T. and Clark, V.L. The major anaerobically induced outermembraane protein of *Neisseria gonorrhoeae*, Pan 1, is a lipoprotein. *Infect. Immun.* **60**, 4704-4708. **1992b**.

Hoffmann, T.; Frankenberg, N.; Marino, M. and Jahn, D. Ammonification in *Bacillus subtilis* utilizing dissimilatory nitrite reductase is dependent on resDE. *J. Bacteriol.* **180**, 189. **1998**.

Hormel, S.; Adman, E.; Walsh, K.A.; Beppu, T. and Titani, K. The amino acid sequence of the blue copper protein of *Alcaligenes faecalis. FEBS Lett.* **197**, 301-304. **1986**.

Howes, B.D.; Abraham, Z.H.; Lowe, D.J.; Bruser, T.; Eady, R.R. and Smith, B.E. EPR and electron nuclear double resonance (ENDOR) studies show nitrite binding to the type 2 copper centers of the dissimilatory nitrite reductase of *Alcaligenes xylosoxidans* (NCIMB 11015). *Biochemistry* **33**, 3171-3177. **1994**.

Huber, R.; Kukla, D.; Bode, W.; Schwager, P.; Bartels, K.; Deisenho, J. and Steigema, W. Structure of complex formed by bovine trypsin and bovine pancreatic trypsin-Inhibitor .2. Crystallographic refinement at 1.9 Å resolution. *J. Mol. Biol.* **89**, 73-101. **1974**.

Hussain, H.; Grove, J.; Griffiths, L.; Busby, S. and Cole, J. A seven-gene operon essential for formate-dependent nitrite reduction to ammonia by enteric bacteria. *Mol. Microbiol.* **12**, 153-163. **1994**.

Huynh, B.H.; Liu, M.-C.; Moura, J.J.G.; Moura, I.; Ljungdahl, P.O.; Münck, E.; Payne, W.J.; Peck, H.D. Mössbauer and EPR studies on nitrite reductase from *Thiobacillus denitrificans*. *J. Biol. Chem.* **257**, 9576-9581. **2004**.

Inoue, T.; Gotowda M.; Deligeer; Kataoka, K.; Yamaguchi, K.; Suzuki, S. and et al. Type I Cu structure of blue nitrite reductase from *Alcaligenes xylosoxidans* GIFU 1051 at 2.05 Å resolution: comparison of blue and green nitrite reductase. *J. Biochem. (Tokyo)* **124**, 876-879. **1998**.

Inoue, T.; Kai Y.; Harada S.; Kasai N.; Ohshiro Y.; Suzuki, S.; Kohzuma, T. and Tobari J. Structure of pseudoazurin from *Methylobacterium Extorquens* AM1 at 1.5-Angstrom resolution. *Crystallograph* **50**, 317. **1994**.

Inoue, T.; Nishio, N.; Kai, Y.; Harada, S.; Ohshiro, Y.; Suzuki, S.; Kohzuma, T.; Shidara, S. Crystallization and preliminary X-ray studies on pseudoazurin from *Achromobacter cycloclastes* IAM1013. *J. Biochem. (Tokyo)* **114**, 761-762. **1993**.

Inoue, T.; Nishio, N.; Suzuki, S. and Kataoka, K. Crystal structure determinations of oxidized and reduced pseudoazurins from *Achromobacter cycloclastes*. *J. Biol. Chem.* **274**, 17845-17852. **1999**.

Iwasaki, H. and Matsubara T. Purification and some properties of *Achromobacter cycloclastes* azurin. *J. Biochem. (Tokyo)* **73**, 659-661. **1973**.

Janin, J. The kinetics of protein-protein recognition. *Proteins* **28**, 153-161. **1997**.

Jetten, M.S.; Sliekers, O.; Kuypers, M.; Dalsgaard, T.; van Niftrik, L.; Cirpus, I.; Pas-Schoonen, K.; Lavik, G. Anaerobic ammonium oxidation by marine and freshwater planctomycete-like bacteria. *Appl. Microbiol. Biotechnol.* **63**, 107-114. **2003**.

Jetten, M.S.; Wagner, M.; Fuerst, J.; van Loosdrecht, M.; Kuenen, G. and Strous, M. Microbiology and application of the anaerobic ammonium oxidation ('anammox') process. *Curr. Opin. Biotechnol.* **12**, 283-288. **2001**.

Jeuken, L.J.; Ubbink, M.; Bitter, J.H.; van Vliet, P.; Meyer-Klaucke, W. and Canters, G.W. The structural role of the copper-coordinating and surface-exposed histidine residue in the blue copper protein azurin. *J. Mol. Biol.* **299**, 737-755. **2000**.

Johnstone, I.L.; McCabe, P.C.; Greaves, P.; Gurr, S.J.; Cole, G.E.; Brow, M.A.D.; Unkles, S.E.; Clutterbuck, A.J. Isolation and characterisation of the crnA-niiA-niaD gene cluster for nitrate assimilation in *Aspergillus nidulans*. *Gene* **90**, 181-192. **1990**.

Kakutani, T.; Beppu, T. and Arima, K. Regulation of nitrite reductase in the denitrifying bacterium *Alcaligenes faecalis* . *Agr. Biol. Chem. Tokyo* **45**, 23-28. **1981a**.

Kakutani, T.; Watanabe, H.; Arima, K. and Beppu, T. A blue protein as an inactivating factor for nitrite reductase from *Alcaligenes faecalis* strain S-6. *J. Biochem. (Tokyo)* **89**, 463-472. **1981b**.

Kakutani, T.; Watanabe, H.; Arima, K. and Beppu, T. Purification and properties of a copper-containing nitrite reductase from a denitrifying bacterium, *Alcaligenes faecalis* strain S-6. *J. Biochem. (Tokyo)* **89**, 453-461. **1981c**.

Kalk, A. and Berendsen, H.J.C. Proton magnetic relaxation and spin diffusion in proteins. *J. Magn. Reson.* **24**, 343-366. **1976**.

Kalverda, A.P.; Ubbink, M.; Gilardi, G.; Wijmenga, S.S.; Crawford, A.; Jeuken, L.J and Canters, G.W. Backbone dynamics of azurin in solution: slow conformational change associated with deprotonation of histidine 35. *Biochemestry* **38**, 12690-12697. **1999**.

Kannt, A.; Young, S. and Bendall, D.S. The role of acidic residues of plastocyanin in its interaction with cytochrome *f*. *Biochim. Biophys. Acta* **1277**, 115-126. **1996**.

Kataoka, K.; Furusawa, H.; Takagi, K.; Yamaguchi, K. and Suzuki, S. Functional anallysis of conserved aspartate and hitidine residues located around the type 2 copper site of copper-containing nitrite reductase. *J. Biochem. (Tokyo)* **127**, 345. **2000**.

Katoh, S.; Shiratori, I. and Takamiya, A. Purification and some properties of spinach plastocyanin. *J. Biochem. (Tokyo)* **51**, 32-40. **1962**.

Knapp, J.S. and Clark, V.L. Anaerobic growth of *Neisseria gonorrhoeae* coupled to nitrate reduction. *Infect. Immun.* **46**, 176-181. **1984**.

Kobayashi, M. and Shoun, H. The copper containing dissimilatory nitrite reductase involved in the denitrifying system of the *Fungus oxysporum*. *J. Biol. Chem.* **270**, 4146-4151. **1995**.

Kraulis, P.J. Ansig - A program for the assignment of protein H-1 2D-NMR spectra by interactive computer-graphics. *J. Magn. Reson.* **84**, 627-633. **1989**.

Kukimoto, M.; Nishiyama, M.; Murphy, M.E.; Turley, S.; Adman, E.T.; Horinouchi, S. and Beppu, T. X-ray structure and site-directed mutagenesis of a nitrite reductase from *Alcaligenes faecalis* S-6: roles of two copper atoms in nitrite reduction. *Biochemistry* **33**, 5246-5252. **1994**.

Kukimoto, M.; Nishiyama, M.; Ohnuki, T.; Turley, S.; Adman, E.T.; Horinouchi, S. and Beppu, T. Identification of interaction site of pseudoazurin with its redox partner, copper-containing nitrite reductase from *Alcaligenes faecalis* S-6. *Protein Eng.* **8**, 153-158. **1995**.

Kukimoto, M.; Nishiyama, M.; Tanokura, M.; Adman, E.T. and Horinouchi, S. Studies on protein-protein interaction between copper-containing nitrite reductase and pseudoazurin from *Alcaligenes faecalis* S-6. *J. Biol. Chem.* **271**, 13680-13683. **1996**.

Kupce, E. and Freeman, R. Adiabatic pulses for wideband inversion and broadband decouplig. *J. Magn. Reson.* **A115**, 273-276. **1995**.

Lahners, K.; Kramer, V.; Back, E.; Privalle, L. and Rothstein, S. Molecular cloning of complementary DNA encoding maize nitrite reductase: molecular analysis and nitrate induction. *Plant Physiol.* **88**, 741-746. **1988**.

Larsson, S. Energy saving electron pathways in proteins. *J. Biol. Inorg. Chem.* **5**, 560-564. **2000**.

Li, C.; Inoue, T.; Gotowda, M.; Suzuki, S.; Yamaguchi, K.; Kunishige, K. and Kai, Y. Structure of azurin I from the denitrifying bacterium *Alcaligenes xylosoxidans* NCIMB 11015 at 2.45 A resolution. *Acta Crystall. B* **54 (Pt 3)**, 347-354. **1998**.

Liang, Z.X.; Jiang, M.; Ning, Q. and Hoffman, B.M. Dynamic docking and electron transfer between myoglobin and cytochrome *b*(5**)**. *J. Biol. Inorg. Chem.* **7**, 588. **2002**.

Libby, E. and Averill, B.A. Evidence that the type 2 copper centers are the site of nitrite reduction by *Achromobacter cycloclastes* nitrite reductase. *Biochem. Biophys. Res. Co.* **187**, 1529-1535. **1992**.

Libeu, C.A.P.; Kukimoto, M.; Nishiyama, M.; Horinouchi, S. and Adman, E.T. Site-directed mutants of pseudoazurin: Explanation of increased redox potentials from X-ray structures and from calculation of redox potential differences. *Biochemistry* **36**, 13160-13179. **1997**.

Lin, J.T.; Goldman, B.S. and Stewart, V. Structures of genes nasA and nasB, encoding assimilatory nitrate and nitrite reductases in *Klebsiella pneumoniae* M5al. *J. Bacteriol.* **175**, 2370-2378. **1993**.

Liu, M.-Y.; Liu, M.-C.; Payne, W.J.; Peck, H.D. and LeGall, J. Cytochrome *c* components of denitrifying *Pseudomonas stutzeri*. *Curr. Microbiol.* **9**, 87-92. **1983**.

Lommen, A. and Canters, G.W. pH-dependent redox activity and fluxionality of the copper site in amicyanin from *Thiobacillus yersutus* as studied by 300- and 600- MHz ^{1}H NMR. *J. Biol. Chem.* **265**, 2768-2774. **2004**.

Lommen, A.; Canters, G.W. and Van Beeumen, J. A ^{1}H-NMR study on the blue copper protein amicyanin from *Thiobacillus versutus*. Resonance identifications, structural rearrangements and determination of the electron self-exchange rate constant. *Eur. J. Biochem.* **176**, 213-223. **1988**.

Luque, I.; Flores, E. and Herrero, A. Nitrite reductase gene from *Synechococcus sp.* PCC 7942: homology between cyanobacterial and higher-plant nitrite reductases. *Plant Mol. Biol.* **21**, 1201-1205. **1993**.

Machczynski, M.C.; Gray, H.B. and Richards, J.H. An outer sphere hydrogen-bond network constrains copper coordination in blue proteins. *J. Inorg. Biochem.* **88**, 375-380. **2002**.

Mancinelli, R.L.; Cronin, S. and Hochstein, L.I. The purification and properties of a *cd*-cytocrome nitrite reductase from *Paracoccus halodenitrificans*. *Arch. Microbiol.* **145**, 202-208. **1986**.

Marcus, R.A. and Sutin, N. Electron transfers in chemistry and biology. *Biochim. Biophys. Acta* **811**, 265-322. **1985**.

Matthew, J.B.; Weber, P.C.; Salemme, F.R. and Richards, F.M. Electrostatic orientation during electron transfer between flavodoxin and cytochrome *c*. *Nature* **301**, 169-171. **1983**.

Mellies, J.; Jose, J. and Meyer, T.F. The *Neisseria gonorrhoeae* gene aniA encodes an inducible nitrite reductase. *Mol. Genet. Genomics* **256**, 525-532. **1997**.

Merchan, F.; Prieto, R.; Kindle, K.L.; Llama, M.J.; Serra, J.L. and Fernandez, E. Isolation, sequence and expression in *Escherichia coli* of the nitrite reductase gene from

the filamentous, thermophilic cyanobacterium *Phormidium laminosum*. *Plant. Mol. Biol.* **27**, 1037-1042. **1995**.

(2001) *Handbook of Metalloproteins* Messerschmidt, A., Huber, R., Poulos, T.L., and Wieghardt, K. John Wiley & Sons Chichester

Moir, J.W.; Baratta, D.; Richardson, D.J. and Ferguson, S.J. The purification of a cd_1 type nitrite reductase from, and the absence of a copper-type nitrite reductase from, the aerobic denitrifier *Thiosphaera pantotropha*; the role of pseudoazurin as an electron donor. *Eur. J. Biochem.* **212**, 377-385. **1993**.

Moratal, J.M.; Romero, A.; Salgado, J.; Perales-Alarcon, A. and Jiminez, H.R. The crystal structure of nickel(II)-azurin. *Eur. J. Biochem.* **228**, 653-657. **1995**.

Morelli, X.; Czjzek, A.; Hatchikian, C.E.; Bornet, O.; Fontecilla-Camps, J.C.; Palma, P.N.; Moura J.J.G. and Guerlesquin, F. Structural model of the Fe-hydrogenase/cytochrome *c*553 complex combining transverse relaxation-optimized spectroscopy experiments and soft docking calculations. *J. Biol. Chem.* **275**, 23204-23210. **2000a**.

Morelli, X.; Dolla, A.; Czjzek, A.; Palma, P.N.; Blasco, F.; Krippahl, L.; Moura, J.J.G. and Guerlesquin, F. Heteronuclear NMR and soft docking: an experimental approach for a structural model of the cytochrome *c*553-ferredoxin complex. *Biochemestry* **39**, 2530-2537. **2000b**.

Morelli, X.J.; Palma, P.N.; Guerlesquin, F. and Rigby, A.C. A novel approach for assessing macromolecular complexes combining soft-docking calculations with NMR data. *Protein Sci.* **10**, 2131-2137. **2001**.

Murphy, L.M.; Dodd, F.E.; Yousafzai, F.K.; Eady, R.R. and Hasnain, S.S. Electron donation between copper containing nitrite reductases and cupredoxins: the nature of protein-protein interaction in complex formation. *J. Mol. Biol.* **315**, 859-871. **2002**.

Murphy, M.E.; Turley, S. and Adman, E.T. Structure of nitrite bound to copper-containing nitrite reductase from *Alcaligenes faecalis*. Mechanistic implications. *J. Biol. Chem.* **272**, 28455-28460. **1997**.

Murphy, M.J.; Siegel, L.M.; Tove, S.R. and Kamin, H. Siroheme: a new prosthetic group participating in six-electron reduction reactions catalyzed by both sulfite and nitrite reductases. *Proc. Natl. Acad. Sci. USA* **71**, 616. **1974**.

Nakanishi, T.; Miyazawa, M.; Sakakura, M.; Terasawa, H.; Takahashi, H. and Shimada, I. Determination of the interface of a large protein complex by transferred cross-saturation measurements. *J. Mol. Biol.* **318**, 245-249. **2002**.

Nar, H.; Messerschmidt, A.; Filippou, A.C.; Barth, M.; Jaquinod, M.; Van de Kamp, M. and Canters, G.W. Characterization and crystal structure of zinc azurin, a by-product of heterologous expression in *Escherichia coli* of *Pseudomonas aeruginosa* copper azurin. *Eur. J. Biochem.* **205**, 1123-1129. **1992**.

Nar, H.; Messerschmidt, A.; Huber, R.; van de, K.M. and Canters, G.W. Crystal structure analysis of oxidized *Pseudomonas aeruginosa* azurin at pH 5.5 and pH 9.0. A pH-induced conformational transition involves a peptide bond flip. *J. Mol. Biol.* **221**, 765-772. **1991**.

Neininger, A.; Seith, B.; Hoch, B. and Mohr, H. Gene expression of nitrite reductase in Scots pine (*Pinus sylvestris L.*) as affected by light and nitrate. *Plant Mol. Biol.* **25**, 449-457. **1994**.

Nicholls, A.; Sharp, K.A. and Honig, B. Protein folding and association- insights from the interfacial and thermodynamic properties of hydrocarbons. *Prot. Struc. Funct. Genet.* **11**, 281-296. **1991**.

Nishiyama, M.; Suzuki, J.; Kukimoto, M.; Ohnuki, T.; Horinouchi, S. and Beppu, T. Cloning and characterization of a nitrite reductase gene from *Alcaligenes faecalis* and its expression in *Escherichia coli*. *J. Gen. Microbiol.* **139**, 725-733. **1993**.

Northrup, S.H. and Erickson, H.P. Kinetics of protein-protein association explained by Brownian dynamics computer simulatio. *Proc. Natl. Acad. Sci. USA* **89**, 3338-3342. **1992**.

Ogawa, K.I.; Akagawa, E.; Yamane, K.; Sun, Z.W.; Lacelle, M.; Zuber, P. and Nakano, M.M. The nasB operon and nasA gene are required for nitrate/nitrite assimilation in *Bacillus subtilis*. *J. Bacteriol.* **177**, 1409-1413. **1995**.

Ota, A. and Okonuki, K. A nitrite reducing system reconstructed with purified cytochrome components of *Pseudomonas aeruginosa*. *Biochim. Biophys. Acta* **53**, 294-308. **1961**.

Palma, P.N.; Krippahl, L.; Wampler, J.E. and Moura, J.J. BiGGER: a new (soft) docking algorithm for predicting protein interactions. *Proteins* **39**, 372-384. **2000**.

Parr, S.R.; Barber, D.; Greenwood, C. and Brunori, M. The electron-transfer reaction between azurin and the cytochrome *c* oxidase from *Pseudomonas aeruginosa*. *Biochem J.* **167**, 447-455. **1977**.

Pauleta, S.R.; Guerlesquin, F.; Goodhew, C.F.; Devreese, B.; Van Beeumen, J.; Pereira, A.S.; Moura, I. and Pettigrew, G.W. *Paracoccus pantotrophus* pseudoazurin is anelectron donor to cytochrome *c* peroxidase. *Biochemestry* **43**, 11214-11225. **2004**.

Peitsch, M.C. Protein modeling by E-mail. *Bio-Technol.* **13**, 658-660. **1995**.

Pervushin, K.; Riek, R.; Wider, G. and Wuthrich, K. Attenuated T-2 relaxation by mutual cancellation of dipole-dipole coupling and chemical shift anisotropy indicates an avenue to NMR structures of very large biological macromolecules in solution. *Proc. Natl. Acad. Sci. USA* **94**, 12366-12371. **1997**.

Pervushin, K.; Riek, R.; Wider, G. and Wuthrich, K. Transverse relaxation-optimized spectroscopy (TROSY) for NMR studies of aromatic spin systems in C-13-labeled proteins. *J. Am. Chem. Soc.* **120**, 6394-6400. **1998**.

Petratos, K.; Dauter, D. and Wilson, K.S. Refinement of the structure of pseudoazurin from *Alcaligenes faecalis* S-6 at 1.55 A resolution. *Acta Crystallogr.* **B44**, 628-636. **1988**.

Petratos, K.Z.; Papadovasilaki, M. and Dauter, Z. The crystal structure of apo-pseudoazurin from Alcaligenes faecalis S-6. *FEBS Lett.* **368**, 442. **1995**.

Pettigrew, G.W.; Prazeres, S.; Costa, C.; Palma, N.; Krippahl, L.; Moura, I. and Moura J.J.G. The structure of electron transfer complex containing a cytocrome *c* and a peroxidase. *J. Biol. Chem.* **274**, 11383-11389. **1999**.

Pinho, D.; Besson, S.; Brondino, C.D.; de Castro, B. and Moura, I. Copper-containing nitrite reductase from *Pseudomonas chlororaphis* DSM 50135. *Eur. J. Biochem.* **271**, 2361-2369. **2004**.

Prudêncio, M.; Eady, R.R. and Sawers, G. The Blue Copper-Containing Nitrite reductase form *Alcaligenes xylosoxidans*: clining of the nirA gene and charactrization of the ricombinant enzyme. *J. Bacteriol.* **181**, 2323-2329. **1999**.

Prudêncio, M.; Eady, R.R. and Sawers, G. Catalytic and spectroscopic analysis of blue copper-containing nitrite reductase mutants altered in the environment of the type 2 copper centre: implications for substrate interaction. *Biochem J.* **353**, 259-266. **2001**.

Prudêncio, M.; Rohovec, J.; Peters, J.A.; Tocheva, E.I.; Boulanger, M.J.; Murphy, M.E.P.; Hupkes, H.J.; Kosters, W. A caged lanthanide complex as a paramagnetic shift agent for protein NMR. *Chem. Eur. J.* **10**, 3252-3260. **2004**.

Randall, D.W.; Gamelin, D.R.; LaCroix, L.B. and Salomon, E.I. Electronic structure contributions to electron transfer in blue Cu and Cu(A). *J. Biol. Inorg. Chem.* **5**, 16-29. **2000**.

Robertson, G.P.; Paul, E.A. and Harwood, R.R. Greenhouse gases in intensive agriculture: contributions of individual gases to the radiative forcing of the atmosphere. *Science* **289**, 1922-1925. **2000**.

Ryde, U.; Olsson, M.H.M.; Roos, B.O.; De Kerpel, J.O.A. and Pierloot, K. On the role of strain in blue copper proteins. *J. Biol. Inorg. Chem.* **5**, 565-574. **2000**.

Sasaki, S.; Karube, I.; Hirota, N.; Arikawa, Y.; Nishiyama, M.; Kukimoto, M.; Horinouchi, S. and Beppu, T. Application of nitrite reductase from *Alcaligenes faecalis* S-6 for nitrite measurement. *Biosens. Bioelectron.* **13**, 1-5. **1998**.

Sato, K. and Dennison, C. Effect of Histidine 6 protonation on the active site structure and electron transfer capabilities of pseudoazurin from *Achromobacter cycloclastes*. *Biochemestry* **41**, 120-130. **2002**.

Schreiber, G. and Fersht, A.R. Interaction of barnase with its polypeptide inhibitor studied by protein engineering. *Biochemestry* **32**, 5145-5150. **1993**.

Schwede, T.; Kopp, J.; Guex, N. and Peitsch, M.C. SWISS-MODEL: an automated protein homology-modeling server. *Nucleic Acids Res.* **31**, 3381-3385. **2003**.

Sheinerman, F.B.; Norel, R. and Honig, B. Electrostatics aspects of protein-protein interaction. *Curr. Opin. Struc. Biol.* **10**, 153-159. **2000**.

Shepard, W.E.B.; Anderson, B.F.; Lewandowski, D.A.; Norris, G.A. and Baker, E.N. Copper coordination geometry in azurin undergoes minimal change on reduction of copper(II) to copper(I). *J. Am. Chem. Soc.* **112**, 7817-7819. **1990**.

Sheriff, S.; Silverton, E.W.; Padlan, E.A.; Cohen, G.H.; Smithgill, S.J.; Finzel, B.C. and Davies, D.R. 3-Dimensional structure of an antibody-antigen complex. *Proc. Natl. Acad. Sci. USA* **84**, 8075-8079. **1987**.

Silvestrini, M.C.; Tordi, M.G.; Musci, G. and Brunori, M. The reaction of *Pseudomonas* nitrite reductase and nitrite. A stopped-flow and EPR study. *J. Biol. Chem.* **265**, 11783-11787. **1990**.

Strous, M.; Kuenen, J.G. and Jetten, M.S. Key physiology of anaerobic ammonium oxidation. *Appl. Environ. Microbiol.* **65**, 3248-3250. **1999**.

Suzuki, S.; Deligeer; Yamaguchi, K.; Kataoka, K.; Kobayashi, K.; Tagawa, S.; Kohzuma, T.; Shidara, S. Spectroscopic characterization and intramolecular electron transfer processes of native and type 2 Cu-depleted nitrite reductases. *J. Biol. Inorg. Chem.* **2**, 265-274. **1997**.

Suzuki, S.; Deligeer; Yamaguchi, K.; Kataoka, K.; Shidara, S.; Iwasaki, H. and Sakurai, T. Spectroscopic distinction between two Co(II) ions substituted for types 1 and 2 Cu in nitrite reductase. *Inorg. Chim. Acta* **276**, 289-294. **1998**.

Suzuki, S.; Kataoka, K. and Yamaguchi, K. Metal coordination and mechanism of multicopper nitite reductase. *Acc. Chem Res.* **33**, 728-735. **2000**.

Suzuki, S.; Kataoka, K.; Yamaguchi, K.; Inoue, T. and Kai, Y. Structure-function relationships of copper-containing nitrite reductases. *Coordin. Chem. Rev.* **192**, 245-265. **1999**.

Suzuki, S.; Kohzuma, T.; Delingeer Yamaguchi K.; Nakamura N.; Shidara, S. and et al. Pulse radiolysis on itrite reductase from *Achromobacter cycloclastes* IAM 1013: evidence for intramolecular electron transfer from type I Cu to type II Cu. *J. Am. Chem. Soc.* **116**, 1145-1146. **1994**.

Takahashi, H.; Nakanishi, T.; Kami, K.; Arata, Y. and Shimada, I. A novel NMR method for determining the interfaces of large protein-protein complexes. *Nat. Struct. Biol.* **7**, 220-223. **2000**.

Tanaka, T.; Ida, S.; Irifune, K.; Oeda, K. and Morikawa, H. Nucleotide sequence of a gene for nitrite reductase from *Arabidopsis thaliana*. *DNA Seq.* **5**, 57-61. **1994**.

Thamdrup, B. and Dalsgaard, T. Production of N(2) through anaerobic ammonium oxidation coupled to nitrate reduction in marine sediments. *Appl. Environ. Microbiol.* **68**, 1312-1318. **2002**.

Thompson, G.S.; Leung, Y.C.; Ferguson, S.J.; Radford, S.E. and Redfield, C. The structure and dynamics in solution of Cu(I) pseudoazurin from *Paracoccus pantotrophus*. *Protein Sci.* **9**, 846-858. **2000**.

Tocheva, E.I.; Rosell, F.I.; Mauk, A.G. and Murphy, M.E.P. Side-On Copper-Nitrosyl coordination by Nitrite Reductase. *Science* **304**, 867. **2004**.

Tosques, I.E.; Kwiatkowski, A.V.; Shi, J. and Shapleigh, J.P. Characterization and regulation of the gene encoding nitrite reductase in *Rhodobacter sphaeroides* 2.4.3. *J. Bacteriol.* **179**, 1090-1095. **1997**.

Tsai, L.-C.; Sjolin, L.; Langer, V.; Bonander, N.; Karlsson, G.; Vanngard, T.; Hammann, C. and Nar, H. Structure of the azurin mutant nickel-Trp48Met from *Pseudomonas aeruginosa* at 2.2 Å resolution. *Acta Crystallogr. D Biol. Crystallogr.* **51**, 711-717. **1995**.

Ubbink, M. and Bendall, D.S. Complex of plastocyanin and cytochrome *c* characterized by NMR chemical shift analysis. *Biochemistry* **36**, 6326-6335. **1997**.

Ubbink, M.; Ejdebäck; Karlsson, B.G. and Bendall, D.S. The structure of the complex of plastocyanin and cytochrome *f*, determined by paramagnetic NMR and restrained rigid-body molecular dynamics. *Structure* **6**, 323-335. **1998**.

Vakoufari, E.; Wilson, K.S. and Petratos, K. The Crystal-structures of reduced pseudoazurin from *Alcaligenes Faecalis* S-6 at two pH values. *FEBS Lett.* **347**, 203-206. **1994**.

Van de Graaf, A.A.; Mulder, A.; de Bruijn, P.; Jetten, M.S.; Robertson, L.A. and Kuenen, J.G. Anaerobic oxidation of ammonium is a biologically mediated process. *Appl. Environ. Microbiol.* **61**, 1246-1251. **1995**.

Van de Kamp, M.; Canters, G.W.; Andrew C.R.; Sanders-Loehr, J.; Bender C.J. and Peisach J. Effect of lysine ionization on the structure and electrochemical behaviour of the Met44-->Lys mutant of the blue-copper protein azurin from *Pseudomonas aeruginosa*. *Eur. J. Biochem.* **218**, 229-238. **1993**.

Walsh, T.A.; Johnson, M.K.; Barber, D.; Thomson, A.J. and Greenwood, C. Studies on heme d_1 extracted from *Pseudomonas aeruginosa* nitrite reductase. *J. Inorg. Biochem.* **14**, 15-31. **1981**.

Wasser, I.M.; de Vries, S.; Moenne-Loccoz, P.; Schroder, I. and Karlin, K.D. Nitric oxide in biological denitrification: Fe/Cu metalloenzyme and metal complex NO(x) redox chemistry. *Chem. Rev.* **102**, 1201-1234. **2002**.

Williams, P.A.; Fulop, V.; Garman, E.F.; Saunders, N.F.; Ferguson, S.J. and Hajdu, J. Haem-ligand switching during catalysis in crystals of a nitrogen-cycle enzyme. *Nature* **389**, 406-412. **1997**.

Williams, R.S.B.; Davis, M.A. and Howlett, B.J. The nitrate and nitrite reductase-encoding genes of *epLtosphaeria maculans* are closely linked and transcribed in the same direction. *Gene* **158**, 153-154. **1995**.

Wishart, D.S.; Sykes, B.D. and Richards, F.M. The chemical shift index: a fast and simple method for the assignment of protein secondary structure through NMR spectroscopy. *Biochemestry* **31**, 1647-1651. **1992**.

Woods, J.P.D.; Kawula, T.H.; Barritt, D.S. and Cannon, J.G. Characterizatiion of the Neisserial lipid-modified azurin bearing the H. 8 epitope. *Mol. Microbiol.* **3**, 583-591. **1989**.

Worrall, J.A.R.; Liu, Y.; Crowley, P.B.; Nocek, J.M.; Hoffman, B.M. and Ubbink, M. Myoglobin and cytochrome b_5: a nuclear magnetic resonance study of a higly dynamic protein complex . *Biochemistry* **41**, 11721-11730. **2002**.

Worrall, J.A.R.; Kolczak, U.; Canters, G.W. and Ubbink, M. Interaction of yeast iso-1-cytochrome *c* with cytochrome c peroxidase investigated by [^{15}N, ^{1}H] heteronuclear NMR spectroscopy. *Biochemistry* **40**, 7069-7076. **2001**.

Worrall, J.A.R.; Reinle, W.; Bernhardt, R. and Ubbink, M. Transient protein interactions studied by NMR spectroscopy: the case of cytochrome *c* and adrenodoxin. *Biochemistry* **42**, 7068-7076. **2003**.

Yamamoto, K.; Uozumi, T. and Beppu, T. The blue copper protein gene of *Alcaligenes faecalis* S-6 directs secretion of blue copper protein from *E. coli* cells. *J. Bacteriol.* **169**, 5648-5652. **1987**.

Zhao, Y.; Lukoyanov, D.A.; Toropov, Y.V.; Wu, K.; Shapleigh, J.P. and Scholes, C.P. Catalytic function and local proton structure at the type 2 copper of nitrite reductase: the correlation of enzymatic pH dependence, conserved residues, and proton hyperfine structure. *Biochemistry* **41**, 7464. **2002**.

Zhu, D.W.; Dahms, T.; Willis, K.; Szabo, A.G. and Lee, X. Crystallization and preliminary crystallographic studies of the crystals of the azurin *Pseudomonas fluorescens*. *Arch. Biochem. Biophys.* **308**, 469-470. **1994**.

Zhu, Z.; Cunane, L.M.; Chen, Z.; Durley, R.C.; Mathews, F.S. and Davidson, V.L. Molecular basis for interprotein complex-dependent effects on the redox properties of amicyanin. *Biochemestry* **37**, 17128-17136. **1998**.

Zuiderweg, E.R. Mapping protein-protein interactions in solution by NMR spectroscopy. *Biochemistry* **41**, 1-7. **2002**.

Zumft, W.G. Cell biology and molecular basis of denitrification. *Microbiol. Mol. Biol. R.* **61**, 533-616. **1997**.

.

Summary

Electron transfer complexes of metallo-proteins are fundamental in many metabolic processes. They differ from many other protein complexes in their characteristic compromise between specificity and affinity. Specificity is a requirement for complex formation in a context where many proteins are present. The binding needs to be selective for specific partners and furthermore, it needs to be localized to an area close to the active site in order to be productive. However, the strength of the binding (the affinity), cannot be high because this limits the turn-over of the complex, which needs to be high in the case of electron transfer. These opposing requirements need to be balanced in order to guarantee formation and functionality of the complex. This balance is determined by the molecular details of transient complex formation, more specifically in the characteristics of the residues involved in the complex formation and the kind of forces under which the complex is formed. The aim of the thesis is to characterize the molecular interactions between the proteins pseudoazurin (PAZ) and nitrite reductase (NiR), both metallo-proteins forming an electron transfer complex.

In the introduction the role of this complex in nature is discussed. PAZ and NiR complex occur in a soil bacterium called *Alcaligenes faecalis* S-6. This bacterium participates in the fundamental biological process of denitrification. In the denitrification process, nitrate is reduced in several steps to elementary nitrogen. NiR catalyses nitrite reduction to nitric oxide upon receiving electrons from PAZ.

Nuclear magnetic resonance (NMR) was the primary tool in this investigation: chemical shift perturbation analysis and cross saturation transfer have been used to characterize binding kinetics and to identify the binding area on PAZ surface.

The first step of this work has been the assignment of NMR PAZ spectra, which is presented in Chapter II. The near complete assignment for the nuclei ^{1}H, ^{15}N, ^{13}C is listed for copper containing PAZ in its reduced form. Zn substituted PAZ, used as the equivalent for the oxidized form of copper PAZ, was also analyzed and the amide resonances (^{1}H and ^{15}N) have been assigned.

In Chapter III binding studies of NiR and PAZ are described. Metal substituted forms of PAZ and NiR have been used to mimic the different oxidation states of the proteins. It is shown that binding proprieties are dependent on the redox state of PAZ. PAZ in its reduced form exhibits a complex binding behaviour that differs from its oxidized state. Interestingly the reduced form exhibits two binding modalities between PAZ and NiR which occur simultaneously, one in fast exchange and the other one in slow exchange on the NMR time scale. In the oxidized form of PAZ only a fast modality is present. The experimental observations of protein interactions in the reduced form have been modelled using a four-state model. In Chapter IV the influence of the pH on PAZ-NiR binding has been analyzed in order to find a possible explanation of the two binding modes in the reduced state of PAZ. It is shown that pH affects the affinity between the two proteins. It is concluded that protonation of the surface exposed His6 is unlikely to explain the observation. The

protonation of copper ligand His81 in the reduced form is suggested to be a more probable explanation. His81 is in fact in the middle of the hydrophobic patch involved in the complex interface and in the electron transfer to NiR.

In Chapter V cross saturation transfer is used as tool to determine the interface of binding between PAZ and NiR both in the reduced state. This method allowed the determination of the binding area for the proteins under slow exchange conditions. In this chapter the procedure to express efficiently ^{2}H-^{15}N PAZ required for this type of experiment is also described.

For the oxidized form of PAZ which associates in fast exchanges mode with NiR, the binding surface has been determined via chemical shift perturbation mappings, described in Chapter VI. On the basis of the results and docking simulations, a model for the structure of the complex is suggested.

The interaction between nitrite reductase and azurin from the pathogenic *Neisseria gonorrhoeae* has also been analysed in this thesis. Remarkably, these proteins show no detectable complex formation and thus must interact in a fashion that is very different from PAZ and NiR from *Al. faecalis*.

In the general discussion some conclusions from the work are discussed. In previous kinetic studies it was suggested that the recognition of positively charged residues of PAZ by negatively charged ones from NiR is important for complex formation.

From the analysis of our results it is possible to conclude that the complex involving PAZ in the reduced state as well as in the oxidized one involves the hydrophobic patch on PAZ located around the His81 copper ligand. A combination of electrostatic and hydrophobic forces, localized around the copper site, thus provides an optimized binding which on the one hand guarantees rapid electron transfer from PAZ to NiR and on the other ensures a high turnover rate essential for an electron transfer complex. The oxidation state of the metal centre, although it does not modify the binding area, affects the binding modalities of the two forms, oxidized and reduced. The explanation for such phenomena needs further investigations.

Samenvatting

De vorming van eiwit:eiwit-complexen om elektronen over te dragen is een essentieel onderdeel van veel metabolische processen. Een kenmerk dat deze complexen onderscheidt van andere eiwitcomplexen, is het compromis tussen specificiteit en affiniteit. Specificiteit van het complex is noodzakelijk in een omgeving waar vele verschillende eiwitten aanwezig zijn. De associatie moet plaatsvinden tussen specifieke partners en bovendien op een specifieke locatie op het oppervlak van de eiwitten (de bindingsplaats). De sterkte van de binding (affiniteit) mag echter niet te hoog zijn, want dit zou de omzettingssnelheid van het complex beperken en snel elektrontransport verhinderen. Beide voorwaarden moeten in elektronoverdrachtscomplexen in evenwicht zijn, hetgeen bereikt wordt met behulp van de juiste moleculaire interacties tussen de aminozuurresiduen in de bindingsplaatsen op de eiwitten. Het zijn deze residuen die het karakter van de interactie bepalen.

Het doel van het werk beschreven in dit proefschrift is de karakterisatie van de moleculaire interactie tussen de koperbevattende eiwitten pseudoazurine (PAZ) en nitrietreductase (NiR). In de inleiding wordt de fysiologische rol van dit complex besproken. De eiwitten komen voor in de grondbacterie *Alcaligenes faecalis* S-6, welke een rol heeft in het fundamentele proces van de denitrificatie. In dit proces wordt nitraat in enkele stappen omgezet in elementaire stikstof. NiR reduceert nitriet (NO_2^-) tot stikstofmonoxide (NO), met behulp van elektronen die gedoneerd worden door het elektrontransporteiwit PAZ. Kernspinresonantie (Nuclear Magnetic Resonance, NMR) spectroscopie is de belangrijkste techniek die voor het onderzoek gebruikt is. De analyse van veranderingen in de chemische verschuivingen van de NMR signalen en intermoleculaire verzadigingsoverdracht (cross saturation transfer) zijn toegepast om de kinetiek van binding alsmede de bindingsplaatsen te bestuderen.

De eerste stap in dit werk is het toekennen van de NMR spectra van PAZ, welk in Hoofdstuk II is beschreven. De ^1H, ^{15}N en ^{13}C spectra van PAZ met het koperion in de monovalente toestand zijn bijna volledig toegekend. Van PAZ waarin de koper was vervangen door zink (II) - als redoxinactief substituut voor koper (II) - zijn de ^1H en ^{15}N resonanties van de amidegroepen toegekend.

In Hoofdstuk III zijn bindingstudies van NiR en PAZ beschreven. Met behulp van metaalgesubstitueerde vormen van beide eiwitten is het mogelijk de verschillende redoxtoestanden na te bootsen. Zo is aangetoond dat de manier van binden afhankelijk is van de oxidatietoestand van PAZ, maar niet van die van NiR. In de gereduceerde vorm laat PAZ een complex bindingsmechanisme zien, terwijl dat voor geoxideerd PAZ simpeler is. Het gereduceerde PAZ vertoont tegelijkertijd twee bindingsmanieren, waarvan de ene snel is op de NMR-tijdsschaal, terwijl de andere langzaam is. Een model met vier toestanden is geformuleerd om dit verschijnsel te beschrijven.

In Hoofdstuk IV is de invloed van de pH op het complex van PAZ en NiR beschreven, met als doel de moleculaire oorzaak van de twee bindingsmanieren van gereduceerd PAZ bloot te leggen. Het blijkt dat met toenemende pH de bindingssterkte van de interactie afneemt, maar dat het mechanisme niet fundamenteel verandert. Deze resultaten suggeren dat

protonering van de aan het eiwitoppervlak gelegen zijketen van aminozuurresidu His6 niet de oorzaak is van de dubbele bindingsmodus. Protonering van de koperligand His81 zou dit verschijnsel wel kunnen verklaren.

In Hoofdstuk V is cross saturation transfer gebruikt om de bindingsplaats voor NiR op PAZ te bepalen voor de modus van langzame complexvorming en -dissociatie. In dit hoofdstuk wordt ook de procedure beschreven voor de efficiënte productie van ^{2}H,^{15}N-verrijkte PAZ, die noodzakelijk was voor dit experiment.

Voor de geoxideerde vorm van PAZ, die een snelle bindingsinteractie vertoont met NiR, is de bindingsplaats bepaald door analyse van de chemische verschuivingen van de amideresonanties, hetgeen beschreven is in Hoofdstuk VI. Op basis van de experimentele resultaten en een bindingssimulatie, is gekomen tot een model voor de structuur van het complex van NiR en PAZ.

In hoofdstuk VII is een studie naar de interactie van azurine en NiR uit de pathogene bacterie *Neisseria gonorrhoeae* beschreven. Het blijkt dat deze vermeende fysiologische partners geen complexvorming van betekenis laten zien. De interactie tussen deze eiwitten moet dus van een geheel andere aard zijn dan die tussen PAZ en NIR uit *Al. faecalis*.

In het laatste hoofdstuk worden enige conclusies van het werk besproken en in verband gebracht met eerdere studies. Eerder werk aan de kinetiek van elektronoverdracht tussen PAZ en NiR had aangetoond dat bepaalde geladen residuen belangrijk zijn voor de complexvorming. Het hier beschreven werk geeft aan dat de bindingsplaats voor NiR op PAZ het goeddeels hydrofobe gebied rond His81 omvat. Dit residu is naar alle waarschijnlijkheid de poort voor het elektron vanuit PAZ naar NiR. Het hydrofobe karakter van de bindingsplaats, in samenhang met het belang van geladen residuen, geeft aan dat zowel hydrofobe interacties als elektrostatische krachten een rol spelen bij de complexvorming. Deze combinatie garandeert zowel een snelle binding (door de ladingsinteracties) als voldoende specificiteit (door de hydrofobe contacten). Het is opmerkelijk dat de oxidatietoestand van PAZ een zo grote invloed heeft op het bindingsmechanisme en toch geen effect heeft op de bindingsplaats. De verklaring van dit verschijnsel behoeft nog verder onderzoek.

Appendix: Color pictures

a) Pseudoazurin
Alcaligenes faecalis **S-6**
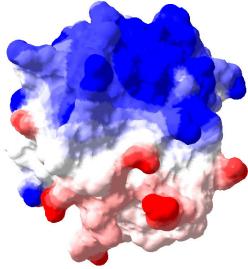
c)Azurin *(model)*
Neisseria gonorrhoeae
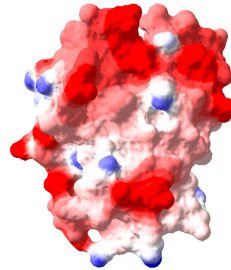
Figure 1.5: (Top panel) a) Ribbon structure of pseudoazurin (PDB entry: 8PAZ) with lysines and aspartate residues together with ligand His81 shown with sticks. Model ribbon diagram of Laz (c) obtained using homology modelling of Swiss – Model server (Schwede, 2003; Guex, 1997b; Peitsch, 1995) and using as model azurin from *Ps. aeruginosa* (PDB entry:1E5Y). Copper in both pictures a) and c), is indicated with a black sphere. The bottom panel shows the electrostatic potential surfaces of pseudoazurin (b) and azurin (d). The surfaces were created with Swiss-Pdb Viewer 3.7 with a colour range from blue for positive residues to red for negative ones.

Figure 5.3.: Binding map**.** A) Surface representation of the PAZ Cu I structure using the colour code according to the classification shown in Figure 5.2; with intensity ratios <0.41 in red, 0.41-0.51 in orange, 0.52-0.55 in yellow and >0.54 in blue. Residues for which no data are available (prolines, K46, D47) are shown in grey. Relevant residues are indicated. B) Semi-transparent representation, tilted relative to A) to show the location of the copper site. The figure was produced using GRASP (Nicholls, 1991).

a) PAZ Cu I : NiR Cu I-T2D

(inverse titration)
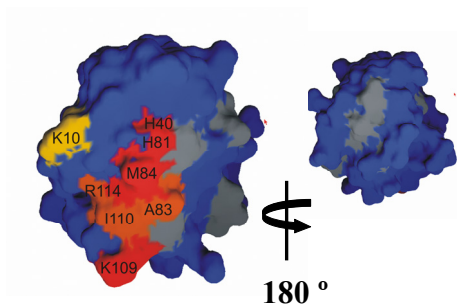
b) PAZ Zn II : NiR CuI-T2D
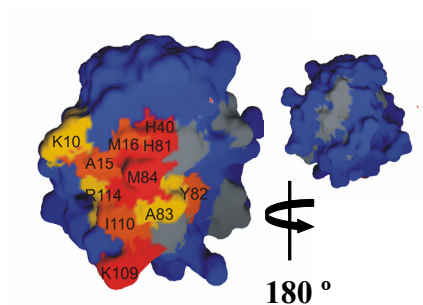
(direct titration)

c) PAZ Zn II : NiR Cu II-Cu II

(direct titration)

d) PAZ Cu I : NiR Cu I-T2D

(cross saturation transfer method)

Figure 6.3: Mapping of the $\Delta\delta_{avg}$ on the surface of PAZ (front side on the left and back side on the right) for the complexes a) NiR Cu I-T2D : ^{15}N-PAZ Cu I at a ratio of 1.7 in the inverse titration; b) NiR Cu I-T2D :[15]N-PAZ Zn II at a ratio 0.15 in the direct titration; c) NiR Cu II-Cu II :[15]N-PAZ Zn II at a ratio of 0.10 in the direct titration and d) map obtained with cross saturation transfer for complex formation between NiR Cu I-T2D and ^{15}N-PAZ Cu I at a ratio of 0.7. Residues are colour-coded according with the horizontal line in Figure 6.2a, b and c (for Figure 6.3a, b and c respectively). In figure 6.3d the colour code according to the classification shown in Figure 5.2 in Chapter 5 has been used.

Figure 6.4: The experimentally ranked docking geometries generated by BIGGER programme. NiR is depicted as C^{α} trace with the type1 and type2 coppers shown as green spheres. The geometric centre of PAZ is represented by spheres in each of the top 200 orientations. The colour indicates the ranking position on a scale from blue to red with red indicating the highest ranking.
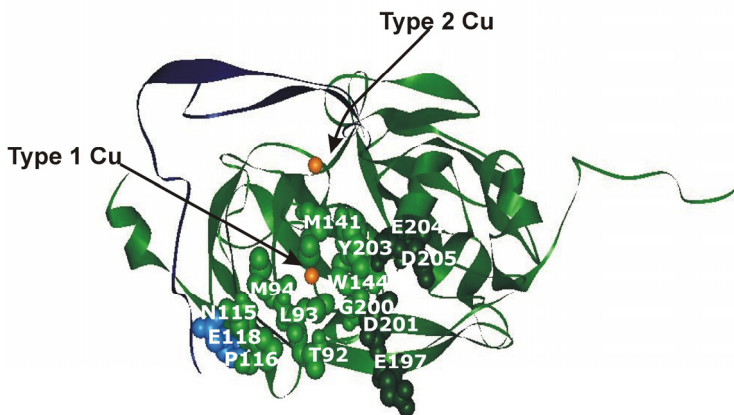

Figure 6.7: Binding site on the surface of NiR subunit surface. The residues involved in the interaction are depicted as green spheres and labelled, the dark green spheres indicate those residues that have been also identified as involved in the binding in the mutagenesis and kinetic studies (Kukimoto, 1996). E118 which also results involved in the binding in the mutagenesis and kinetic studies is depicted as blue spheres. The remaining protein is depicted in ribbons (one monomer in green and the tail of the adjacent monomer in blue) and the two copper atoms as orange spheres.

Publications

^{1}H, ^{13}C and ^{15}N resonance assignment of Cu(I)-pseudoazurin from *Alcaligenes faecalis S-6*
A. Impagliazzo and M. Ubbink (**2004**)
Journal of Biomolecular NMR **29**: 541-542

Mapping of the binding site on pseudoazurin in the transient 152 kDa complex with nitrite reductase
A. Impagliazzo and M. Ubbink (**2004**)
J Am Chem Soc. **126**: 5658-5659.

A caged lanthanide complex as paramagnetic shift agent for protein NMR
M. Prudêncio, J. Rohovec, J.A. Peters, E. Tocheva, M.J. Boulanger, M.E.P. Murphy, H. Hupkes, W. Kosters, A. Impagliazzo and M. Ubbink (**2004**)
Chemistry **10**: 3252-60

Pseudoazurin : nitrite reductase interactions
A. Impagliazzo, L. Krippahl. and M. Ubbink (**2004**)
Submitted for publication.

Redox state dependent binding between pseudoazurin and nitrite reductase
A. Impagliazzo, M.J. Cliff, J.E. Ladbury, M. Prudêncio, G.W. Canters and M. Ubbink (**2004**)
In preparation.

Acknowledgments

Curriculum Vitae

Antonietta Impagliazzo was born in Rome on the 2nd of August 1971. She attended the secondary school; "Liceo Vivona" for her classical studies before getting her Chemistry degree in 1997 at the Università degli Studi di Roma "La Sapienza".

Her dissertation, under the supervision of Prof. M. Delfini, had as the subject: *The β-carbolyns: a ligand for the paramagnetic metal as hypothetical contrast agents for Image NMR by means of ^{1}H- ^{13}C NMR and UV spectoscopy*. In September 1997 she received a grant from the Second University of Rome, Tor Vergata (Italy) under the supervision of Prof. M. Paci to work on the project: *Structural study of SPR-3 proteins of the corneous layer of the skin by means of 2D NMR and Circular Dychroism*.

From May 1999 she worked for the Istituto dell'Enciclopedia Italiana Treccani (Rome,Italy) involved in the project "*I Saperi del Novecento*" (Science education for schools) and in the quality control of the CD-ROM enclosed with the encyclopaedia "*Frontiere della Vita*".

In May 2000 she started her Ph.D. study at University of Leiden supervised by Dr. M. Ubbink in the Metallo-Protein group of Prof. G.W. Canters.

Parts of this thesis were presented at the Annual Meeting of the Studiegroep Eiwitonderzoek (Lunteren, The Netherlands, 2003). This seminar was awarded a prize for the best oral presentation.